ROLES OF TWO INTERHELICAL INSERTIONS IN CATALASE-PEROXIDASE CATALYSIS: TRACING THE IMPACT OF PERIPHERAL PROTEIN STRUCTURES ON HEME ENZYME FUNCTION

Except where reference is made to the work of others, the work described in this dissertation is my own or was done in collaboration with my advisory committee. This dissertation does not include proprietary or classified information.

_____

Yongjiang Li

Certificate of Approval:

_____	_____
Stewart W. Schneller, Dean Professor Chemistry and Biochemistry	Douglas C. Goodwin, Chair Associate Professor Chemistry and Biochemistry
_____	_____
Holly R. Ellis Assistant Professor Chemistry and Biochemistry	Evert C. Duin Assistant Professor Chemistry and Biochemistry
_____	_____
John Aull Professor Chemistry and Biochemistry	Stephen L. McFarland Dean Graduate School

ROLES OF TWO INTERHELICAL INSERTIONS IN CATALASE-PEROXIDASE CATALYSIS: TRACING THE IMPACT OF PERIPHERAL PROTEIN STRUCTURES ON HEME ENZYME FUNCTION

Yongjiang Li

A Dissertation

Submitted to

the Graduate Faculty of

Auburn University

in Partial Fulfillment of the

Requirements for the

Degree of

Doctor of Philosophy

Auburn, Alabama
December 16, 2005

ROLES OF TWO INTERHELICAL INSERTIONS IN CATALASE-PEROXIDASE CATALYSIS: TRACING THE IMPACT OF PERIPHERAL PROTEIN STRUCTURES ON HEME ENZYME FUNCTION

Yongjiang Li

_____
Signature of Author

_____
Date of Graduation

VITA

Yongjiang Li, son of Baozeng Li and Junguo Dong, was born in Mianxian, Shanxi Province, P.R. China, on November 20, 1976. He graduated from Hefei No.1 High School, Anhui Province in June of 1994. He then attended Fudan University in Shanghai, P. R. China and graduated with a Bachelor of Chemistry in July of 1998. Then he worked as an Assistant Researcher in National Key Lab of Bio-organic Chemistry, Shanghai Institute of Organic Chemistry, China Academy of Sciences, in Shanghai, P. R. China, from 1998 to 2000. In August 2000, he entered graduate school at Auburn University in the Department of Chemistry and Biochemistry for Ph.D degree.

DISSERTATION ABSTRACT

ROLES OF TWO INTERHELICAL INSERTIONS IN CATALASE-PEROXIDASE CATALYSIS: TRACING THE IMPACT OF PERIPHERAL PROTEIN STRUCTURES ON HEME ENZYME FUNCTION

Yongjiang Li

Doctor of Philosophy, December 16, 2005
(B.S., Fudan University, Shanghai, P.R. China, July, 1998)

206 Typed Pages

Directed by Dr. Douglas C. Goodwin

Monofunctional peroxidases and bifunctional catalase-peroxidases share almost superimposable active sites, yet peroxidases lack appreciable catalase activity. Moreover, catalase-peroxidases catalyze both catalase and peroxidase reactions with a *single* active site. Given that catalase-peroxidases have two extra interhelical insertions that connect the D and E helices (the DE insertion), and F and G helices (the FG insertion), it is rational to suggest that these two insertions may serve to fine-tune the active site for bifunctionality. To explore the roles of these two insertions, we produced

variants of *E. coli* catalase-peroxidase (KatG) lacking either the DE insertion ($KatG^{\Delta DE}$), the FG insertion ($KatG^{\Delta FG}$), or both insertions ($KatG^{\Delta DE/FG}$). All variants retained peroxidase activity that was comparable or greater than that of wtKatG. However, $KatG^{\Delta FG}$ retained only 0.2% catalase activity, whereas $KatG^{\Delta DE}$ and $KatG^{\Delta DE/FG}$ lost all catalase activity, indicating both insertions are critical for KatG bifunctional ability. $KatG^{\Delta FG}$ absorption and EPR spectra suggested little change in heme coordination state occurred when FG insertion was removed. Kinetic parameters suggested that the FG insertion poises the active site geometrically or electronically to help peroxide substrates access to the active site. In contrast, $KatG^{\Delta DE}$ appeared to have more hexa-coordinate heme species present, suggesting this insertion is important for maintaining the correct heme coordination environment. The kinetic parameters suggest that the DE insertion serves to regulate the access of reducing substrates to the heme edge. As a result, the rate limiting step of the $KatG^{\Delta DE}$ peroxidase catalytic cycle changed from compound I reduction as for wtKatG to compound II reduction. This led to an increased propensity to the formation of compound III for $KatG^{\Delta DE}$. This phenomenon is also commonly observed in monofunctional peroxidases. This inactivation could be prevented by the reducing substrate due to its competition with H_2O_2 in reacting with compound II. Furthermore, the inactive compound III could also be rescued back to the catalytic cycle by reducing substrate cation radicals. Both insertions, despite of their peripheral positions to the active site, serve to fine-tune the active site for its bifunctional properties and cooperate with other peripheral protein structures to achieve the full catalytic potential of the catalase-peroxidases.

ACKNOWLEDGEMENTS

The research conducted in this dissertation would not have been possible without the help and support of many people whom I wish to thank. First, I would like to thank my research advisor, Dr. Douglas C. Goodwin. Dr. Goodwin not only guided me through the whole graduate process, gave me help on both of my academic and personal life, but taught me how to be a good researcher. To me he is much more than an advisor. I hope that I will continue to make him proud. Second, I would like to thank my committee members, Drs. Holly Ellis, Evert Duin, John Aull, and Stewart Schneller for their constructive suggestions and all the professional assistance. To all of my co-workers at Auburn University, especially Ruletha Baker, Cornelius Varnado, Carma Cook, Robert Moore, Sonya Savage, Ron Marcy, and Kimberly Laband for all the intelligent discussions, selfless help, and pleasant lab environment. Special thanks to my family, my sweet girlfriend Shichu Huang, and all my friends, for their continuous understanding, support, and encouragement. Finally, I would like to thank the Department of Chemistry and Biochemistry, Auburn University, the American Chemical Society's Petroleum Research Fund for their funding support for my research, and COSAM alumni and friends for their generous donations to PRISM (Promoting Research in Sciences and Mathematics) for the CD spectropolarinmeter.

Style Manual Used: Biochemical and Biophysical Research Communications

Computer Software Used: Microsoft Word, Microsoft Excel, Prism, ChemDraw, SwissPdbViewer, MegaPov

TABLE OF CONTENTS

ABSTRACT……..……..……..... v

ACKNOWLEDGEMENTS……..…….. vii

TABLE OF CONTENTS…… ix

LIST OF TABLES AND FIGURES……... xi

INTRODUCTION…….. 1

CHAPTER ONE: LITERATURE REVIEW.…… 8

1.1 Heme and Heme Environments…….. 8

1.2 Heme Enzymes……... 13

1.3 Summary……..……... 48

CHAPTER TWO: MATERIALS AND METHODS…….…..…….. 50

2.1 Reagent……... 50

2.2 Cloning and Expression of wtKatG and the Variants…….…… 51

2.3 Enzyme Reconstitution…….…….. 65

2.4 Recombination of $KatG^{N\text{-}term/\Delta DE}$ and $KatG^{N\text{-}term/\Delta FG}$ with $KatG^{C\text{-}term}$…..... 66

2.5 Protein Characterization……...…….….. 67

CHAPTER THREE: RESULTS…… 73

3.1 wtKatG……..…….. 73

3.2 $KatG^{\Delta FG}$……..... 91

3.3 KatG$^{\Delta DE}$ 104

3.4 KatG$^{\Delta DE/FG}$ 126

3.5 KatG$^{N\text{-}term/\Delta DE}$ and KatG$^{N\text{-}term/\Delta FG}$ 134

CHAPTER FOUR: DISCUSSION 149

4.1 Impacts of the FG insertion 152

4.2 Impacts of the DE insertion 161

4.3 Collaboration of the Two Insertions and C-terminal Domain 169

4.4 Summary 172

REFERENCES 176

LIST OF TABLES AND FIGURES

Table 4.1.	Steady-state Kinetic Parameters for Catalase and Peroxidase Activities of wtKatG and theVariants……..	153
Figure 1.1.	Structure of the Most Common Hemes…….....	10
Figure 1.2.	Catalytic Cycle of P450s……..	16
Figure 1.3.	Functions of Myoglobin……..	20
Figure 1.4.	Schemes of Structural Changes between T-state and R-state of Hemoglobin……..	23
Figure 1.5.	Catalytic Cycle of Catalases……..	26
Figure 1.6.	Catalytic Cycle of Peroxidases…….	31
Figure 1.7.	Catalytic Cycle of Catalase-peroxidases.…….	35
Figure 1.8.	Structure of Isoniazid and Ethioamide…….	39
Figure 1.9.	Proposed Mechanism of INH……...	41

Figure 1.10. Scheme of Structural Comparison of Peroxidases and Catalase-peroxidases…….. 46

Figure 1.11. Models of the Trp-Tyr-Met Covalent Adduct of Catalase-peroxidases……..... 47

Figure 2.1. Structure of IPTG and Lactose……. 54

Figure 2.2. Structural Scheme of Ni-NTA Resin and Bound Six-His tag…….. 61

Figure 2.3. Structure of ABTS……... 69

Figure 2.4. Diagram of Single Mixing Mode of Stopped Flow Reaction Analyzer……..... 71

Figure 3.1. Change in Catalase Activity of wtKatG with Hemin Reconstitution……... 75

Figure 3.2. Change in Ratio of Absorbance at 408 nm and 370 nm of wtKatG with Hemin Reconstitution……... 76

Figure 3.3. Absorption Spectra Recorded for Ferric, Ferrous, and Ferri-cyano Forms of wtKatG…….. 78

Figure 3.4. Effect of pH on Catalase Activity of wtKatG……... 80

Figure 3.5. Effect of pH on Peroxidase Activity of wtKatG……... 81

Figure 3.6. Effect of H_2O_2 Concentration on the Catalase Activity of wtKatG…….. 83

Figure 3.7. Effect of H_2O_2 Concentration on the Peroxidase Activity of wtKatG…….. 84

Figure 3.8. Effect of ABTS Concentration on the Peroxidase Activity of wtKatG…….. 85

Figure 3.9. Far-UV CD Spectrum Recorded for Reconstituted wtKatG…… 86

Figure 3.10. Effect of Cyanide Concentration on the Rate of Formation of the Fe^{III}-CN Complex of wtKatG..……. 88

Figure 3.11. Change in Absorbance at 423.6 nm with Cyanide Added to wtKatG..... 90

Figure 3.12. Absorption Spectra Recorded for Ferric, Ferrous, and Ferri-cyano Forms of $KatG^{\Delta FG}$……. 93

Figure 3.13. EPR Spectrum Recorded for $KatG^{\Delta FG}$……... 95

Figure 3.14. Comparison of pH Optima for Catalase Activity of wtKatG and $KatG^{\Delta FG}$……. 96

Figure 3.15. Effect of H_2O_2 Concentration on Peroxidase Activity of $KatG^{\Delta FG}$……. 97

Figure 3.16. Effect of ABTS Concentration on Peroxidase Activity of $KatG^{\Delta FG}$……. 99

Figure 3.17. Effect of pH on Peroxidase Activity of $KatG^{\Delta FG}$…….. 100

Figure 3.18. Far-UV CD Spectra of apo-$KatG^{\Delta FG}$ and Reconstituted $KatG^{\Delta FG}$..... 102

Figure 3.19. Change in Absorbance at 423.5 nm with Cyanide Added to $KatG^{\Delta FG}$……. 103

Figure 3.20. Absorption Spectra Recorded for Ferric, Ferrous, and Ferri-cyano Forms of $KatG^{\Delta DE}$ 106

Figure 3.21. Far-UV CD Spectra of apo $KatG^{\Delta DE}$, $KatG^{\Delta DE}$ 0 Hour, and 22 hours After Reconstitution..... 107

Figure 3.22. EPR Spectrum of $KatG^{\Delta DE}$ 109

Figure 3.23. Comparison of Peroxidase Activity of wtKatG and $KatG^{\Delta DE}$ with Respect to H_2O_2 as the Substrate..... 111

Figure 3.24. Comparison of Peroxidase Activity of wtKatG and $KatG^{\Delta DE}$ with Respect to ABTS as the Substrate..... 112

Figure 3.25. Effect of ABTS Concentration on Lag Phase of Peroxidase Activity of $KatG^{\Delta DE}$ 113

Figure 3.26. Effect of ABTS Concentration on Lag Time of Peroxidase Activity of $KatG^{\Delta DE}$ 115

Figure 3.27. Effect of H_2O_2 Concentration on Lag Phase of Peroxidase Activity of $KatG^{\Delta DE}$ 116

Figure 3.28. Effect of H_2O_2 Concentration on Lag Time of Peroxidase Activity of $KatG^{\Delta DE}$ 117

Figure 3.29. Heme Absorption Spectra of $KatG^{\Delta DE}$ Before and After the Addition of 0.1 mM H_2O_2 119

Figure 3.30. Effect of ABTS radical Concentration on Lag Time of Peroxidase Activity of $KatG^{\Delta DE}$ 121

Figure 3.31. Effect of ABTS radical Concentration on Peroxidase Activity of $KatG^{\Delta DE}$ 122

Figure 3.32. Effect of Cyanide Concentration on Observed Rate of Cyanide Binding to KatG$^{\Delta DE}$…….. 123

Figure 3.33. Change in Absorbance at 420 nm with Cyanide Added to KatG$^{\Delta DE}$……..... 125

Figure 3.34. Absorption Spectra Recorded for Ferric, Ferrous, and Ferri-cyano Forms of KatG$^{\Delta DE/FG}$…… 128

Figure 3.35. Effect of H_2O_2 Concentration on Peroxidase Activity of KatG$^{\Delta DE/FG}$…… 129

Figure 3.36. Effect of ABTS Concentration on Peroxidase Activity of KatG$^{\Delta DE/FG}$…… 131

Figure 3.37. Change in Absorbance at 401 nm with Cyanide Added to KatG$^{\Delta DE/FG}$…… 132

Figure 3.38. Effect of Cyanide Concentration on Observed Constant of Cyanide Binding for KatG$^{\Delta DE/FG}$…….. 133

Figure 3.39. Spectra of KatG$^{N\text{-term}/\Delta FG}$ Immediately Following and 24 Hours After Recombination with Equimolar KatG$^{C\text{-term}}$ ……. 136

Figure 3.40. Spectra of KatG$^{N\text{-term}/\Delta DE}$ Immediately Following and 48 Hours After Recombination with Equimolar KatG$^{C\text{-term}}$ ……. 138

Figure 3.41. Effect of ABTS Concentration on Peroxidase Activity of Recombined KatG$^{N\text{-term}/\Delta FG}$……... 139

Figure 3.42. Effect of H_2O_2 Concentration on Peroxidase Activity of Recombined KatG$^{N\text{-term}/\Delta FG}$……... 140

Figure 3.43. Effect of ABTS Concentration on Peroxidase Activity of Recombined KatG$^{N\text{-term}/\Delta DE}$……... 141

Figure 3.44. Effect of H_2O_2 Concentration on Peroxidase Activity of Recombined $KatG^{N\text{-}term/\Delta DE}$..... 142

Figure 3.45. Effect of H_2O_2 Concentration on Lag Time of Peroxidase Activity of Recombined $KatG^{N\text{-}term/\Delta DE}$..... 144

Figure 3.46. Effect of ABTS Concentration on Lag Time of Peroxidase Activity of Recombined $KatG^{N\text{-}term/\Delta DE}$..... 145

Figure 3.47. EPR Spectrum Recorded for $KatG^{N\text{-}term/\Delta FG}$..... 146

Figure 3.48. EPR Spectrum Recorded for $KatG^{N\text{-}term/\Delta FG}$ 24 Hours after Recombination with $KatG^{C\text{-}term}$..... 148

Figure 4.1. Active Site Comparison of Cytochrome *c* Peroxidase and *E. coli* Catalase-peroxidase..... 150

Figure 4.2. Position of the Insertions and Key Amino Acids within KatG Active Site..... 158

Figure 4.3. Position of the FG Insertion and the H-bonding Network Outlined by His 106, Asn 136, and Leu 130..... 159

Figure 4.4. Proposed Catalytic Cycle of $KatG^{\Delta DE}$..... 168

INTRODUCTION

Many enzymes need cofactors to execute their biological functions. Heme is a highly versatile cofactor that is widely used by enzymes to catalyze a variety of chemical transformations. Indeed, heme enzymes play essential roles in redox reactions, oxygen storage and transport, electron transfer, ligand binding, signal transduction, gene expression control, and other processes. In general, the catalytic properties of the heme group in hemoproteins are dictated at four structural levels: the structure of heme itself, the identity of protein-derived heme ligands, the non-ligand heme environment, and the global structure of the protein. Among them, the outermost, global protein structure, is the least understood. Nevertheless, it is clearly an indispensable part of hemoprotein function. Lack of progress in understanding the impact of global protein structure is primarily due to the lack of a proper model for rational investigation of such phenomena.

Catalase-peroxidases are heme enzymes that have generated much interest for numerous reasons. First, *Mycobacterium tuberculosis* catalase-peroxidase has been shown to be essential for the activation of isoniazid (INH), a front-line anti-tubercular drug. Furthermore, several highly virulent pathogens, such as *E. coli* O157:H7, *L.*

pneumophila, and *Y. pestis*, carry unique periplasmic catalase-peroxidases that are absent from nonpathogenic strains. This suggests that catalase-peroxidases may be used by these pathogens as virulence factors. Finally, these enzymes are able to efficiently catalyze both catalase and peroxidase reactions. This unique bifunctional capability is accomplished with a *single* active site. For reasons outlined below, this feature of catalase-peroxidases makes them great models for evaluating hemoprotein structure and function, particularly at the global protein structural level.

Both catalase and peroxidase catalytic cycles begin with the oxidation of the ferric form of the enzyme by a hydroperoxide molecule to form a ferryl-oxo porphyrin/protein radical intermediate, known as compound I. Compound I is two oxidizing equivalents above the ferric form of the enzyme. The mechanism of compound I reduction is the key point of divergence between catalase activity and peroxidase activity. In the catalase cycle, compound I is reduced back to ferric enzyme by a second equivalent of H_2O_2 along with the production of O_2. In contrast, the peroxidase cycle is completed by two consecutive one-electron reduction reactions of compound I by an exogenous reducing substrate. This occurs via the formation of a ferryl-oxo intermediate known as compound II. In the process, two equivalents of substrate radical are generated. For catalase-peroxidases, the rate limiting step of peroxidase catalytic cycle is typically the reduction of compound I. Catalase- peroxidases are susceptible to peroxide-dependent inactivation. In the presence of high concentrations H_2O_2 (0.4 M and above), compound II can react with H_2O_2 and lead to the formation of inactive compound III, a ferrous-dioxy/ferric-superoxide intermediate. Additional reactions with H_2O_2 result in irreversible

inactivation of the enzyme. This phenomenon is much more frequently observed in monofunctional peroxidases, even with H_2O_2 as low as 0.1 mM. This is due mainly to the accumulation of compound II during catalysis. Compound II reduction is the rate-determining step for monofunctional peroxidases.

In spite of their efficient catalase activity, catalase–peroxidases bear no sequential or structural resemblance to monofunctional catalases. Instead, they are closely related to monofunctional peroxidases. Indeed, the inner three structural levels of these two important groups of enzymes are nearly indistinguishable. Nevertheless, the monofunctional peroxidases lack appreciable catalase activity. Given the high similarity of the monofunctional peroxidase and catalase–peroxidase active sites, it is reasonable to suggest that the global protein structure of catalase–peroxidases has an important role in fine-tuning the active site for its bifunctional abilities. Thereby, we realized that catalase-peroxidases further provided ideal models for the study of global protein structure and its influence on heme enzyme function.

Comparison of the global structures of these two groups of enzymes reveals that the bifunctional catalase-peroxidases contain three prominent structural features that are absent from monofunctional peroxidases. They are two interhelical insertions (~ 35 amino acids each) and a C-terminal domain (~ 300 amino acids). Importantly, *all three* are peripheral to the active site. The two interhelical insertions appear within loops that connect the D and E helices, and the F and G helices of the catalase–peroxidase N-terminal domain. Thus, we refer to these structures as the DE insertion

and the FG insertion, respectively.

Due to their absence from monofunctional peroxidases, we propose that these two insertions are critical for the catalase activity of these bifunctional enzymes. We also propose that other properties unique to either the catalase-peroxidases or monofunctional peroxidases (e.g., insensitivity of catalase-peroxidases to peroxide-dependent inactivation, a property that monofunctional peroxidases lack) may also be explained by the presence of these interhelical insertions.

To test this hypothesis, we employed a novel deletion mutagenesis procedure to generate clones of recombinant *Escherichia coli* catalase–peroxidase (KatG) lacking its DE insertion ($KatG^{\Delta DE}$), FG insertion ($KatG^{\Delta FG}$), and both insertions ($KatG^{\Delta DE/FG}$). We also generated variants in which only the N-terminal domain of KatG lacking the DE insertion ($KatG^{N\text{-}term/\Delta DE}$) or the FG insertion ($KatG^{N\text{-}term/\Delta FG}$) were expressed. These variants were expressed and isolated for characterization.

Absorption and EPR (electron paramagnetic resonance) spectra were taken to inspect the heme coordination state inside the proteins. Steady-state kinetic analyses were performed to observe the extent of change in catalytic properties of the proteins. Cyanide binding experiments were performed to test the active site accessibility before and after these peripheral structures were removed. Circular dichroism (CD) spectra were taken to determine whether or not there were fundamental changes in protein global folding when the insertion(s) was (were) removed from the structure.

Visible absorption spectra and EPR spectra both indicated that the heme coordination state of KatG$^{\Delta FG}$ was highly similar to wtKatG. KatG$^{\Delta FG}$ retained peroxidase activity that was comparable to the wild-type enzyme, indicating that the non-ligand heme environment was also similar to wtKatG. However, the variant retained only 0.2 % catalase activity, confirming that the FG insertion fine-tunes the active site for its bifunctionality. The structural position of the FG insertion along with the kinetic parameters and pH dependence of KatG$^{\Delta FG}$ activity suggest that the FG insertion may support hydrogen-bonded networks that are integral to catalase activity. Furthermore, the rate limiting step of peroxidase catalytic cycle of KatG$^{\Delta FG}$ changed from compound I reduction (observed for wtKatG) to compound I formation, suggesting that the FG insertion helps align the active site geometrically or electronically for the reaction with hydroperoxides.

The critical role of the DE insertion in enzyme bifunctionality was confirmed by the total loss of catalase activity of KatG$^{\Delta DE}$. Furthermore, KatG$^{\Delta DE}$ appeared to have more hexa-coordinate heme species present than wtKatG and KatG$^{\Delta FG}$. Interestingly, KatG$^{\Delta DE}$ showed a peroxidase activity about *seven fold greater* than that of wtKatG, together with the accumulation of compound II, indicating the rate limiting step is changed to compound II reduction. This was confirmed by the kinetic parameters for peroxidase activity, suggesting that DE insertion functions to regulate the access of reducing substrates to the heme edge. As observed in monofunctional peroxidases, the accumulation of compound II led to the formation of inactive compound III in the presence of excess H_2O_2, followed by peroxide-dependent

inactivation. This inactivation could be prevented by the reducing substrate due to its competition with H_2O_2 in reacting with compound II. Furthermore, we observed that the inactive compound III could also be rescued back to the catalytic cycle by means of peroxidase-generated cation radicals. These are all properties observed in the monofunctional peroxidases.

Like KatG$^{\Delta DE}$, KatG$^{\Delta DE/FG}$ also lost all catalase activity and showed more hexa-coordinate heme species present than wtKatG and KatG$^{\Delta FG}$. However, though still greater than that of wtKatG, the peroxidase activity was less than half of that of KatG$^{\Delta DE}$, and no peroxide-dependent inactivation was observed. KatG$^{\Delta DE/FG}$ also showed an apparent second-order rate constant with respect to H_2O_2 much lower than that of KatG$^{\Delta DE}$, and a higher apparent second-order rate constant with respect to ABTS. These results confirm that the FG insertion helps poise the active site for reaction with peroxide, and regulates the access of reducing substrates to the heme edge. Compared to KatG$^{\Delta FG}$, KatG$^{\Delta DE/FG}$ showed much higher peroxidase activity, and a higher apparent second-order rate constant with respect to ABTS, confirming that the DE insertion serves to regulate the access of reducing substrate to the heme edge.

The C-terminal domain of KatG, which is also peripheral to the active site, cooperates with the interhelical insertions for the enzyme function. The C-terminal domain serves to maintain the active site architecture by holding the so-called distal histidine in position, preventing it from becoming a sixth ligand to the heme. The C-terminal domain executes this role of supporting the distal histidine by sustaining the

B-helix of the N-terminal domain via several ionic interactions between the surfaces of both N- and C-terminal domains. Our lab expressed and purified the C-terminal domain of KatG ($KatG^{C\text{-}term}$), as well as the N-terminal domain of KatG lacking each of the insertions, ($KatG^{N\text{-}term/\Delta DE}$ and $KatG^{N\text{-}term/\Delta FG}$). None of them exhibited any activity. However, recombination of $KatG^{C\text{-}term}$ with $KatG^{N\text{-}term/\Delta DE}$ and $KatG^{N\text{-}term/\Delta FG}$ led to recovery of activity and active site characteristics observed for $KatG^{\Delta DE}$ and $KatG^{\Delta FG}$, respectively. These data suggest that all three peripheral structures (each for unique reasons) are required for the full function of catalase-peroxidases.

Both insertions, despite of their peripheral positions to the active site, have a profound impact on KatG function. Alone and cooperatively, they serve to fine-tune the active site for enzyme bifunctionality. These studies demonstrate that the catalase-peroxidases are exceptional models to probe heme enzyme function at the global structural level. The ability to manipulate enzyme function at this level will be a critical aspect of engineering enzymes to carry out new functions. Similarly, understanding catalase-peroxidase structure and function at this level will be essential to understanding and thwarting antibiotic resistance of *M. tuberculosis* and the use of these enzymes as virulence factors by other pathogenic bacteria.

CHAPTER ONE

LITERATURE REVIEW

1.1 Heme and Heme Environments

Nature has made extensive use of metal ions as cofactors to assist in catalysis. These cofactors include metal ions such as Fe^{3+}, Cu^{2+}, or Mn^{2+}, as well as metallo-organic molecules such as heme (Fe), cobalamin (Co), and chlorophyll (Mg). Indeed, approximately 40 percent of all enzymes have metal ions in their active sites.

Hemes are prosthetic groups widely used in nature to perform diverse biological functions. In 1853, Ludwig Carl Teichmann-Stawiarski reported the oxygen transport properties of hemoglobin and the crystallization of hemin from blood i.e., Teichmann's crystals [1]. In 1886, electron transfer proteins containing myohematin and histohematin were reported by McMunn [2]. In 1925, Keilin named these electron transfer proteins "cytochromes" (literally "cellular pigments"), and classified them based on maximum absorption of what is now known as the α-band in their reduced state: cytochromes *a* (605 nm), *b* (~ 565 nm), and *c* (550 nm) [3]. Heme

enzymes have drawn intense attention over the last 50 years because of their versatility. Heme enzymes mainly perform three functions: catalysis of peroxide/oxygen dependent redox reactions (e.g., cytochromes P450, catalases, peroxidases, and catalase-peroxidases), oxygen storage and transport (e.g., hemoglobin, and myoglobin), and electron transfer (e.g., cytochromes P450) [4, 5]. Other than these, hemoproteins also participate in ligand binding, signal transduction, and gene expression control [5].

One basic question can be raised is this: how does heme, a simple metalloorganic compound, get used for so many different functions? The answer lies in the variety of heme environments created by different heme-protein interactions. The application of heme to a particular function must be dictated by structure at four levels: the structure of heme itself, the identity of protein-derived heme ligands, the non-ligand heme environment, and the global structure of the protein.

1.1.1 Hemes

In the structure of heme, a tetrapyrrole macrocycle ring is complexed with iron (Figure 1.1). Four equatorial ligands are the porphyrin nitrogens. The remaining two axial ligands lie above and below the plane of the heme. The most commonly observed heme is heme *b* (iron protoporphyrin IX), which is found in *b*-type cytochromes, hemoglobins, myoglobins, cytochromes P450, and hemesensor proteins.

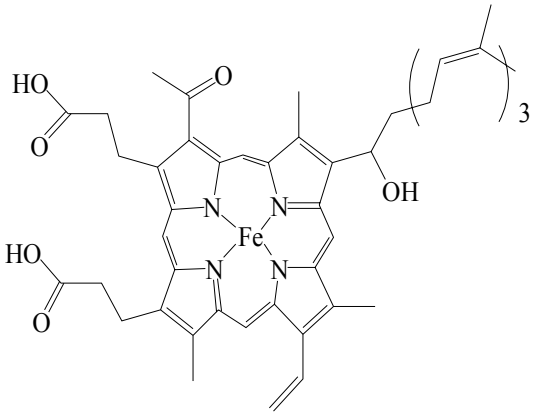

Heme *a*

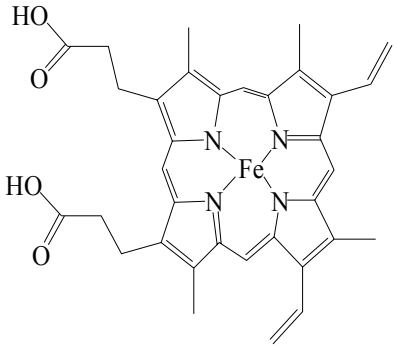

Heme *b*

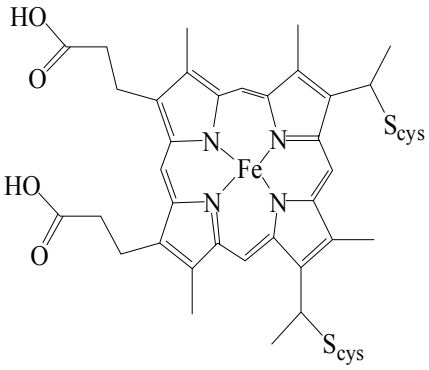

Heme *c*

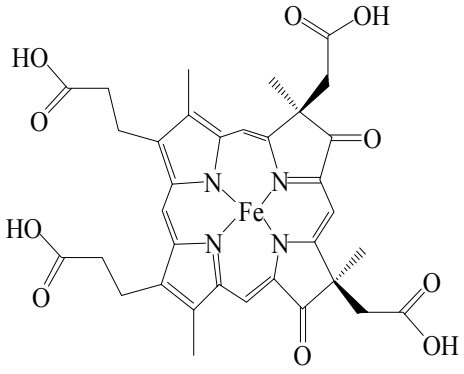

Heme *d*

Figure 1.1. Structure of the Most Common Hemes.

Indeed, the term "heme" specifically refers to heme *b*, and ferric-hydroxy and ferric-chloride complexes are referred to as hematin and hemin, respectively. Heme *a* is derived from heme *b* by substitution of position 2 vinyl group by a hydroxyethylfarnesyl side chain, followed by oxidation of the methyl group at position 8 to a formyl group, as found in mammalian cytochrome *c* oxidase [6]. These changes make heme *a* both more hydrophobic and electron-withdrawing, with a higher reduction potential. This higher reduction potential explains why enzymes at the end of electron transport chains have heme *a*. Compared to heme *b*, heme *c* replaces both of the vinyl groups by thioether bonds formed with cysteine residues of surrounding protein, as observed in cytochrome *c* [7]. The surrounding protein normally has a heme binding motif, CXXCH, with two cysteine sulfurs to covalently bond with heme [8, 9], and a proximal histidine to bind heme iron [10]. Because of the existence of the thioether bonds, proteins with heme *c* are more stable, both chemically and thermally [11]. However, these extra thioether bonds do not affect the heme reduction potential much, probably because the vinyl groups in heme *b* are not dominant in setting the reduction potential [11]. In rare cases, the absence of one thioether bond, which is formed with the first cysteine in the heme binding motif, is observed [12-14]. Heme *d* is less commonly used compared to other hemes. Examples of enzymes using heme *d* are *Penicillium vitale* catalase and *E. coli* catalase [15, 16]. The reduction potential of heme *d* is close to that of heme *b* [16], and the particular reasons for enzymes to adopt heme *d* is under investigation. Some have suggested the change from heme *b* to heme *d* stabilized the heme moiety by

introducing additional hydrogen bonds [17]. Others thought it was a "silent mutation" that did not affect the heme function [16].

1.1.2 Protein-derived heme iron ligands

Heme iron is coordinated with a tetrapyrrole macrocyclic ring. The four equatorial coordination sites are occupied by porphyrin nitrogens. Furthermore, heme iron has two axial coordination sites that are above and below the plane of the tetrapyrrole macrocycle ring. These are available for ligands from proteins to bind. The diversity of protein-derived ligands plays an important role in the versatility of heme enzymes. Histidine is a widely used coordination ligand. Among heme enzymes, penta-coordinate with mono-histidine coordination is the most common motif, as in hemoglobin and myoglobin, with an open site for substrate binding. Very few amino acids other than histidine are observed in penta-coordinate heme enzymes. Exceptions include cysteine thiolate ligation in cytochromes P450 [18] and nitric oxide synthase [19], and tyrosine phenozide in heme catalase [15]. The second most common motif is hexa-coordinate with bis-histidine coordination, followed by hexa-coordinate with histidine and methionine, as in cytochromes *c* [20]. All other combinations of coordination ligands are relatively rare, such as the histidine and lysine combination observed in cytochrome *f*.

1.1.3 Non-ligand heme environment around heme iron

In addition to properties of hemes themselves and the protein-derived ligands attached to them, the immediate protein environment of the heme (i.e., the protein residues around the active site that are not directly bound to the heme), also influences the properties of these enzymes. These residues play important roles in determining the polarity of the proximal and distal heme environment, and the degree of the accessibility of the heme iron center and heme edge [21]. Indeed, metalloproteins that have exactly the same metal centers can have different functions. For instance, though cytochromes P450 and chloroperoxidase have identical thiolate-ligated heme iron at the active sites, cytochromes P450 are mono-oxygenases, but chloroperoxidase halogenates substrates.

1.2 Heme Enzymes

So far, it has been shown that functions of hemoproteins rely on the nature of heme, the proximal and axial ligand(s), and the non-ligand heme environment. In this section heme enzymes cytochromes P450, hemoglobin and myoglobin, catalases, peroxidases, and catalase-peroxidases are taken as examples to better understand how heme environment influences the function of heme enzymes.

1.2.1 Cytochromes P450

The cytochrome P450 superfamily is a group of hemoproteins that contains about 1000 members from a variety of species including bacteria, yeast, plants, insects and mammals. In eukaryotic cells, P450s are present as membrane-bound enzymes, containing about 500 amino acids. In most mammals, including humans, P450s are crucial for many processes, including: (a) the biosynthesis of steroid hormones, (b) protection of hosts through detoxifying xenobiotics, (c) the oxidation of unsaturated fatty acids to intracellular messengers, and (d) the stereo-specific metabolism of fat-soluble vitamins. The P450s were so-named because when CO is present, a unique absorption band with a maximum at ~ 450 nm is observed, corresponding to the formation of the Fe^{II}-CO complex [22]. With the exception of chloroperoxidase and NO synthase, this spectral feature is not observed in other hemoproteins.

The P450s are monooxygenases (also called "mixed-function oxidases") [23, 24] which primarily catalyze insertion of oxygen into carbon-hydrogen bonds at physiological temperature. The overall reaction is:

$$RH + NAD(P)H + H^+ + O_2 \xrightarrow{\text{P450}} ROH + NAD(P)^+ + H_2O$$

The P450 reactions require a cofactor (NADH or NADPH) as the source of electrons and a protein electron transport system. In the presence of O_2, two electrons are transferred from NAD(P)H to the hemoprotein via cytochrome P450 reductase. One oxygen atom from molecular oxygen is incorporated into the substrate. During the process, one or more highly oxidizing intermediates at the heme iron and near the bound substrate are generated.

Typically, P450s undergo an eight-step cyclic series of reactions (Figure 1.2) [25]: (a) the hexa-coordinate ferric form of the hemoprotein, with water as the sixth ligand, initially binds a substrate and results in the dehydration of the heme to form a penta-coordinate ferric intermediate, (b) this intermediate is reduced to the ferrous state by one electron from NADPH, (c) this penta-coordinate ferrous 450-substrate complex reacts with oxygen to form an unstable ternary hexa-coordinate complex of ferrous P450-oxygen-substrate, (d) this ternary intermediate is reduced by a second electron from NADPH, with the formation of a hexa-coordinate ferric peroxo-iron intermediate, which is the rate-limiting step of the catalytic cycle [26], (e) one proton is then incorporated, forming a ferric hexa- coordinate hydroperoxo-iron intermediate, (f) the O-O bond is then heterolytically cleaved, yielding water and a hexa-coordinate oxy-ferryl cation radical species, which is analogous to peroxidase compound I, (g) the bound substrate reacts with the radical intermediate and generates a ferric hexa-coordinate P450-product intermediate, and (h) the product dissociates from the complex, regenerating the uncomplexed ferric P450 which can participate in the next catalytic cycle. In the year 2000, X-ray structures of intermediates after steps b, c,

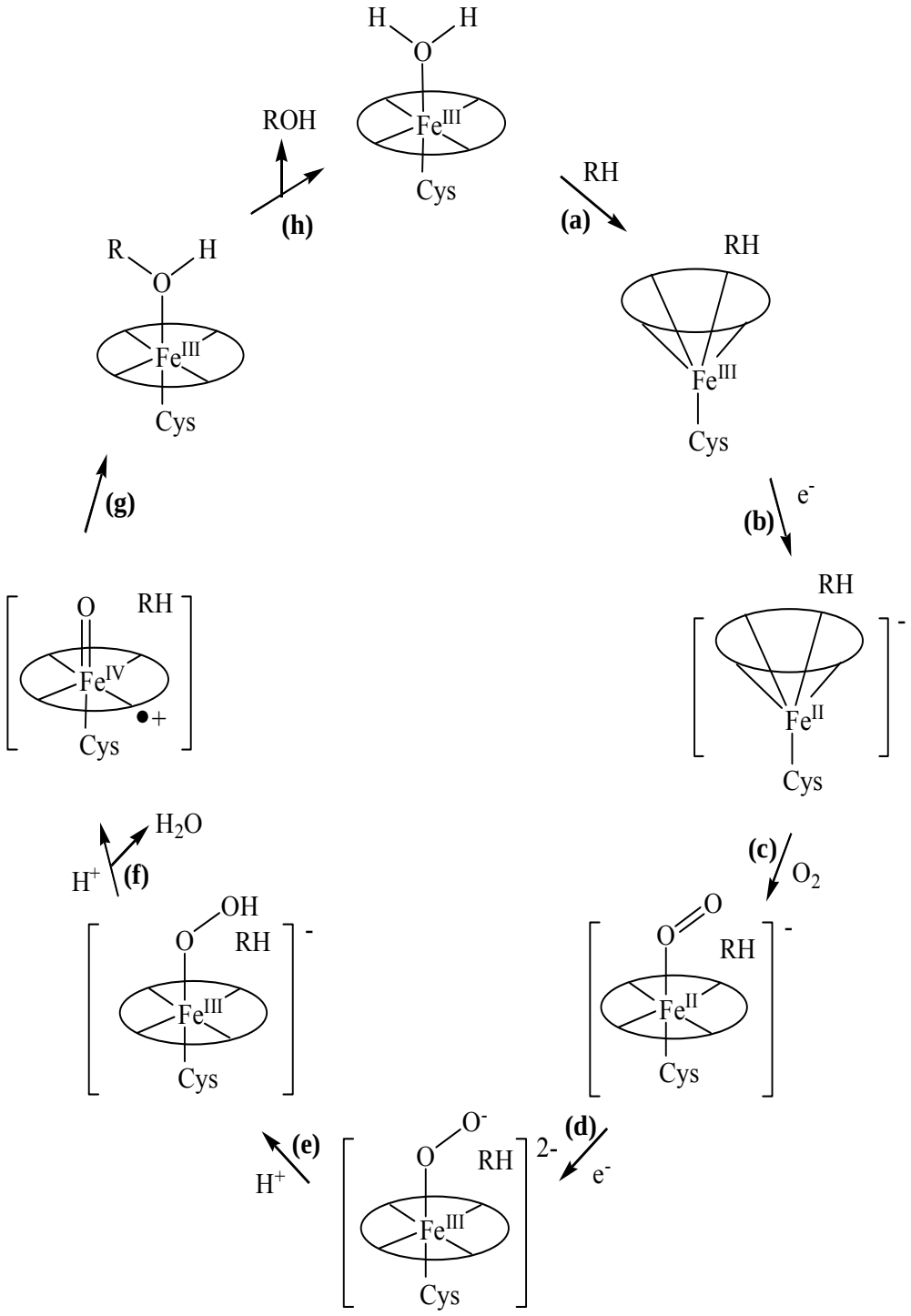

Figure 1.2. Catalytic Cycle of P450s.

and d were determined and it was suggested that the protons needed for the reactions were from a network of bound water molecules [27]. Moreover, P450s can catalyze oxidative reactions with substrates ranging from simple alkanes to complex molecules such as steroids and fatty acids. These enzymes can also catalyze non-oxidative dehydrase, reductase, and isomerase reactions [28].

Like many other hemoproteins, P450s have heme *b* at their active sites; however, P450s catalyze completely different reactions. The reasons for the unique features of P450s lie in the differences at the levels of both protein-derived heme ligands and the non-ligand heme environment. Instead of the nitrogen from the imidazole group of a histidine, typical of many hemoproteins, P450s use a thiolate group from a cysteine as the proximal ligand to bind the heme iron. This thiolate serves as an electron donor [29] and increases the electron density of the resonant porphyrin ring of the heme and further provides an electronic center for the activation and cleavage of the oxygen [29, 30]. The increased electron density also helps to stabilize higher oxidation states of the heme required for catalysis.

However, the thiolate ligand alone is not enough to explain the unique features of P450s, because chloroperoxidase, an enzyme that catalyzes chlorination reaction,

$$X^- + H^+ + H_2O_2 \xrightarrow{\text{chloroperoxidase}} HOX + H_2O$$

$$HOX + AH \longrightarrow AX + H_2O$$

(AH = substrate, X = Cl, Br, I, but not F)

also uses a thiol group from a cysteine as the proximal ligand. This thiolate ligand allows chloroperoxidase to generate high-valent iron-oxo intermediates also. However, the high-valent iron-oxo is directed at fundamentally different reactions. What makes cytochrome P450 different from chloroperoxidase lies after the high-valent iron-oxo intermediate is generated. Chlorination reactions take place at the edge of the heme prosthetic group, while oxo transfer reactions take place at the heme iron center. In cytochrome P450, the edge of the heme is buried, whereas the heme iron center is accessible to the substrate, therefore oxo transfer becomes the dominant reaction. However, compared to cytochrome P450, the heme edge of chloroperoxidase is more accessible to the substrates, which allows chlorination to take place [31].

1.2.2 Myoglobin (Mb) and Hemoglobin (Hb)

Fifteen times more energy can be obtained from metabolizing glucose aerobically rather than anaerobically. However, the solubility of oxygen in water is relatively low, and the diffusion efficiency of oxygen through membranes is poor. Furthermore, no natural amino acid is able to bind oxygen directly. To overcome these limitations, nature has adopted a means of using hemoproteins, mainly myoglobin (Mb) and hemoglobin (Hb), for oxygen storage and transportation. To bind oxygen, these hemoproteins have ferrous heme, instead of ferric heme, at their active sites. One role of the outside protein structures is to prevent this ferrous heme

from being oxidized by the bound oxygen, and this role is achieved by sterically preventing the formation of a heme-O_2-heme "sandwich" complex, which is required for ferrous heme oxidation.

Myoglobin is a cytoplasmic protein, mainly found in vertebrate cardiac, striated and smooth muscle cells. It is a relatively small monomeric protein with a molecular weight around 17 kD. Being able to release oxygen during periods of hypoxia or anoxia, myoglobin serves as an oxygen reservoir, as well as facilitates delivery of oxygen to the mitochondria [32]. Myoglobin also serves to regulate the storage and delivery of NO, which is an important intercellular and intracellular messenger. In addition, myoglobin plays a role as a scavenger of reactive oxygen species to reduce their toxic effects, and has peroxidase activity, though at a much slower rate compared to peroxidases [33], probably due to the ferrous state of heme, and the lack of some specific charged residues in the active site [34] (Figure 1.3).

Myoglobin is the first protein for which the crystal structure was determined. Its structure was first delineated in 1958 [35]. In myoglobin there is one heme prosthetic group per molecule, and one oxygen molecule can be bound reversibly. The outside of the fully folded protein is composed mainly of hydrophilic residues [36], which is considered to help myoglobin molecules slide past each other, and as a result, favor myoglobin-facilitated oxygen diffusion in the sarcoplasm [37, 38]. The overall structure of myoglobin consists of eight α-helices, namely helix A-H, alphabetically. The heme prosthetic group at the active site is a ferrous heme *b*. The heme pocket is surrounded by these helices, and is relatively hydrophobic compared

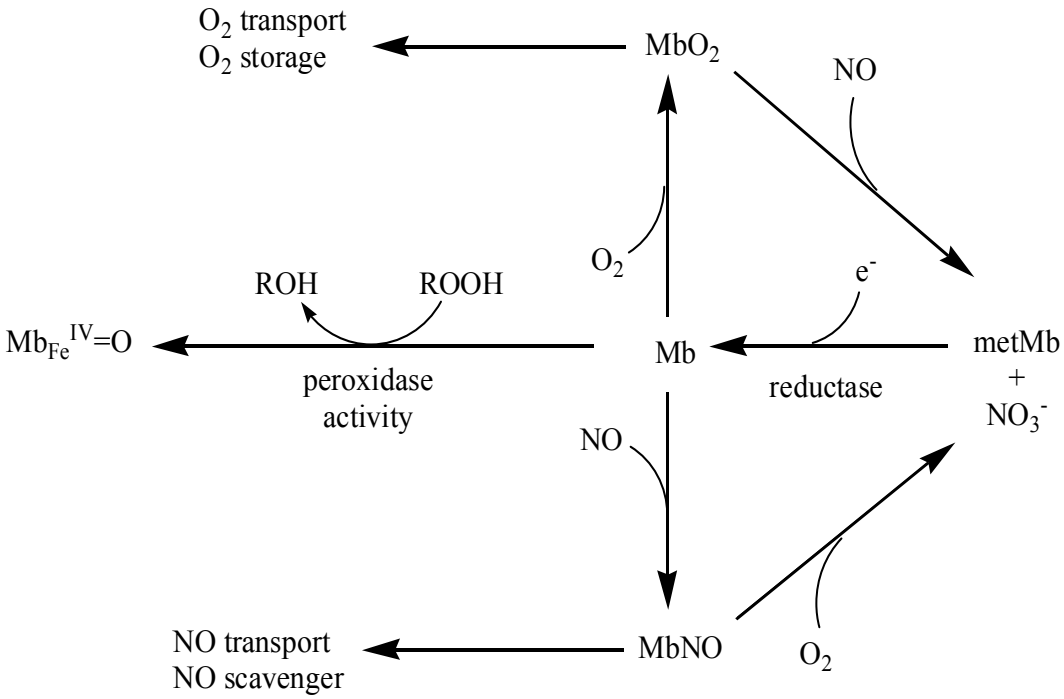

Figure 1.3. Functions of Myoglobin.

to peroxidases. A histidine residue on the heme proximal side serves as the fifth coordination ligand to the heme group. The sixth coordination site is for the binding of a target molecule (e.g., oxygen, nitric oxide [NO], carbon monoxide [CO], etc.) [39].

Myoglobin shows a hyperbolic curve for oxygen binding, which means Mb will bind oxygen when the oxygen partial pressure is high, and will release oxygen when tissues are oxygen-deficient. This property makes myoglobin a good candidate for oxygen storage.

Contrary to myoglobin, which is mainly found in muscle cells, hemoglobin is the oxygen carrier in blood. It carries oxygen from lungs to tissues and bringscarbon dioxide from tissues back to lungs to expel. Hemoglobin is a tetramer with two α chains and two β chains. Each chain has a heme prosthetic group in it, and is folded in much the same way as a myoglobin molecule, with only minor differences, such as truncated H helices in both α and β chains, and additional truncated D helices in α chains. Like myoglobin, the heme inside hemoglobin is also ferrous heme *b*. The major difference between hemoglobin and myoglobin occurs at the intersubunit contacts of hemoglobin. In these areas the side chains of hemoglobin have to be hydrophobic while as in the corresponding areas in myoglobin the side chains are hydrophilic because they are exposed to the hydrophilic surroundings. Moreover, in hemoglobin there are also several H-bonds and salt bridges (ionic interactions) between the subunits. The quaternary structure of hemoglobin is stabilized by these interactions.

One structural feature of hemoglobin is that upon the addition of oxygen to one subunit, the subunit conformation undergoes a slight change. When there is no oxygen present, the heme iron is slightly out of the plane of the heme ring, and the heme ring is a little distorted. This state is called "t (tense) state". When oxygen binds, the heme iron will be pulled back to the heme ring plane, and this state is called "r (relaxed) state". Another structural feature of hemoglobin is that upon the addition of oxygen to one subunit, the quaternary structure changes. Compared to deoxyhemoglobin, the oxygenation rotates one αβ subunit ~ 15° with respect to the other αβ subunit, and the quaternary structural states of deoxyhemoglobin and oxyhemoglobin are termed as T (tense) state, and R (relaxed) state, respectively (Figure 1.4) [40]. An interesting property here is that the R state has a higher oxygen affinity than the T state, which means when there is oxygen bound, hemoglobin tends to change its conformation to bind oxygen more easily, and vice versa [41]. The detailed mechanism for the conformational change between T and R states is still under investigation. However, it is clear that the changes in heme coordination state have a great influence on heme environment, and even protein quaternary structure.

This conformational change gives rise to the positive cooperativity of oxygen binding to hemoglobin. Unlike myoglobin, which shows a hyperbolic curve on oxygen binding, hemoglobin shows a sigmoidal curve, which means when oxygen is bound, succeeding oxygen molecules will be bound more easily. This property makes hemoglobin ideal for oxygen transport. When there is adequate amount of oxygen

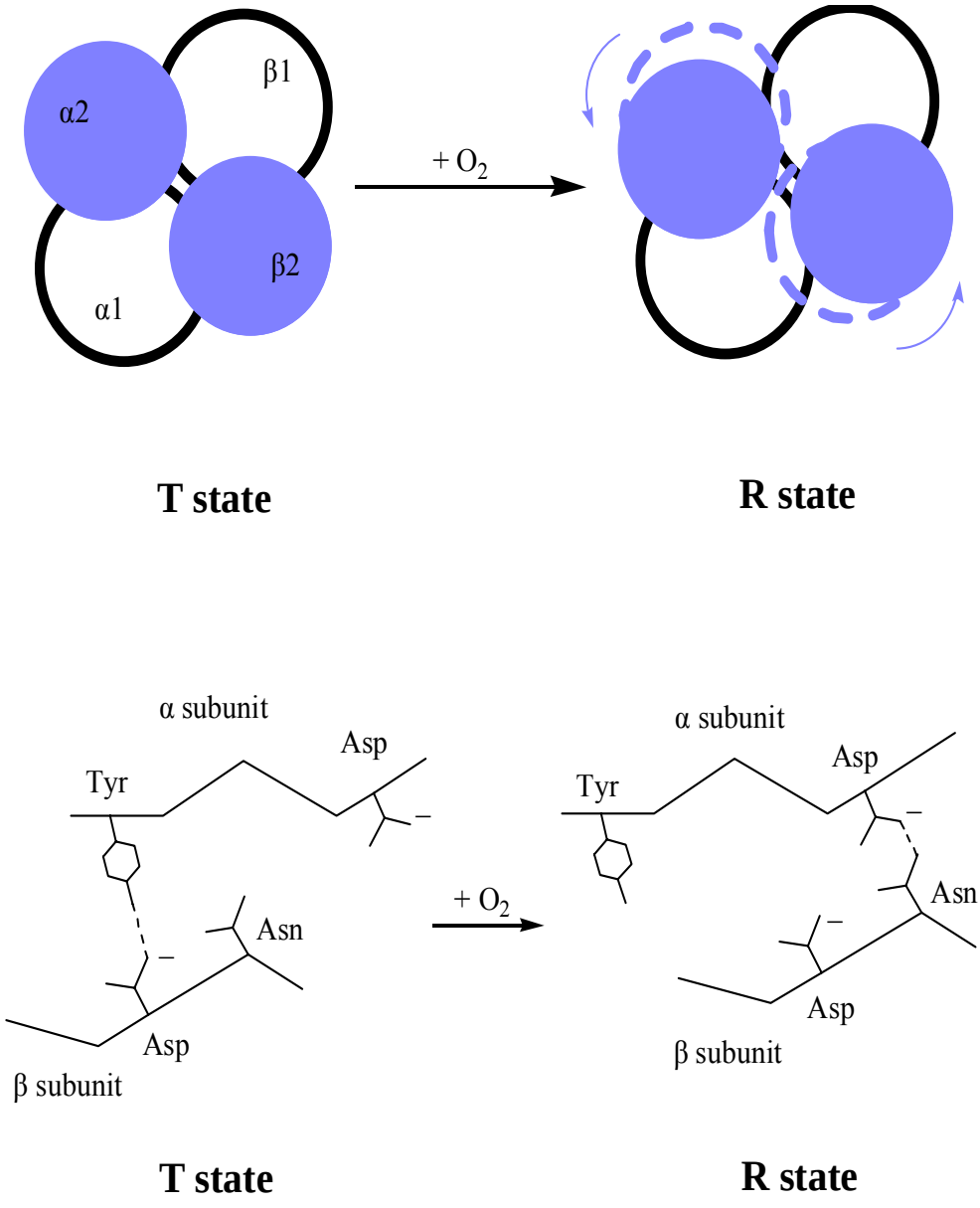

Figure 1.4. Schemes of Structural Changes between T-state and R-state of Hemoglobin.

present, hemoglobin will bind oxygen efficiently. In places where oxygen is deficient, hemoglobin will also efficiently release the bound oxygen.

Many other hemoproteins, like peroxidases, also use histidine as the fifth coordination ligand to the heme. What makes myoglobin and hemoglobin different from those hemoproteins lies at both distal and proximal sides. The distal histidine is positioned much closer to the heme compared to peroxidases, serving to stabilize the coordination of the target molecule. Moreover, peroxidases possess a distal side arginine and a proximal side aspartate, which are both important for peroxidase activity, though by different mechanisms. The positively charged side chain of the distal side arginine favors the heterolytic cleavage of O-O bond. The proximal aspartate serves to increase the donor strength of the proximal histidine by contributing some anionic character to it [34]. This negatively charged aspartate may also serves to stabilize the ferric state of the heme. In myoglobin and hemoglobin these charged residues have been replaced by uncharged residues.

1.2.3 Catalases

The first catalase was found and identified in 1863 by Schonbein [42]. Sixty years later, Warburg verified that the active site of catalase contains iron [43]. Catalases are found in almost all aerobically respiring organisms, including prokaryotes and eukaryotes. Many organisms have multiple isoforms of catalase.

Non-heme catalases have also been identified. These catalases contain either Mn or Fe within their active sites. Because they do not use heme for activity and because they have no structural resemblance to typical heme-dependent catalases, they are classified as "pseudocatalases" and will not be covered in this section.

The main role of catalases is to detoxify endogenous H_2O_2 generated as a by-product of aerobic metabolism. H_2O_2 is a powerful oxidizing agent and is potentially damaging to cells. By preventing excessive H_2O_2 accumulation, catalases prevent damage to critical cellular components and damage to tissues by the formation of an $OH^{\bullet}$ radical and other highly reactive species.

The reaction by which catalases disproportionate H_2O_2 is:

$$2\ H_2O_2 \xrightarrow{\text{catalase}} 2\ H_2O + O_2$$

This is a two-step reaction (Figure 1.5). In the first step the resting ferric enzyme is oxidized by H_2O_2 in a heterolytic O-O cleavage mechanism to generate one equivalent of H_2O and the intermediate is known as compound I. Compound I has been shown to be an oxyferryl porphyrin cation radical intermediate, and the oxygen bound to the iron is derived from H_2O_2 [44]. Compound I is then reduced by another equivalent of H_2O_2, generating the ferric form of the enzyme, H_2O and O_2.

Most catalases are homotetramers. There is one heme prosthetic group in each subunit. In most cases the heme is ferric heme *b*, but in some fungal and bacterial catalases, heme *d* has been observed. The structure of catalases is well conserved.

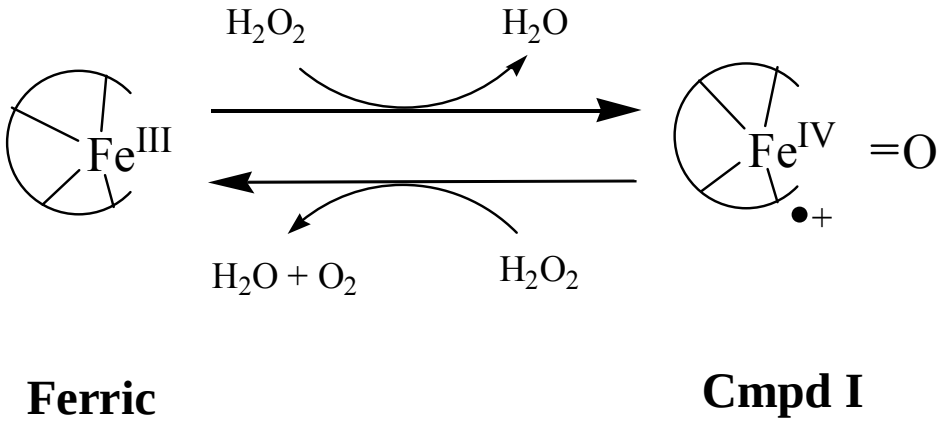

Figure 1.5. Catalytic Cycle of Catalases.

The subunit shows a characteristic globular form with an N-terminal arm. In each subunit four domains can be identified: the N-terminal arm domain, the β-barrel domain, the wrapping domain, and the α-helical domain. Among these domains the β-barrel domain is the most conserved in species from prokaryotes to eukaryotes [45-50].

The N-terminal domain forms a hairpin structure and participates in a remarkable intersubunit knot-like structure [51]. It is buried between adjacent subunits and may serve to stabilize the homotetramer [52]. The highly conserved distal histidine is situated at the C-terminus of this N-terminal domain. Its position is restricted by the hydrogen bonding system formed by the conserved side chain architecture of residues from the β-barrel domain. However, unlike all other hemoproteins in which the imidazole ring of the distal histidine is perpendicular to the heme plane, the imidazole ring of this essential histidine in catalases is parallel to the heme plane. This parallel orientation is energetically favored, because it favors intensive π–π interactions between this histidine imidazole ring and the porphyrin ring, thus presumably lowering the reactivity of compound I with reducing substrates [53].

The most highly conserved β-barrel domain has an eight-stranded antiparallel β-barrel with six α-helical insertions in the turns between the strands [51, 54]. This domain forms a hydrophobic substrate channel with a narrow bottom which allows the small peroxides to rapidly diffuse to the active site [55]. Together with a water molecule, an essential serine in this domain forms a hydrogen bonding system that serves to orient the essential distal histidine [53]. Another highly conserved

asparagine in this β-barrel domain has been proved to be important for peroxide binding and heterolytic cleavage. This is most likely accomplished by promoting H^+ transfer to essential distal histidine imidazole, thus stabilizing a transition state for heterolytic cleavage of the O–O bond [53, 56].

The wrapping domain, also known as "the domain connection", is found between the β-barrel domain and the α-helical domain. This domain wraps around half of the β-barrel domain. Except for a highly conserved 18-residue α-helix, it lacks apparent secondary structure. However, the fifth coordination ligand of the heme iron is located in this domain. Though catalase-peroxidases also have comparable catalase activity, catalases and catalase-peroxidases use different heme-bound ligands. Catalase-peroxidases use a histidine as the coordination ligand, while catalases use a tyrosine. The phenolate ligand provided by this tyrosine may increase the electron density of the heme, thus lowering the heme iron reduction potential and helping to oxidize the ferric heme to the oxyferryl porphyrin cation radical. This also explains why this ferric heme of catalases can not be readily reduced to ferrous form by sodium dithionite while the heme in catalase-peroxidases, which is also a ferric heme *b*, can.

The α-helical domain is named for its high α-helical composition contributed by four contiguous α-helices. This region is responsible for binding NADPH and is not highly conserved. Based on the binding strength of NADPH, catalases can be divided into three groups: those with tight NADPH binding, those with moderate NADPH binding, and those which are not capable of binding NADPH. NADPH

serves to prevent and reverse the accumulation of compound II, derived from compound I via one-electron reduction [57]. Accordingly, the absence of bound NADPH leads to the increased tendency to the formation of compound II [53, 58]. NADPH is about 13-14 Å away from the heme iron, which is rather long for the rapid transfer of electrons, which indicates a tunneling mechanism. It is suggested that NADPH exerts this function via a highly conserved serine as the electron tunnel. More recent research indicates that NADPH may also serve to stabilize the quaternary structure of the enzyme [49].

1.2.4 Peroxidases

Peroxidases utilize heme iron to transfer electrons from a reducing substrate to H_2O_2. The overall reaction can be shown as:

$$H_2O_2 + 2RH \longrightarrow 2R^{\bullet} + 2H_2O$$

Peroxidases can be classified into two distinct groups, the so-called animal peroxidases, and plant peroxidases [59]. The designation "plant peroxidase" is not entirely accurate because members of this group have been identified not only in plants, but also in fungi and prokaryotes. Most plant peroxidases utilize ferric heme *b* as the prosthetic group. In contrast, the heme utilized in most animal peroxidases is

covalently linked to the enzyme [60, 61]. The plant peroxidases share similar folding features and active sites, and can be further divided into three classes based on their sequence comparison [62, 63]. Class I contains the intracellular enzymes, including yeast cytochrome *c* peroxidase, ascorbate peroxidase, and bacterial gene-duplicated catalase-peroxidases. These peroxidases function as peroxide scavengers to protect cells. Class II contains the secretory fungal peroxidases, such as lignin peroxidase, manganese peroxidase from *Phanerochaete chrysosporium*, as well as *Arthromyces ramosus* peroxidase. The main role of class II peroxidases is to degrade lignin in wood, and participate in secondary metabolism under conditions of limited nutritional supply [64]. Class III contains the secretory plant peroxidases such as peroxidases from horseradish, barley, and soybean. They play important roles in defense and stress related processes, as well as lignin synthesis and auxin degradation.

The quaternary structure of plant peroxidases (i.e., the number of subunits or chains) varies depending on the peroxidase. However, all plant peroxidase monomers share similar structural features [65-69]. The major secondary structural component in their overall structure is α–helix. There are 10 major helices, namely helices A-J, with a heme prosthetic group in each monomer. The heme plane divides the monomer of peroxidases into two domains, domain I, which consists of helices A-D, and domain II, which consists of helices F-J. These two domains are connected by helix E [65-69].

All peroxidases studied to date share the same catalytic cycle with three irreversible steps (Figure 1.6) [70]. The first step of peroxidase reaction is the same

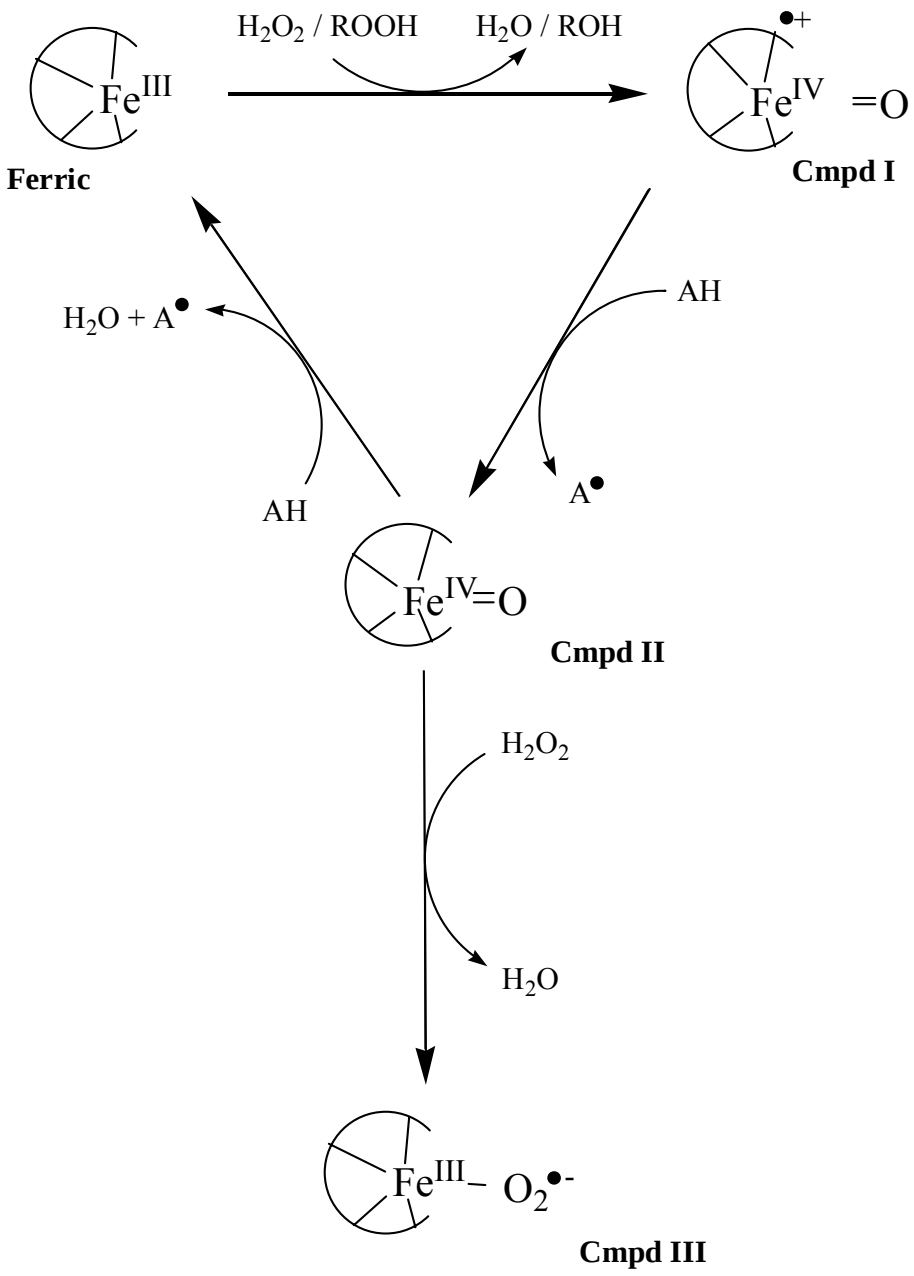

(AH: reducing substrate)

Figure 1.6. Catalytic Cycle of Peroxidases.

as that of a catalase, which is the oxidation of resting ferric enzyme by H_2O_2 to generate H_2O and compound I [71, 72]. Compound I is then reduced by one electron from a reducing substrate to generate one equivalent of substrate radical and compound II, a ferryl-oxo form of the enzyme [60]. However, unlike compound I, which contains a porphyrin π cation radical, compound II is a neutral, non-radical intermediate [72, 73]. To complete the catalytic cycle, compound II is reduced back to the ferric form by a subsequent one-electron transfer from the reducing substrate, with the generation of another equivalent of substrate radical and one equivalent of H_2O. In the catalytic cycle, the reduction of compound II is usually the rate-limiting step [60, 74]. The main difference between compound I and compound II is their heme states. Compound I has a porphyrin cation radical heme, and its reduction needs only an outer sphere electron transfer from the substrate to the heme, whereas compound II has a low-spin ferryl-oxo neutral non-radical heme, and the reactions of compound II require a change in the heme state to a high-spin ferric state [75]. This reorganizational event may be the barrier that makes the reduction of compound II the rate-limiting step of the cycle.

In the presence of excess H_2O_2, the formation of compound III, a ferrous-dioxy/ferric-superoxide inactive intermediate is observed (Figure 1.6) [76]. Compound III is formed by the reaction of compound II with H_2O_2. In addition, two other mechanisms for compound III formation have also been shown: (a) the reaction of ferrous enzyme with O_2, and (b) the reaction of ferric enzyme with superoxide anion [59]. Though compound III is inactive, the latter pathways of its formation are

reversible [77]. However, the reversion of compound III is relatively slow [78]. Meanwhile, in the presence of excess H_2O_2, compound III can undergo additional reactions which lead to irreversible inactivation [79-81]. Therefore, formation of compound III during turnover would represent a substantial and potentially irreversible inhibition of peroxidase-catalyzed oxidation. The mechanism of this irreversible inactivation by H_2O_2 is not completely clear. However, the process usually involves the "bleaching" of the heme (i.e., the decrease in visible absorption peak intensity without a compensatory increase at other wavelengths).

Meanwhile, the presence of an efficient reducing substrate can prevent this irreversible inactivation of peroxidases [81-84]. Furthermore, it has been suggested that some radicals such as phenoxyl radical can react with compound III to turn this intermediate back to active enzyme [85].

1.2.5 Catalase-peroxidases

Catalase-peroxidases are unique because these bifunctional enzymes, though with a *single* active site, catalyze both catalase and peroxidase reactions. These two types of reactions are mechanistically different; they even have different pH optima [86-88]. What is particularly striking about catalase-peroxidases is that with very few exceptions, which will be discussed below, the structure of the N-terminal domain of catalase-peroxidases, including the heme structure, the heme-bound ligand and the

non-ligand heme environment, is almost identical to monofunctional peroxidases, yet the latter lacks appreciable catalase activity. This demonstrates the critical nature of the fourth level of structure, global protein structure, in hemoprotein function. Clearly, structural components peripheral to the active site have a profound influence on the catalytic abilities of the heme in catalase-peroxidases. Finally, these enzymes are of great biomedical importance. Among them, *Mycobacterium tuberculosis* catalase-peroxidase is essential for the activation of INH, the front-line anti-tubercular drug. Furthermore, several highly virulent pathogens, such as *E. coli* O157:H7, *L. pneumophila*, and *Y. pestis*, possess extra periplasmic catalase-peroxidases, which are believed to be virulence factors.

1.2.5.1 Catalytic Cycles

Both catalase and peroxidase activities of these enzymes start with the peroxide-dependent conversion of ferric enzyme to the ferryl-oxo porphyrin radical intermediate known as compound I, with one equivalent of H_2O_2 reduced to H_2O (Figure 1.7). Compound I is two oxidizing equivalents above the ferric form of the enzyme and is the key point of divergence of catalase activity from peroxidase activity. In the catalase cycle, compound I is reduced back to the ferric state by H_2O_2 with the production of O_2. In contrast, the peroxidase cycle is completed by two consecutive one-electron reduction reactions of compound I by an exogenous reducing substrate, with the production of two equivalents of substrate radical and one

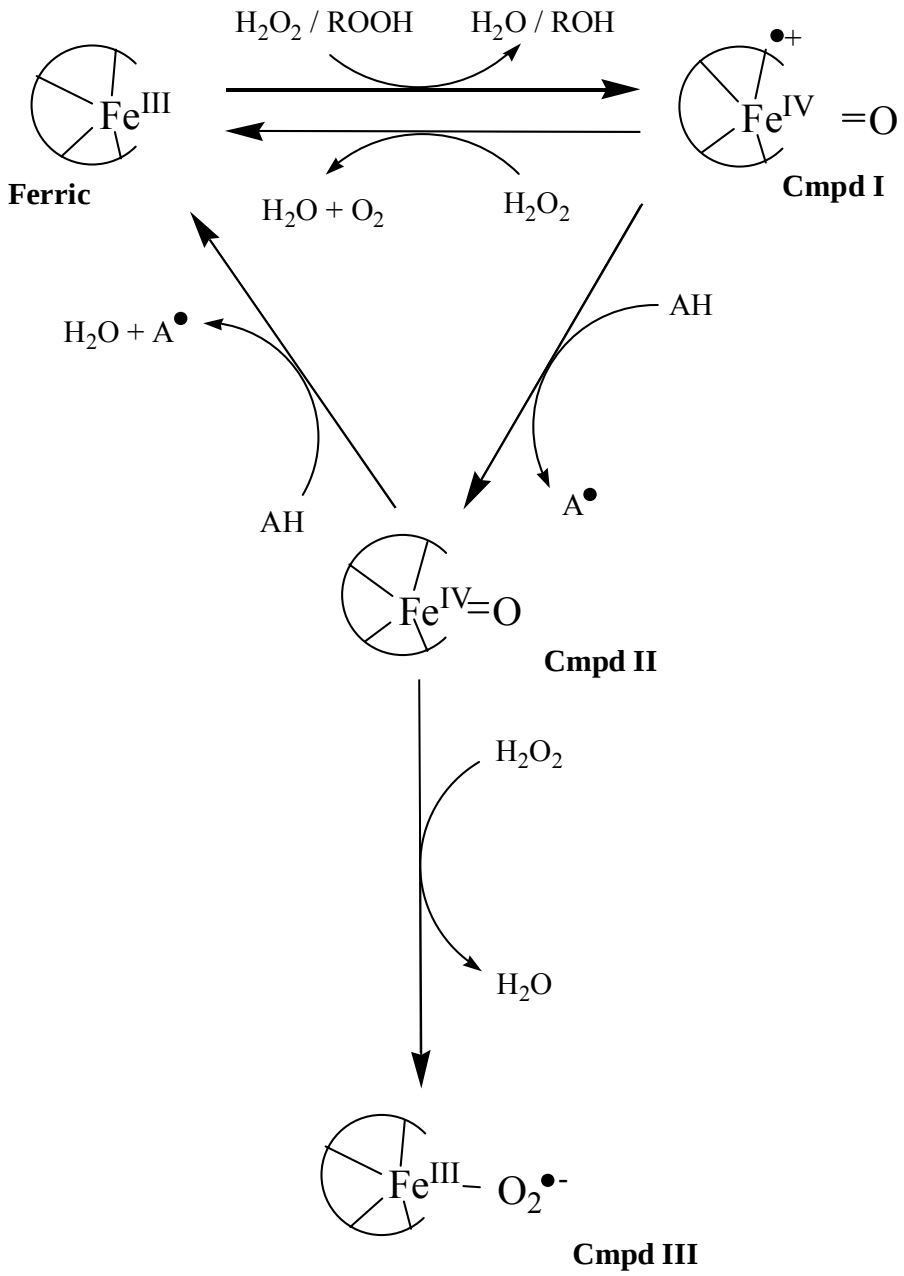

Figure 1.7. Catalytic Cycle of Catalase-peroxidases.

equivalent of H_2O. The first one-electron step reduces compound I to the ferryl-oxo intermediate, also known as compound II, and the second reduces compound II to the ferric form of the enzyme.

1.2.5.2 Virulence factors

Catalase–peroxidases are believed to be virulence factors of *Escherichia coli* O157:H7, *Yersina pestis* and *Legionella pneumophila* [89-92]. Among them, *Escherichia coli* O157:H7 is a highly virulent and deadly food-borne pathogen; *Yersina pestis* is the causative organism of bubonic plage; and *Legionella pneumophila* is an intracellular parasite and the causative organism of Legionnaires' pneumonia. Catalase–peroxidases are thought to be virulence factors because they are absent from the less pathogenic or non-pathogenic relatives of these organisms. This hypothesis is supported by the facts that KatP is encoded on a plasmid known to correlate with *E. coli* virulence; KatY from pathogenic *Yersinia* species is expressed at 37 °C, but not 26 °C, the temperatures representing the mammalian host and the flea, respectively [90, 92]; and when *katA* gene is inactivated in *L. pneumophila*, this pathogen is more sensitive to exogenous hydrogen peroxide and less virulent [89].

These enzymes, KatP (from *E. coli* O157:H7), KatA (from *L. pneumophila*), and KatY (from *Y. pestis*), are part of one subgroup among the family of the bifunctional catalase–peroxidases called periplasmic catalase-peroxidases. Most

catalase-peroxidases are cytoplasmic [93, 94]. They lack the signal peptide sequence targeting them to the periplasm. Conversely, KatP, KatY, and KatA are all periplasmic, and are more closely related to each other than they are to their cytoplasmic counterparts based on sequence information [95, 96]. Furthermore, these periplasmic enzymes form a cluster that is distinct from other catalase–peroxidases [96].

The mechanisms by which these catalase–peroxidases may contribute to virulence have not been determined. Interestingly, these pathogens also produce another set of cytoplasmic catalase-peroxidases. Thus, it is suggested that the primary benefit to these pathogens for producing a periplasmic catalase–peroxidase is to protect the pathogens from being killed by phagocytes [91]. Professional phagocytes mediate oxygen-dependent processes of bacterial killing by a series of reactions including the formation of superoxide radical ($O_2^{\bullet -}$) by NADPH oxidase, superoxide dismutation and the formation of H_2O_2 by superoxide dismutase (SOD), and the generation of bactericidal HOCl from H_2O_2 by myeloperoxidase [97]. Accordingly, a logical function for these ideally positioned pathogen periplasmic catalase-peroxidases would be to destroy H_2O_2 generated during phagocytosis, thereby protecting these pathogenic cells against external threats whereas their cytoplasmic counterparts can not. The peroxidase activity of the periplasmic catalase–peroxidases may also protect the pathogens by reducing some reactive peroxides, e.g., peroxynitrite ($ONOO^-$) and its conjugate peroxynitrous acid (ONOOH), which are produced as a result of the immune response.

1.2.5.3 Isoniazid activation

Tuberculosis is responsible for one fourth of all avoidable adult deaths in developing countries. Each year over 8 million people are diagnosed with tuberculosis and nearly 2 million of these patients die [98, 99]. The continued rise in multidrug-resistant strains of tuberculosis and its highly contagious property have called for research to explicate the molecular mechanism of anti-tubercular drugs, including isoniazid (isoniacotinic acid hydrazide, INH), and ethionamide, which is used in cases when INH is not effective (Figure 1.8). Isoniazid is the most effective drug for the treatment and prophylaxis of tuberculosis. This bactericidal drug was first reported in the treatment of *Mycobacterium tuberculosis* in 1952 [100], yet the details of its mechanism of action are still incomplete.

Early studies of isoniazid-resistant clinical strains of *M. tuberculosis* revealed a correlation between the resistance and loss of catalase-peroxidase activities [101, 102]. In 1992, based on the facts that: (i) many INH-resistant isolates of *M. tuberculosis* have decreased catalase activity, (ii) the most highly resistant isolates are completely catalase-negative, (iii) deletion of *katG* gene from the chromosome was associated with INH resistance in two patient isolates of *M. tuberculosis*, and (iv) transformation of a INH-resistant mutant of *M. smegmatis* with *katG* gene restored its sensitivity to INH, it was concluded that the resistance to isoniazid can arise from either mutations in or deletion of the mycobacterial *katG* gene, which encodes the *M. tuberculosis* catalase-peroxidase (KatG) [103]. These facts strongly suggest that isoniazid is a prodrug which requires KatG to reach its

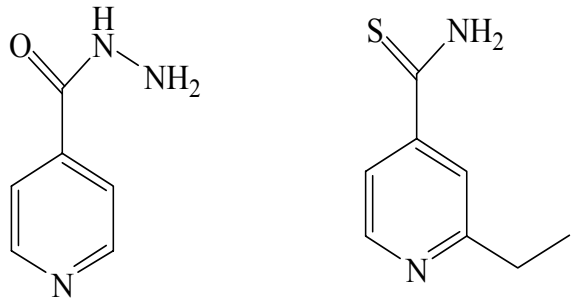

Isoniazid **Ethionamide**

Figure 1.8. Structure of Isoniazid and Ethioamide.

final active form. Since that time intense studies have been undertaken to explain the mechanism of isoniazid action, including a search for a mycobacterial target of drug action. It has been shown that *M. tuberculosis* strains with wild-type *katG* but mutations to *inhA* gene also showed isoniazid resistance. The corresponding InhA protein is an NADH-dependent fatty acyl enoyl ACP reductase, which catalyzes the biosynthesis of long-chain fatty acids, including the mycolic acids, which are essential for the cell wall integrity in mycobacterial species [104]. This suggests that InhA is the target of isoniazid, but the drug first requires activation by KatG before it can effectively inhibit this enzyme (Figure 1.9). Though the oxidation of isoniazid also produces some active oxygen species such as superoxide and hydroxyl radicals, these radicals alone do not account for InhA inactivation [105]. Meanwhile, the inactivation of InhA by INH can be inhibited by the addition of InhA substrate, suggesting that an active site residue is included [105]. Furthermore, inactivation of InhA by isoniazid could only be achieved in the presence of the cofactor NADH/NAD^+, suggesting that a conformational change induced by cofactor binding to make the key InhA residue more accessible to isoniazid is required [105]. This active site key residue has been shown to be Cys243 [105].

In short, the mechanism of isoniazid as the antitubercular drug can be described as follows: 1) Isoniazid is actively taken up by *M. tuberculosis* as a prodrug, 2) it is then oxidized by the mycobacterial catalase-peroxidase to reach the

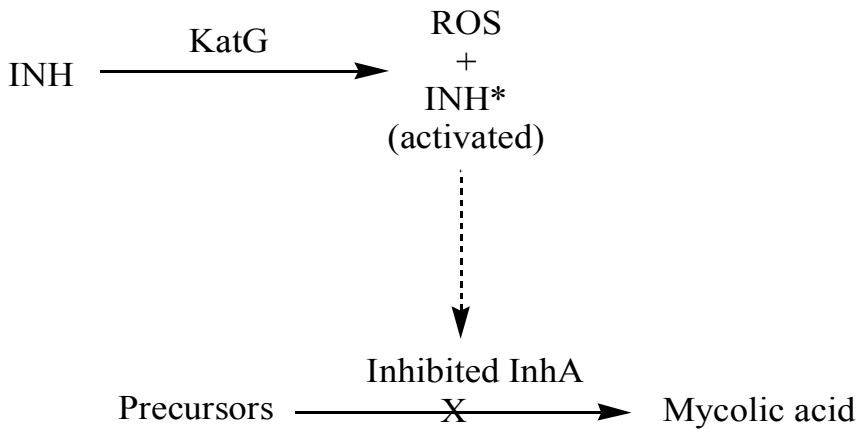

Figure 1.9. Proposed Mechanism of INH.

activated form, and 3) the activated form of INH binds with Cys 243 of the *M. tuberculosis* InhA-NADH complex, inhibiting the activity of InhA and interfering with the biosynthesis of long-chain fatty acids, particularly mycolic acids, the deficiency of which will lead to cell death. However, the details of INH interaction with KatG, the mechanism of INH activation by the enzyme, and the basis for resistance caused by mutations to KatG are still unclear.

1.2.5.4 Two Domains

The catalase-peroxidases that have been characterized to date are either homodimers or homotetramers [106]. Each subunit of catalase-peroxidases has a molecular weight of ~ 80 kDa, and contains one active site highlighted by the presence of the heme prosthetic group. The subunit structure is divided into two domains, the N-terminal domain and the C-terminal domain. These two domains have noteworthy sequence similarity, most likely from gene duplication and fusion events [107, 108]. Though catalase-peroxidases show a much higher catalase activity than peroxidase activity, both domains share sequence similarity and the topological arrangements of secondary structural elements with monofunctional class I peroxidases [108], and share no sequence similarity or secondary structural arrangement with typical monofunctional catalases [50]. Both domains have high α-helical composition with few β-sheets. There are 10 major helices in each domain, namely helices A-J alphabetically. A heme-binding consensus sequence is

present only in the N-terminal domain of each subunit and thus contains the active site. There are also several channels that allow access to the active site in the N-terminal domain [87]. The C-terminal domain does not contain a heme-binding motif and consequently, does not bind heme. Moreover, the space corresponding to the heme pocket is filled with two short β-strands (between helices D and E) and a loop (between helices F and G) [86, 87]. The N-terminal domain and the C-terminal domain are connected by a long loop that does not have any defined secondary structural element [86].

Although the C-terminal domain does not possess an active site, and is absent from monofunctional peroxidases, it is an essential component for catalase–peroxidase catalysis, *even* the peroxidase activity of these bifunctional enzymes [109]. One role that has been realized of the C-terminal domain is to support the architecture of the active site, preventing coordination of the heme iron by a highly conserved and essential distal histidine, which is located in helix B. This essential distal histidine acts as a general base required for the catalytic functions of peroxidases and catalase-peroxidases [60, 110-112]. Without the C-terminal domain, the architecture of the active site collapses and the essential histidine coordinates with heme to form an inactive, hexa-coordinate, low-spin heme species [109]. The C-terminal domain performs this structure-supporting function by the interactions between the loop B'C' and helix E' of its own and the loop BC of the N-terminal domain [109]. In contrast, monofunctional peroxidases keep the architecture of the active site by some other means. For instance, manganese peroxidase and lignin peroxidase use a calcium ion

which is coordinated to the residues from helix B and loop BC [66, 113]. Moreover, it is believed that the C-terminal domain plays multiple roles other than active site supporting. However, these roles are still under investigation.

1.2.5.5 Non-ligand Heme Environment

The heme environment of catalase-peroxidases is similar to that of the class I peroxidases, and the active site residues between catalase-peroxidases and class I peroxidases are almost superimposable [86, 87]. On the distal side of the heme, the active-site triad of Arg, Trp and His is typical of both groups of enzymes. In class III peroxidases, such as horseradish peroxidase, the Trp in the triad is replaced by a Phe. Alteration of Trp by Phe in catalase-peroxidases deeply reduces their catalase activity [110, 111, 114]. On the proximal side, an essential His is the fifth coordination ligand to the heme iron as in the peroxidases, and it is in close hydrogen bonded association with the fully conserved Asp, which also interacts with the indole nitrogen atom from the proximal Trp [87].

1.2.5.6 Insertions

Although the active site and overall tertiary structural arrangement of catalase-peroxidase N-terminal domain closely resembles that of monofunctional class I peroxidases, comparison of these two groups of enzymes reveals two interhelical insertions that are unique to the N-terminal domain of bifunctional catalase-

peroxidases but absent from monofunctional peroxidases (Figure 1.10) [107, 108]. Both insertions are peripheral to the active site [86, 87]. The first insertion, with a length of 36-43 residues, is positioned between conserved helices D and E. The second insertion, with a length of 35-36 residues, is located between helices F and G. Despite their peripheral locations to the active site, these two insertions are believed to play important functional roles based on the facts that the first three structural levels of catalase-peroxidases and peroxidases are almost superimposable, while monofunctional peroxidases lack appreciable catalase activity. These roles undoubtedly have important biomedical applications, for instance, they will help us better understand the virulence of certain pathogenic bacteria, and may help clarify the mechanism of action of isoniazid.

1.2.5.7 Trp-Tyr-Met Covalent Adduct

With the revelation of the first crystal structure of a catalase-peroxidase (*Haloarcula marismortui* KatG), a novel Trp-Tyr-Met adduct was identified [86] (Figure 1.11). This has been observed in two other catalase-peroxidase structures, and the residues involved are strictly conserved, suggesting that this covalent adduct is common to all catalase-peroxidases [87, 88]. The bonds are formed between $C^{\eta 2}$ of Trp and $C^{\varepsilon 1}$ of Tyr, and between $C^{\varepsilon 2}$ of Tyr and S^{δ} of Met. Alterations of the Trp [110, 111] or Tyr [115, 116] result in the loss of catalase activity with little effect upon the peroxidase activity of the enzymes, indicating the role of this adduct is to maintain the

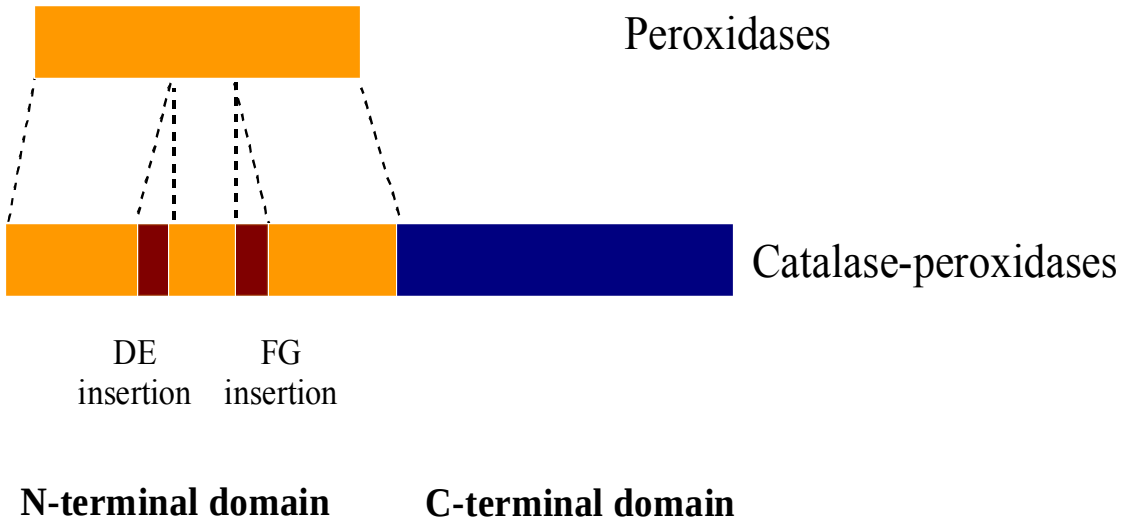

Figure 1.10. Scheme of Structural Comparison of Peroxidases and Catalase-peroxidases.

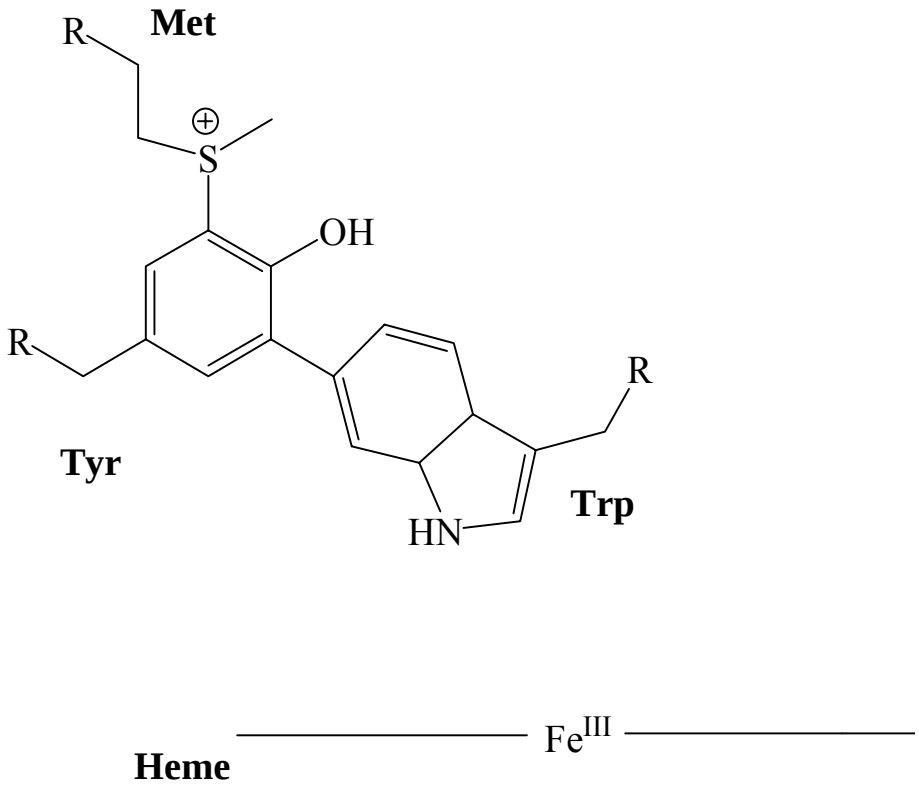

Figure 1.11. Models of the Trp-Tyr-Met Covalent Adduct of Catalase-peroxidases.

catalase activity of these bifunctional enzymes. Further investigation has shown that the formation of the Trp-Tyr-Met covalent crosslinkage requires the presence of heme within the enzyme active site and a peroxide oxidant. This is based on the observations that: (a) reconstitution of apo-KatG with heme results in the partial conversion of catalase-peroxidase to its crosslinked form, (b) the conversion was enhanced upon the addition of a peroxide oxidant, and (c) when using Zn-protoporphyrin IX instead of heme to reconstitute apo-KatG, no formation of the crosslink was observed, regardless of the addition of the peroxide oxidant (Cornelius Varnado and Douglas Goodwin, unpublished results). Furthermore, it has been shown that disruption of this covalent linkage weakens the binding of heme to the active site, as well as contributes to a partial change of heme iron state from penta-coordinate high-spin to hexa-coordinate low-spin [117].

1.3 Summary

Despite its simple structure and small size, the metallo-organic compound heme plays important roles in remarkable heme enzyme versatility. Among the four structural levels that regulate these varieties in function, intense effort has been put into the studies on how the inner three structural levels (i.e., the structure of heme itself, the identity of protein-derived heme ligands, and the non-ligand heme environment), affect heme enzyme functions. In the mean time, though the outermost structural level, the global

protein structure, is clearly indispensable, little is known about how it regulates heme enzyme function.

The catalase-peroxidases provide ideal models for evaluating hemoprotein structure and function, particularly at the global protein structural level. Catalase-peroxidases catalyze both catalase and peroxidase reactions using a *single* active site. The first three structural levels around this active site are almost identical to those of monofunctional peroxidases, yet the latter lacks appreciable catalase activity. This highlights the effects of global protein structure on enzyme function. Comparison of the global structures of these two important classes of enzymes reveals two interhelical insertions which are peripheral to the active site, indicating that these two insertions are functionally important. In this dissertation the roles of these two interhelical insertions in *E. coli* catalase-peroxidase function were explored with the expectation that it would enhance our understanding of the regulation of heme enzyme function by global protein structure.

CHAPTER TWO

MATERIALS AND METHODS

2.1 Reagents

Hydrogen peroxide (30%), peracetic acid, hemin, δ-amino levulinic acid, imidazole, Sephacryl 300 HR, phenyl-sepharose resin, ampicillin, chloramphenicol, ferrous ammonium sulfate, phenylmethylsulfonyl fluoride (PMSF), and 2,2'-azino-bis(3-ethylbenzthiazoline-6-sulfonic acid) (ABTS) were obtained from Sigma (St. Louis, MO). Urea, Luria-Bertani broth, trichloroacedic acid (TCA), isopropyl-β-D-thiogalactopyranoside (IPTG) and tetracycline hydrochloride were obtained from Fisher (Pittsburgh, PA). Bugbuster and benzonase were obtained from Novagen (Madison, WI). All restriction enzymes were obtained from New England Biolabs (Beverly, MA), and all oligonucleotide primers were obtained from Invitrogen (Carlsbad, CA). All *E. coli* strains (BL-21 [DE3] pLysS and XL-1 Blue) and *Pfu* polymerase were obtained from Stratagene (La Jolla, CA). Nickel–nitrilotriacetic acid (Ni–NTA) resin was obtained from Qiagen (Valencia, CA). All buffers and media were prepared using water purified through either Barnstead system (EASYpure II) or Millipore system (MilliQ, QPAK II) (18.2 MΩ/cm resistivity).

2.2 Cloning and Expression of wtKatG and its Variants

2.2.1 Seamless® cloning (Stratagene)

Seamless® cloning (Stratagene) method is based on PCR (polymerase chain reaction). It follows PCR by treating PCR products with the endonuclease *Eam*1104 I. *Eam*1104 I is a type IIS restriction endonuclease that cleaves target DNA downstream of its recognition sequence, and the unique feature of this endonuclease is that its cleavage site is one nucleotide down on the upper strand in the 3' direction and four nucleotides down on the lower strand in the 5' direction, as shown in the scheme below (the cleavage sites are marked with solid triangles). Thus, the resulting overhanging sequence has three nucleotides. Because the PCR primers are designed to contain an *Eam*1104 I recognition sequence, it is possible also to design the overhanging sequences resulting from *Eam*1104 I digestion.

5' – **CTC** **TTC** N▼NN NN – 3'

3' – GAG AAG NNN N▲N – 5'

The PCR product is then digested with *Eam*1104 I, and ligated with a DNA vector, which was pET-20b plasmid in the cases of the studies in this dissertation, using T4 DNA ligase.

2.2.2 The pET expression system

The pET expression system is based on T7 promoter-driven system. The T7 promoter is not recognized by *E. coli* RNA polymerase, minimizing expression of the target gene until T7 RNA polymerase is present. The plasmid used in the studies in this dissertation was pET-20b. The gene of interest was inserted following the T7 RNA polymerase promoter. All genes were inserted such that expression would result in a C-terminal 6-histidine tag. For selection purposes, the pET-20b plasmid encodes an ampicillin resistance gene, conferring ampicillin resistance on cells carrying the plasmid.

2.2.3 Non-expression host E. coli XL-1 Blue

The *E. coli* XL-1 Blue strain was used for amplification of plasmid DNA. To achieve this goal, *E. coli* XL-1 Blue strain was transformed with the ligated DNA plasmid. All transformations using *E. coli* XL-1 Blue were carried out as described below: cells were incubated with the target plasmid and β-mercaptoethanol on ice for 30 minutes. Then the mixture is heat shocked at 42 °C for 45 seconds, followed by quenching on ice for 2 minutes. Cells were allowed to recover for 1 hour at 37 °C in LB (Luria–Bertani) broth lacking added antibiotics with gentle agitation. Following recovery, cells were plated on LB agar plates supplemented with ampicillin (50 mg/l). In all molecular cloning described in this dissertation, transformed *E. coli* XL-1 Blue

strains were grown on LB-agar plates and in LB broth in the presence of ampicillin (100 mg/l). The target plasmids were harvested using standard protocols.

2.2.4 Protein expression host E. coli BL-21 [DE3] pLysS

E. coli strain BL-21 [DE3] pLysS was used to express the proteins studied in this dissertation. First *E. coli* strain BL-21 [DE3] pLysS was transformed with pET-20b plasmid containing the gene for *E. coli* catalase-peroxidase (KatG) or variants thereof. The designation "DE3" in the expression strain indicates that the strain is a λDE3 phage lysogen, that is to say, it contains a chromosomal copy of the gene for T7 RNA polymerase under control of the *lac* UV5 promoter. When there is no lactose or lactose analog (e.g., IPTG) (Figure 2.1) present, *lac* repressor binds to the *lac* promoter, and no T7 RNA polymerase is expressed. As a result, none of the target protein is expressed either. Conversely, in the presence of lactose or a suitable analog, the *lac* repressor dissociates from the *lac* promoter, and T7 RNA polymerase is expressed. Consequently, the target protein is expressed. In the studies, isopropyl-β-D-thiogalactopyranoside (IPTG) was used as a lactose analog. The symbol "pLysS" indicates that plasmid that encodes T7 lysozyme is present in the strain. Lysozyme inhibits T7 RNA polymerase, therefore stops "leakage" expression of the target protein. This tightly controlled protein expression feature is important, especially for the expression of toxic proteins. The *lac* UV5 promoter is known to allow "leakage" expression. That is, there is a small amount of T7 RNA polymerase expressed even in

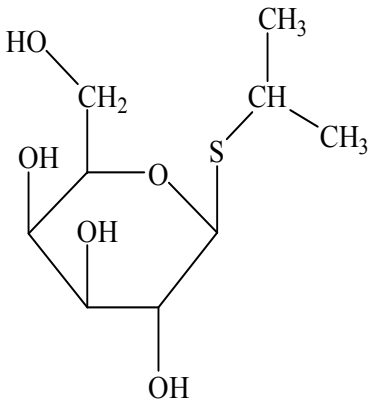

IPTG

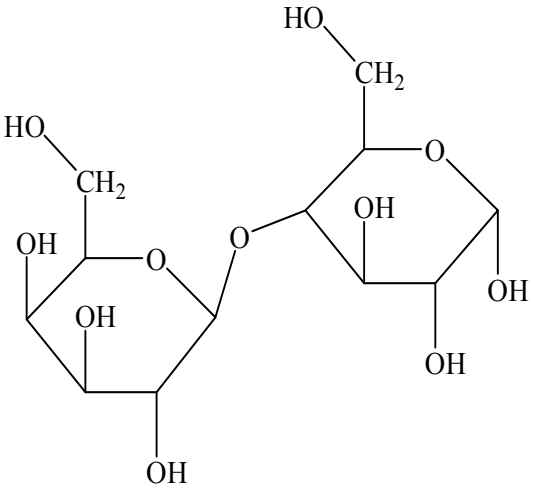

Lactose

Figure 2.1. Structure of IPTG and Lactose.

the absence of lactose or a suitable analog. This in turn induces the expression of target protein. If the protein being overexpressed is toxic, "leakage" expression will substantially slow cell growth or cause cell death. Consequently, the cell density may never reach levels required for efficient and abundant expression of the target protein.

The transformation procedure for *E. coli* BL-21 [DE3] pLysS used for all studies described herein is as follows: cells were incubated with the target plasmid on ice for 30 minutes. Then the mixture was heat-shocked at 42 °C for 20 seconds, followed by quenching on ice for 2 minutes. Cells were allowed to recover for 1 hour at 37 °C in LB broth lacking added antibiotics with gentle agitation. Following recovery, cells were plated on LB agar plates supplemented with ampicillin (50 mg/l) and chloramphenicol (17.5 mg/l).

2.2.5 Cloning and expression of wild-type KatG (wtKatG)

The cloning of wtKatG was accomplished previously by Dr. Douglas Goodwin. Briefly, the *katG* gene was acquired from *E. coli* (K-12) genomic DNA. Two primers, ECCPa03 (GTA GAG GGG AGC ACA *CAT ATG* AGC ACG TCA GAC GAT ATC C), and ECCPa06 (CTG AAC GGG GTC AGA *CTC GAG* CAG GTC GAA ACG GTC) were used to amplify the *katG* gene, using PCR techniques. To incorporate the *katG* gene into pET-20b, the resulting PCR product and the pET-20b plasmid were digested with endonucleases *Nde*I and *Xho*I, and the proper fragments were ligated

together according to standard procedures [118]. Candidate plasmids were sequenced to verify that no accidental mutations had accumulated during the cloning process. By using the *Xho* I restriction site in the multiple cloning sequence of pET-20b, the *katG* gene was followed by six codons for histidine and a stop codon. Thus, wtKatG is expressed with a six-histidine tag on its C-terminus. The *E. coli* protein expression host (BL-21 [DE3] pLysS) was transformed with the pKatG1 plasmid and transformants were selected based on ampicillin resistance.

Expression of wtKatG was achieved by growing in transformed expression host in LB broth (2L) with 100 mg/l ampicillin. Cells were grown to mid-log phase ($OD_{600} = 0.4 \sim 0.6$) and expression of wtKatG was induced by addition of 1 mM IPTG. At the time of induction, cultures were also supplemented with 0.5 mM δ-amino levulinic acid and 0.5 mM ferrous ammonium sulfate for biological synthesis of heme. The expression was carried out at 37 °C with constant shaking for four hours after induction. Cells were then harvested by centrifugation (13,000 × *g*), and the cell pellets were stored at −80 °C until purification.

WtKatG expression was evaluated by treating sample of cells with an equal volume of 10% trichloroacetic acid (4 °C) followed by centrifugation. The pellet was then washed with 1 ml acetone, dried, and resuspended in SDS–PAGE loading buffer. The pH of the resuspended pellet was adjusted with trizma base and separated by SDS–PAGE using a 7.5% acrylamide resolving gel.

2.2.6 Cloning and expression of KatG$^{\Delta FG}$

To generate constructs for the expression of KatG$^{\Delta FG}$ (wtKatG lacking its FG insertion), we developed a deletion mutagenesis procedure adapted from Seamless® cloning (Stratagene). The plasmid for expression of recombinant His-tagged *E. coli* KatG (pKatG1) was used as a template. Primers were designed to: (1) amplify pKatG1 excluding the codons corresponding to the targeted deletion (Pro 277 – Thr 311), (2) include a restriction site for *Eam*1104 I, and (3) yield compatible overhanging sequences upon digestion with *Eam*1104 I. Because *Eam*1104 I is a type IIS endonuclease, it cleaves target DNA downstream of its recognition sequence. Thus, the resulting overhanging sequences were designed for religation such that only the codons corresponding to the targeted deletion were removed. No introduction of new restriction site or extra codon was involved, nor was the removal of codons outside the target sequence required. We used primers ECCP D201 (TAC ATC TCT TCT ***AGA*** ACC GGC ACC GTG GGT TTT ACC CAG) and ECCP D202 (GAT GCC TCT TCC ***TCT*** GGT CTG GAA GTA GTC TGG). The *Eam*1104 I recognition sequence is underlined, and the overhanging sequence generated upon hydrolysis by *Eam*1104 I is in bold italics.

The PCR product was digested with *Eam*1104 I and ligated using T4 DNA ligase. The ligated plasmid was used to transform *E. coli* XL-1 Blue. Colonies were selected on the basis of ampicillin resistance, and candidate plasmids were verified by DNA sequence analysis to ensure the accuracy of the mutagenesis procedure. As we had done with pKatG1, the expression host *E. coli* BL-21 [DE3] pLysS was

transformed with pKatG$^{\Delta FG}$. Expression of KatG$^{\Delta FG}$ was accomplished as described for wtKatG.

2.2.7 Cloning and expression of KatG$^{\Delta DE}$

The expression construct for KatG$^{\Delta DE}$ (wtKatG lacking its DE insertion) was generated using the deletion mutagenesis procedure described for pKatG$^{\Delta FG}$. Primers ECCPD101 (CCA GC TCT TCC ***CGG*** ATC CGG TTC CCA GAC GTC TTC) and ECCPD102 (ATT TAC TCT TCC ***CCG*** GAA GGC CCG GAT CAC AGC) were used. The recognition sequence for *Eam*1104 I is underlined. The overhanging sequence remaining following hydrolysis by *Eam*1104 I is shown in bold italics. The codons and only the codons corresponding to the DE insertion (Leu193 – Asn228) were removed from the sequence.

Digestion, religation of the PCR product, and transformation of the *E. coli* hosts XL-1 Blue and BL21 [DE3] pLysS with the resulting plasmid of KatG$^{\Delta DE}$ were carried out as described for pKatG$^{\Delta FG}$. Candidate plasmids were verified by DNA sequence analysis to ensure the accuracy of the mutagenesis procedure. The expression host *E. coli* BL-21 [DE3] pLysS was transformed with pKatG$^{\Delta DE}$ and transformants were selected based on ampicillin resistance. The expression of KatG$^{\Delta DE}$ was also followed the procedure same as for KatG$^{\Delta FG}$, except for that neither

δ-amino levulinic acid nor ferrous ammonium sulfate were added to the culture medium.

2.2.8 Cloning and expression of KatG$^{\Delta DE/FG}$

The expression construct for KatG$^{\Delta DE/FG}$ (wtKatG lacking Both DE and FG insertions) was generated by applying the deletion mutagenesis procedure described above to the pKatG$^{\Delta FG}$ plasmid. Primers ECCPD101 (CCA GC TCT TCC ***CGG*** ATC CGG TTC CCA GAC GTC TTC) and ECCPD102 (ATT TAC TCT TCC ***CCG*** GAA GGC CCG GAT CAC AGC) were used to eliminate codons corresponding to the DE insertion (Leu 193 – Asn 228) from pkatG$^{\Delta FG}$. The recognition sequence for *Eam*1104 I is underlined. The overhanging sequence remaining following hydrolysis by *Eam*1104 I is shown in bold italics. In comparison to pKatG1, the resulting construct (pKatG$^{\Delta DE/FG}$) had no codons corresponding to either the DE insertion (Leu 193 – Asn 228) or the FG insertion (Pro 277 – Thr 311).

Digestion, religation of the PCR product, and transformation of the *E. coli* hosts XL-1 Blue and BL21[DE3] pLysS by the resulting plasmid (pKatG$^{\Delta DE/FG}$) were all carried out according to the procedure described above for pKatG$^{\Delta FG}$. The expression host *E. coli* BL-21 [DE3] pLysS was transformed with pKatG$^{\Delta DE/FG}$, and transformants were selected based on ampicillin resistance. The expression of KatG$^{\Delta DE/FG}$ was carried out by the same protocol described for KatG$^{\Delta DE}$.

2.2.9 Purification of wtKatG and KatG$^{\Delta FG}$

Cell pellets were resuspended in Bugbuster™ reagent supplemented with 0.1 mM PMSF. Following homogenization, benzonase (250 units) was added, and the mixture was incubated at 23°C with gentle stirring for 1 hour. The cell lysate was then centrifuged at 16,000 × g.

WtKatG and the variants were all purified using Ni-NTA column. The Ni-NTA resin is utilized for purification of proteins with a six-histidine tag. Nitriloacetic acid (NTA) is the chelator which is covalently bound to the resin. Immobilized Ni^{2+} cations are coordinated by the NTA moiety. The target protein, designed to contain a His-tag can tightly bind to the Ni^{2+} cations (Figure 2.2). All other cellular proteins either do not bind or only bind weakly to the resin can be washed off with low concentration imidazole. The target protein can then be eluted with high concentration of imidazole. By this approach, proteins can be purified in either their native or denatured forms.

For wtKatG and KatG$^{\Delta FG}$, the supernatant was loaded onto a Ni-NTA column by recirculating the solution at 1 ml/min through the column bed overnight. Following the loading of the resin with target protein, the column was washed with buffer **A** (50 mM phosphate buffer, pH 8.0; 200 mM NaCl) supplemented with 2 mM imidazole to remove most non-specifically bound proteins. A second wash was then performed with buffer **A** supplemented with 20 mM imidazole to wash off more stringently bound contaminant proteins. Finally, protein was eluted off the column

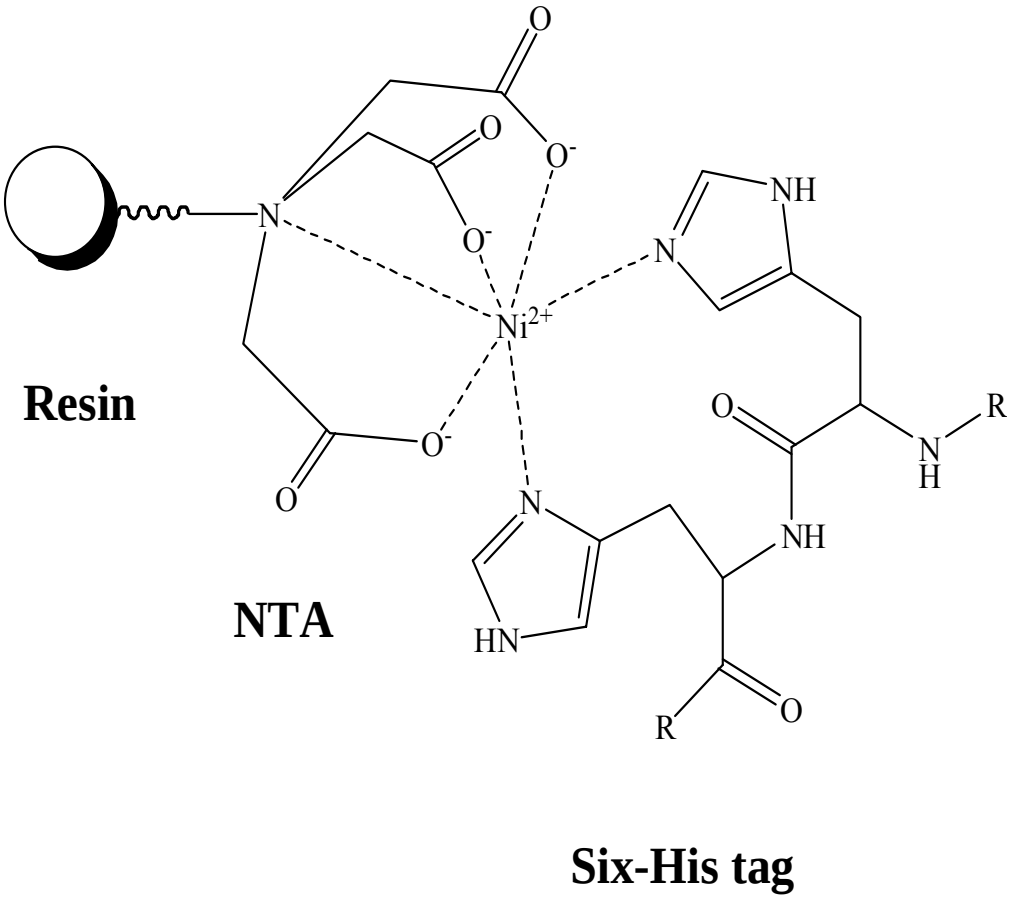

Figure 2.2. Structural Scheme of Ni-NTA Resin and Bound Six-His tag.

with buffer **A** supplemented with 200 mM imidazole. Excess imidazole was then removed by dialysis or gel filtration chromatography. By dialysis, the target protein was dialyzed against buffer **A** for 36 hours.

2.2.10 Purification of KatG$^{\Delta DE}$ and KatG$^{\Delta DE/FG}$

KatG$^{\Delta DE}$ and KatG$^{\Delta DE/FG}$ were both expressed in inclusion bodies, so adenaturing purification procedure was followed. After cells were centrifuged down to pellets, the pellets were resuspended in 200 mM phosphate buffer, pH 7.0, and homogenized. Cells were then lysed by sonication using Branson Sonifier 250 (Branson Ultrasonics Corp., Danbury, CT, USA). Following sonication, benzonase (250 units) was added, and the mixtures were gently stirred at 23 °C for 1 hour.

The cell lysates were then centrifuged at 16,000 × g. The pellets, which contained the included proteins of interest, were then resuspended in 8M urea and homogenized. Centrifugation at 16,000 × g was repeated. This time urea served to solublize the included proteins though they remained in a denatured state. Thus, each supernatant was mixed with Ni-NTA resin and gently agitated at 23 °C overnight. The resin was then loaded into an empty column, washed with 10 mM imidazole in 8 M urea, and then the protein was eluted off the resin with 200 mM imidazole in 8 M urea. Urea and imidazole were then removed by dialysis against buffer **A** for 36 hours. The bulk dialysis buffer was replaced every six hours.

2.2.11 Cloning, expression, and purification of KatG$^{N\text{-}term}$ and KatG$^{C\text{-}term}$

Cloning and expression of KatG$^{N\text{-}term}$ (KatG lacking its C-terminal domain) and KatG$^{C\text{-}term}$ (KatG lacking its N-terminal domain) were accomplished by our group members Ruletha Baker, and Carma Cook. The plasmid for the expression of KatG$^{N\text{-}term}$ was produced following the procedure: (a) primers ECCPm08(+) (GCC GAA AGA AGA TCT G*CT CGA G*TA AGA TCC GCT GCC) and ECCPm08(−) (GGC AGC GGA TCT TA*C TCG AG*C AGA TCT TCT TTC GGC) were used to introduce a *Xho* I restriction site after the codon corresponding to Leu 432 (Quik Change, Stratagene), (b) the non-expression host *E. coli* XL-1 Blue was transformed with the resulting plasmid, (c) amplified plasmid was then digested using *Xho*I, and the band corresponding to the pET-20b plasmid with the codons of the N-terminal domain was isolated by agarose gel electrophoresis and extracted from the gel, (d) the fragment was religated by T4 DNA ligase, and (e) the non-expression host *E. coli* XL-1 Blue was transformed with the ligated plasmid and the target plasmid was amplified. The candidate plasmids were verified by DNA sequence analysis. The resulting expression construct (pKatG$^{N\text{-}term}$) included codons corresponding to the N-terminal domain of KatG (Met 1 through Leu 432) followed by codons for Leu, Glu, and a six-histidine tag. This plasmid was used to transform expression host *E. coli* BL-21 [DE3] pLysS to express KatG$^{N\text{-}term}$.

Generation of an expression construct for KatG$^{C\text{-}term}$ was accomplished by employing the deletion mutagenesis procedure described above. Primers ECCP D301 (GCC GGA CTC TTC G **ATG** GAA GAT CTG ATC TGG CAA GAT CC) and

ECCP D302 (CGT CTG CTC TTC T **CAT** ATG TAT ATC TCC TTC TTA AAG) were used to eliminate codons corresponding to the N-terminal domain from pkatG. The recognition sequence for *Eam*1104 I is underlined. The overhanging sequence remaining following hydrolysis by *Eam*1104 I is shown in bold italics.

The expression of $KatG^{N\text{-}term}$ and $KatG^{C\text{-}term}$ followed the procedure described for $KatG^{\Delta DE}$. The $KatG^{N\text{-}term}$ was expressed in the inclusion bodies and the procedure for purifying $KatG^{\Delta DE}$ was followed. On the contrary, the $KatG^{C\text{-}term}$ was expressed in soluble form, therefore the procedure for purifying wtKatG and $KatG^{\Delta FG}$ was employed.

2.2.12 Cloning, expression, and purification of $KatG^{N\text{-}term/\Delta DE}$ and $KatG^{N\text{-}term/\Delta FG}$

To obtain the KatG N-terminal domain lacking the DE insertion or the FG insertion, the deletion mutagenesis procedure described in sectin 2.2.6 was employed. Primer pairs ECCPD101 (CCA GC TCT TCC ***CGG*** ATC CGG TTC CCA GAC GTC TTC) and ECCPD102 (ATT TAC TCT TCC ***CCG*** GAA GGC CCG GAT CAC AGC) were used to selectively remove the codons corresponding to the DE insertion from $pKatG^{N\text{-}term}$. Primer pairs ECCP D201 (TAC ATC TCT TCT ***AGA*** ACC GGC ACC GTG GGT TTT ACC CAG), and ECCP D202 (GAT GCC TCT TCC ***TCT*** GGT CTG GAA GTA GTC TGG) were used to selectively remove the codons corresponding to the FG insertion from $pKatG^{N\text{-}term}$. The recognition sequence for *Eam*1104 I is

underlined. The overhanging sequence remaining following hydrolysis by *Eam*1104 I is shown in bold italics. The products were used to transform non-expression host *E. coli* XL-1 Blue strain to amplify the target plasmids pKatG$^{N\text{-term}/\Delta DE}$, and pKatG$^{N\text{-term}/\Delta FG}$. These were then used to transform the expression host, *E. coli* BL-21 [DE3] pLysS, for protein expression. Both KatG$^{N\text{-term}/\Delta DE}$ and KatG$^{N\text{-term}/\Delta FG}$ were expressed in inclusion bodies, and the purification procedure of these two proteins followed the procedure used for purifying KatG$^{\Delta DE}$.

2.3 Enzyme Reconstitution

We have observed that wtKatG and KatG$^{\Delta FG}$ can be reconstituted by simply adding hemin following purification. Due to its poor solubility at neutral and acidic pH, hemin solutions for use in reconstitution were prepared by dissolving hemin in 0.1 M KOH. Hemin concentration was determined by the method of Falk [119]. Briefly, a reference solution was made by adding hemin to 20% pyridine, 0.1 M NaOH, followed by the addition of 0.3 mM $K_3Fe(CN)_6$. A reference spectrum from 560 nm to 530 nm was recorded. Roughly 5 mg sodium dithionite was then added to reduce the heme iron and generate a bispyridyl ferrous heme complex. A second spectrum was then recorded. Hemin concentration was calculated by dividing the absorbance difference between the peak (~ 554.5 nm) and valley (~ 539.5 nm) absorbances by the difference in their absorptivities (20.7 $mM^{-1}cm^{-1}$).

Titration of wtKatG and KatG$^{\Delta FG}$ with hemin resulted in a linear increase in their activities up to one equivalent. Addition of hemin beyond this point did not result in any additional increase. To minimize contribution of free hemin or adventitiously bound hemin to spectral or kinetic measurements, each protein was reconstituted with 0.75 equivalents hemin. However, maximal peroxidase activity values of KatG$^{\Delta DE}$ and KatG$^{\Delta DE/FG}$ were observed with 0.25 equivalents hemin and 0.5 equivalents hemin, respectively. Thus, to minimize the effects of free or adventitiously bound hemin, KatG$^{\Delta DE}$ and KatG$^{\Delta DE/FG}$ were reconstituted with 0.25 equivalents and 0.5 equivalents hemin, respectively. Both KatG$^{\text{N-term}/\Delta DE}$ and KatG$^{\text{N-term}/\Delta FG}$ were reconstituted with one equivalent hemin.

2.4 Recombination of KatG$^{N\text{-}term/\Delta DE}$ and KatG$^{N\text{-}term/\Delta FG}$ with KatG$^{C\text{-}term}$

After purification, KatG$^{\text{N-term}/\Delta DE}$ and KatG$^{\text{N-term}/\Delta FG}$ were reconstituted with one equivalent hemin and incubated at 4 °C for 24 hours. Then the reconstituted proteins were mixed with equimolar KatG$^{\text{C-term}}$. Peroxidase activity of the recombined domains was monitored over time. Maximal peroxidase activity was observed at 48 hours and 24 hours for recombined KatG$^{\text{N-term}/\Delta DE}$ and KatG$^{\text{N-term}/\Delta FG}$, respectively. Consequently, all spectral and kinetic measurements were taken 48 hours and 24 hours after recombination for KatG$^{\text{N-term}/\Delta DE}$ and KatG$^{\text{N-term}/\Delta FG}$, respectively, unless otherwise noted.

2.5 Protein Characterization

2.5.1 UV-visible absorption spectra

Following reconstitution of the enzymes, spectra were taken for wtKatG and all variants. These spectra were taken by scanning from 750 nm to 250 nm using Gilford Response-I or Shimadzu UV 1601 UV–Vis spectrophotometer (Shimadzu, Kyoto, Japan). Spectra taken included the ferric, ferrous, and ferri-cyano forms of the enzymes. To obtain the spectra of ferrous form of wtKatG and its variants, ~ 5 mg solid dithionite was added to the corresponding ferric forms. To obtain the spectra of ferri-cyano complexes of these proteins, 2 mM NaCN was added to the corresponding ferric forms. All spectral measurements were carried out at 23 °C in 100 mM phosphate buffer, pH 7.0.

2.5.2 Catalase and peroxidase activities

Catalase activity was evaluated by monitoring the decrease in H_2O_2 concentration over time as monitored at 240 nm. All assays were carried out at 23 °C in 100 mM phosphate buffer, pH 7.0, unless otherwise stated. All activities were normalized based on the heme content which is determined by the method of Falk [119].

Peroxidase activity was measured with both H_2O_2 and ABTS (2,2'-azinobis(3-

ethylbenzthiazoline-6-sulfonate)) (Figure 2.3) as the substrate. Peroxidase activity was evaluated by monitoring the generation of ABTS radical, $ABTS^{\bullet+}$, at 417 nm over time. $ABTS^{\bullet+}$ is generated by the one-electron oxidation of ABTS by the peroxidase activity of catalase-peroxidases. The molar absorptivity of $ABTS^{\bullet+}$ at 417 nm is 34.7 mM^{-1} cm^{-1}. All assays were carried out at 23 °C in 50 mM acetate buffer, pH 5.0. All activities were normalized based on the heme content which is determined by the method of Falk [119]. In some cases the maximal reaction rates were reached not at the beginning of a reaction, but with a lag phase. In these cases the lag time was determined by extrapolating two tangent lines of the initial reaction rate and the maximal reaction rate, and the time point where these two lines intersect is the lag time.

2.5.3 The pH profiles of wtKatG and KatG$^{\Delta FG}$

For their pH profiles on catalase activity, the catalase activities of wtKatG and $KatG^{\Delta FG}$ were measured and standaraized on the basis of their respective activity maxima, in the presence of 20 mM H_2O_2 and 100 mM phosphate buffer, pH ranging from 5.0 to 8.0, with 0.5 pH intervals, at 23 °C.

For their pH profiles on peroxidase activity, the peroxidase activities were measured and standaraized on the basis of their respective activity maxima, in the

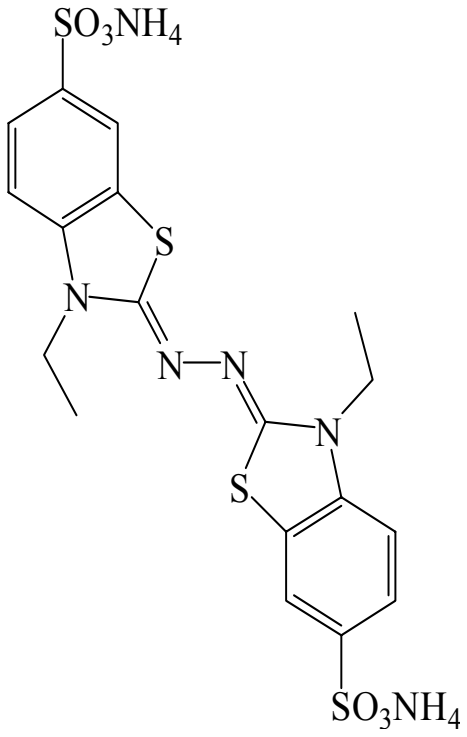

Figure 2.3. Structure of ABTS.

presence of 10 mM H_2O_2, 1 mM ABTS and 50 mM acetate buffer, pH ranging from 3.0 to 7.0, with 0.5 pH intervals, at 23 °C.

2.5.4 Stopped-flow kinetic studies on CN^- binding

CN^- binding by wtKatG and the variants was monitored, and the corresponding CN^- dissociation constants were determined using an SX.18MV Stopped-flow Reaction Analyzer (Applied Photophysics, Surrey, UK). CN^- binding is an effective way to evaluate the accessibility of the heme iron. All reactions were monitored in single mixing mode (Figure 2.4). One syringe contained the proteins of interests and the other syringe contained NaCN (20 μM to 2 mM). Spectral changes during a short period of time were recorded by diode array measurements and a suitable wavelength was chosen for following single wavelength measurements. Kinetic constants were determined from corresponding single wavelength measurement data. All reactions were carried out at 23 °C in 100 mM phosphate buffer, pH 8.0.

2.5.5 CN^- binding to the active site heme iron

CN^- binding to wtKatG and its variants was also monitored by visible spectroscopy on Shimadzu UV 1601 UV–vis spectrophotometer (Kyoto, Japan).

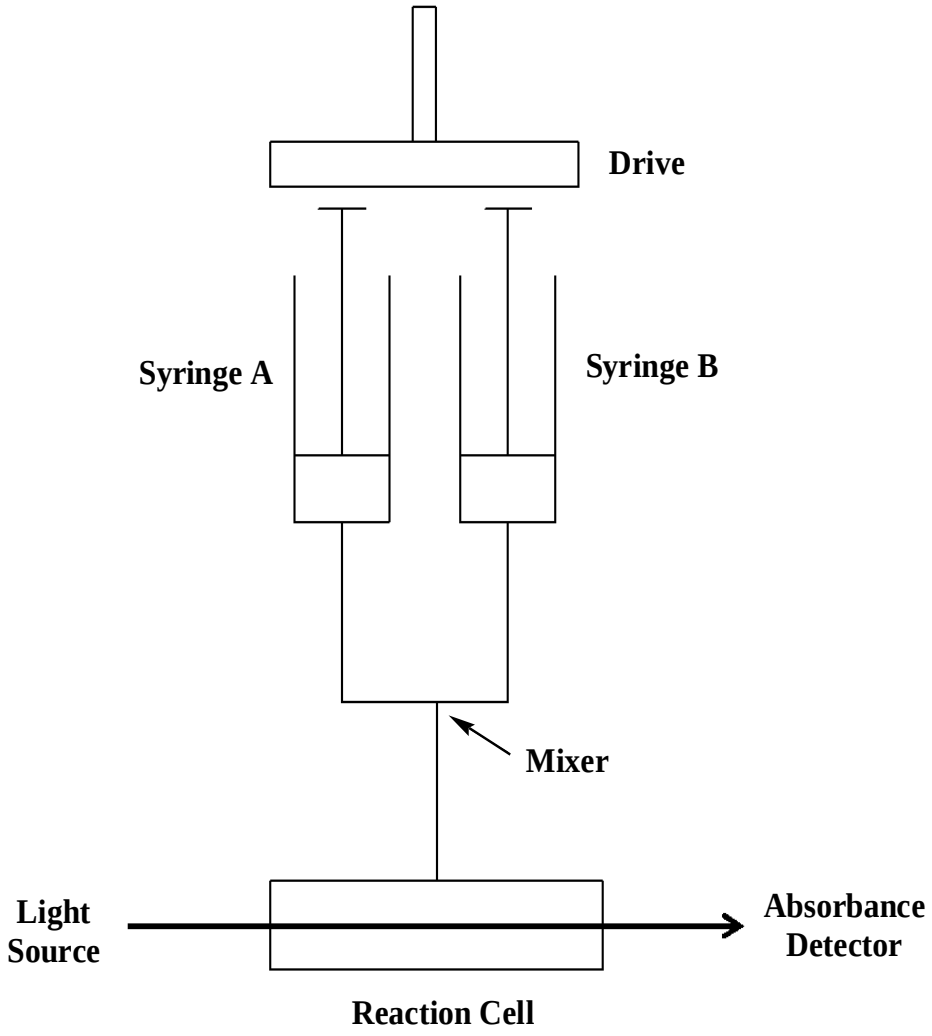

Figure 2.4. Diagram of Single Mixing Mode of Stopped Flow Reaction Analyzer.

These enzymes were treated with series concentrations of NaCN (1 μM to 4.56 mM), and resulting spectra were taken. Optimal wavelengths selected for calculation of dissociation constants for these enzymes were chosen based on the absorbance change extent due to the addition of CN^-. All measurements were taken at 23 °C in 100 mM phosphate buffer, pH 7.0.

2.5.6 Electron paramagnetic resonance spectroscopy

EPR spectra of reconstituted $KatG^{\Delta DE}$, $KatG^{\Delta FG}$, $KatG^{N\text{-}term/\Delta FG}$, and recombined $KatG^{N\text{-}term/\Delta FG}$ with $KatG^{C\text{-}term}$ were recorded on a Bruker EMX spectrometer. Spectrometer settings were as follows: center field, 2700 G; sweep width, 5000 G; microwave frequency, 9.38 GHz; microwave power, 0.10 mW; receiver gain, 1.0×10^5; modulation frequency, 100 kHz; modulation amplitude, 10 G; conversion time, 655.36 ms; time constant, 655.36 ms; and temperature, 10 K.

2.5.7 Far-UV circular dichroism spectra

Far-UV CD spectra (180 – 300 nm) were recorded for wtKatG and $KatG^{\Delta DE}$ prior to and after reconstitution on a Jasco J-810 Spectrapolarimeter (Kyoto, Japan). All measurements were carried out in 10 mM phosphate buffer, pH 7.0, at 23 °C.

CHAPTER THREE

RESULTS

3.1 wtKatG

3.1.1 Expression, and isolation of wtKatG

The *katG* gene was successfully integrated into pET-20b plasmid. The enzyme was expressed in soluble form and included a six His-tag. After purification, roughly 2 x 10^{-6} moles of wtKatG could be obtained per liter of LB broth. The size of the target protein as measured by denaturing electrophoresis was consistent with wtKatG, including a six His-tag (data not shown). Inclusion of δ-amino levulinic acid and ferrous ammonium sulfate has been reported to enhance the heme content of many hemoproteins [120]. However, this effect was not observed with our wtKatG. Routinely, less the 10% of the expressed and isolated wtKatG contained heme. Thus, reconstitution of the purified enzyme with exogenous hemin was required to observe maximal activity.

3.1.2 Reconstitution of wtKatG

Because wtKatG expressed as described above did not have adequate heme content, addition of external heme to the active site was required. We observed that reconstitution of wtKatG can be simply achieved by addition of dissolved hemin (in 100 mM KOH) to solutions containing apo-KatG, and the incorporation of hemin to the active site was very rapid. This highlights one of the major advantages of working with KatG. High-level expression of prosthetic group-requiring enzymes often results in large proportions of apoenzyme. However, this is usually very difficult if not impossible to remedy following expression and purification.

The incorporation of hemin in the active site of wtKatG was evaluated by measuring catalase activity, peroxidase activity, and visible spectral changes reflecting changes in the environment of the hemin. Addition of up to one equivalent hemin resulted in a linear increase in the catalase (Figure 3.1) and peroxidase (data not shown) activities of wtKatG. No further increase in either activity was observed above one equivalent of added hemin (Figure 3.1), indicating exclusive incorporation of hemin within the active site. The binding of hemin to wtKatG as a function of hemin concentration was also monitored by visible absorption spectra. A linear increase in absorbance at 408 nm, the wavelength maximum of the Soret band of heme in wtKatG, was observed with increasing hemin concentration up to one equivalent as well (data not shown). Over the same hemin concentration range, the ratio of absorbance at 408 nm to 370 nm remained constant (Figure 3.2). Together with the activity changes, this confirms that the hemin added was exclusively

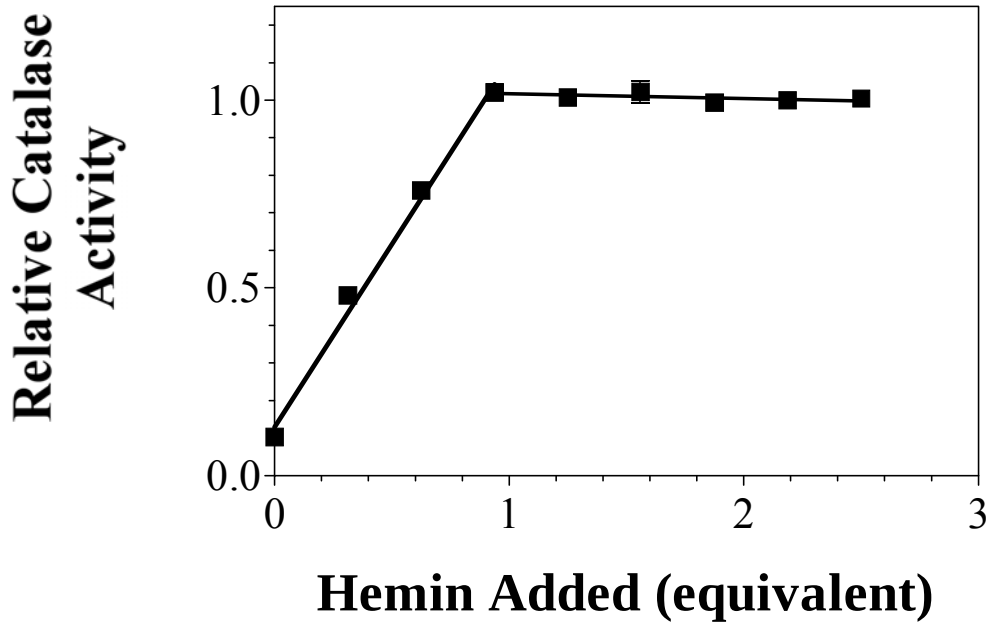

Figure 3.1. Change in Catalase Activity of wtKatG with Hemin Reconstitution.

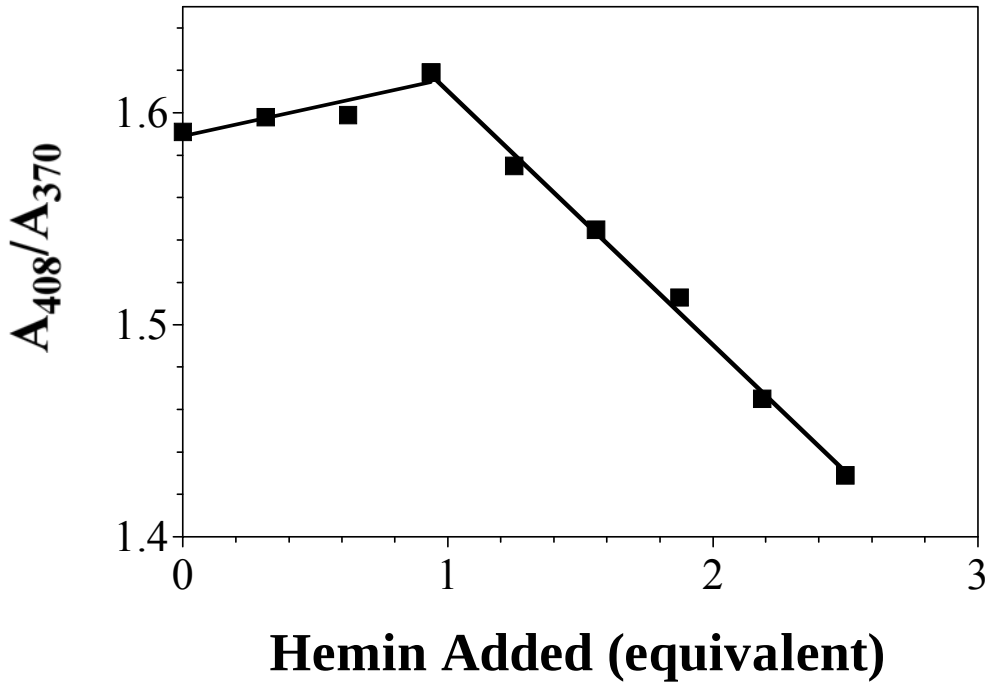

Figure 3.2. Change in Ratio of Absorbance at 408 nm and 370 nm of wtKatG with Hemin Reconstitution.

incorporated in the active site. When hemin was added beyond one equivalent, increases in absorbance at 408 nm were still observed. However, the slope of the increase was smaller (data not shown). More importantly, the ratio of absorbance at 408 nm to 370 nm decreased sharply at hemin concentrations in excess of one equivalent (Figure 3.2), indicating an increase in hemin free in solution or adventitiously bound to wtKatG. Taken together, these data indicated that hemin was taken up in the active site exclusively until the full occupation of the active sites. Given the immediate incorporation of the hemin into the active site, our results suggested that the reconstitution of wtKatG could be easily and effectively achieved by the addition of hemin to the protein. To minimize effects of free hemin or adventitiously bound hemin on spectral or kinetic measurements, wtKatG was reconstituted with 0.75 equivalents hemin in the studies of this dissertation, unless otherwise stated. Hemin concentration was determined by the method of Falk [119].

3.1.3 UV-visible spectra of wtKatG

Following reconstitution with hemin, UV-visible absorption spectra were recorded for the ferric, ferrous, and ferri-cyano forms of wtKatG (Figure 3.3). In the ferric state, the Soret maximum (408 nm) and charge transfer maxima (508 and 642 nm) are consistent with a mixture of states dominated by penta-coordinate and hexa-coordinate high-spin heme iron [116, 121, 122]. The penta-coordinate high-spin species dominates in the ferrous state, as indicated by a Soret maximum of 438 nm in

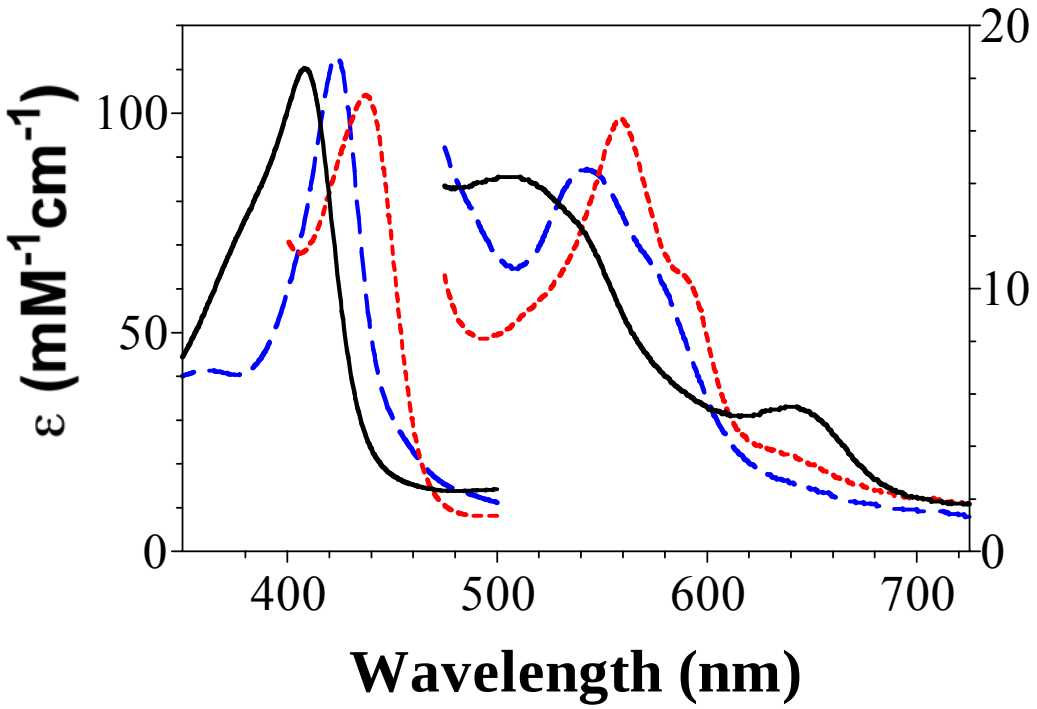

Figure 3.3. Absorption Spectra Recorded for Ferric (solid line), Ferrous (dotted line), and Ferri-cyano (dashed line) Forms of wtKatG.

addition to a strong β band at 560 nm and a relatively weak α band at 588 nm [121]. The addition of cyanide anion to ferric wtKatG resulted in a red-shift in Soret band to 424 nm and an additional maximum at 543 nm, which are indicative of a hexacoordinate, low-sin complex. All UV-visible spectra were consistent with results observed for other catalase-peroxidases [121].

3.1.4 The pH profiles of wtKatG

The activities of KatG are pH dependent. Typically, the optimal pHs for catalase and peroxidase activities are around pH 7.0 [121, 123-125] and pH 5.0 [121, 126], respectively. The pH dependence of the catalase activity of wtKatG followed a well-defined bell-shaped curve. Optimal catalase activity was observed near pH 6.5 (Figure 3.4). Meanwhile, the optimal pH for its peroxidase activity was observed around pH 5.0 (Figure 3.5). The pH optima for both activities are consistent with other catalase-peroxidases.

3.1.5 Kinetic parameters of wtKatG

Consistent with its classification as a catalase-peroxidase, wtKatG showed substantial catalase and peroxidase activities. Both activities were evaluated by steady-state kinetic methods. The catalase activity of wtKatG showed a hyperbolic

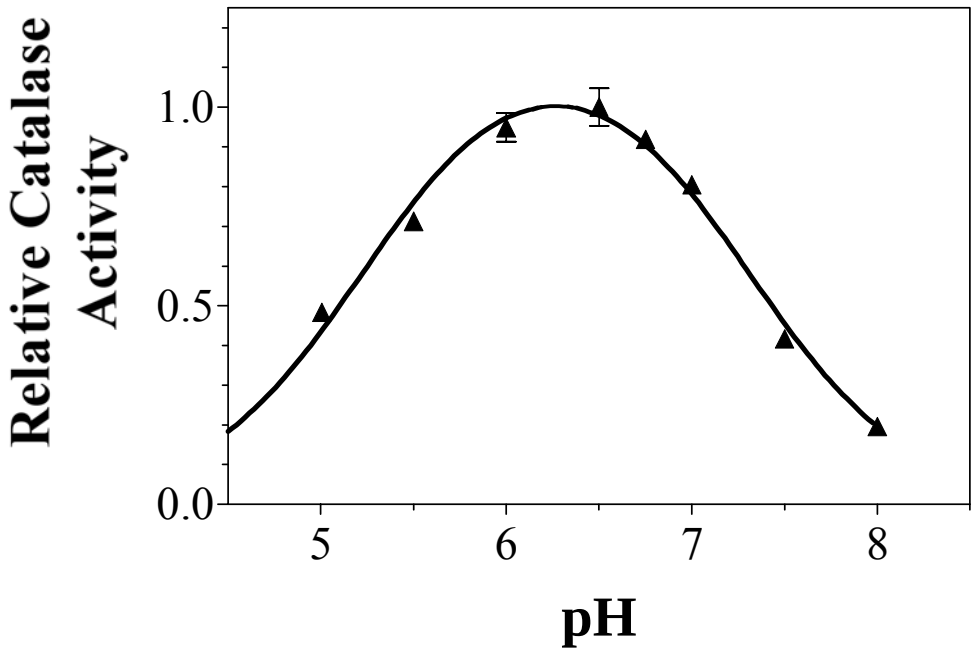

Figure 3.4. Effect of pH on Catalase Activity of wtKatG.

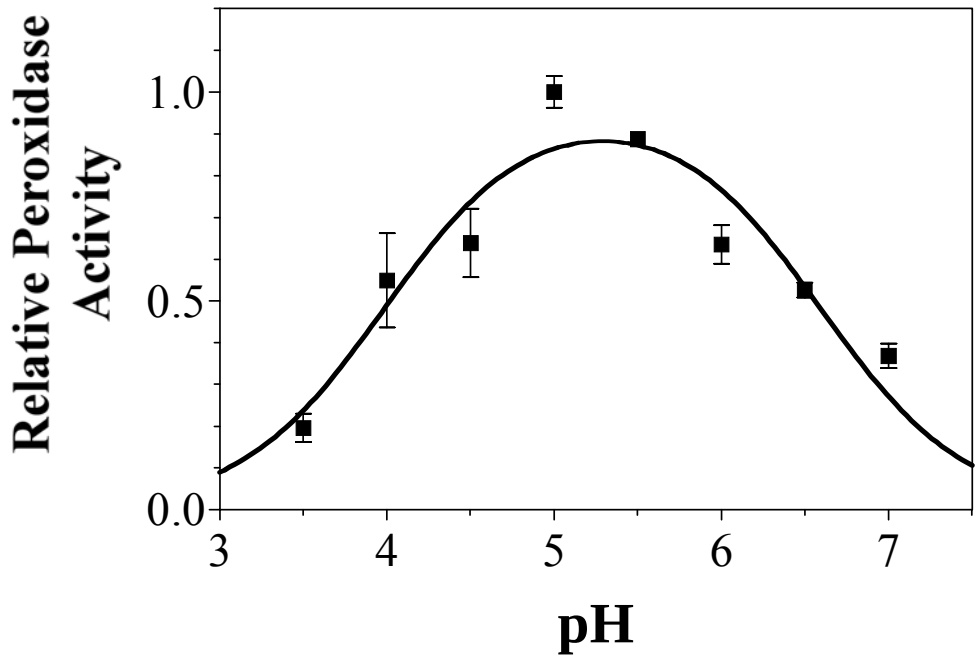

Figure 3.5. Effect of pH on Peroxidase Activity of wtKatG.

dependence on H_2O_2 concentration (Figure 3.6). From these data, an apparent k_{cat} of 1.1×10^4 s^{-1} and an apparent K_M of 3.9 mM for H_2O_2 were obtained. An apparent second-order rate constant of 2.8×10^6 $M^{-1}s^{-1}$ was calculated from these results.

In light of the fact that peroxidase activity requires both a hydroperoxide substrate and a reducing substrate, the dependence of activity was measured as a function of H_2O_2 concentration and ABTS concentration. The peroxidase activity of wtKatG showed a hyperbolic dependence on both H_2O_2 concentration and ABTS concentration (Figure 3.7 and Figure 3.8). With respect to H_2O_2, the peroxidase activity of wtKatG showed an apparent k_{cat} of 58 s^{-1} and an apparent K_M of 0.83 mM, which gave an apparent second-order rate constant of 7.1×10^4 $M^{-1}s^{-1}$. With respect to ABTS, the peroxidase activity of wtKatG showed an apparent k_{cat} of 52 s^{-1} and an apparent K_M of 0.23 mM, which gave an apparent second-order rate constant of 2.2×10^5 $M^{-1}s^{-1}$.

3.1.6 Far-UV CD spectrum of wtKatG

To evaluate the composition of secondary structural features in wtKatG, far-UV CD spectrum of reconstituted wtKatG was recorded using a Jasco J-810 Spectrapolarimeter (Tokyo, Japan) (Figure 3.9). This spectrum bears high resemblance to CD spectra recorded for other catalase-peroxidases [116]. The strong

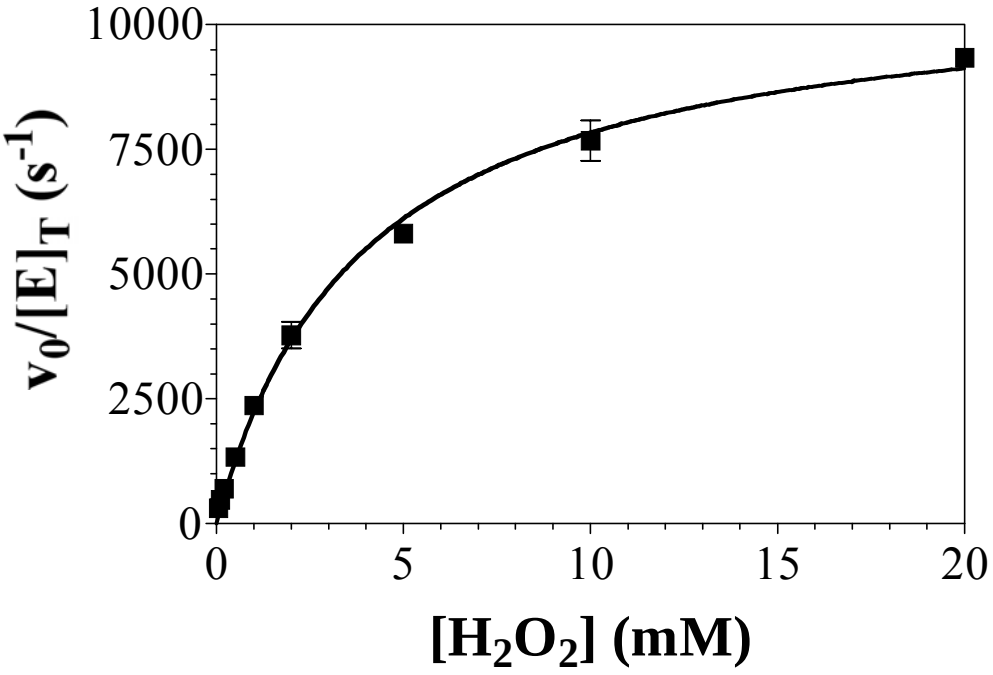

Figure 3.6. Effect of H_2O_2 Concentration on the Catalase Activity of wtKatG.

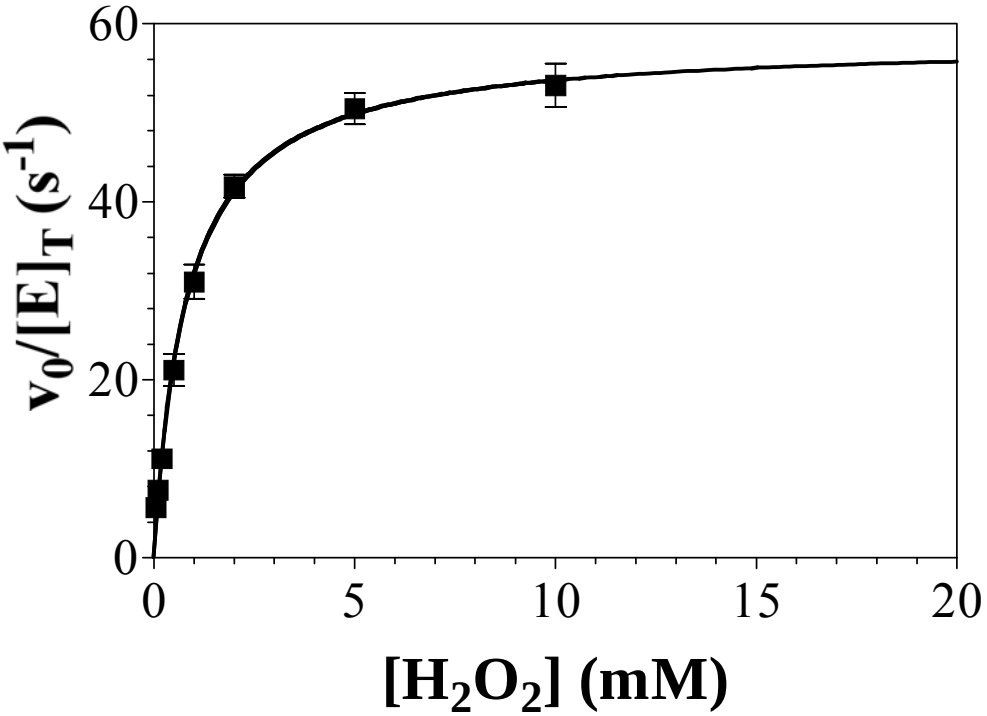

Figure 3.7. Effect of H_2O_2 Concentration on the Peroxidase Activity of wtKatG.

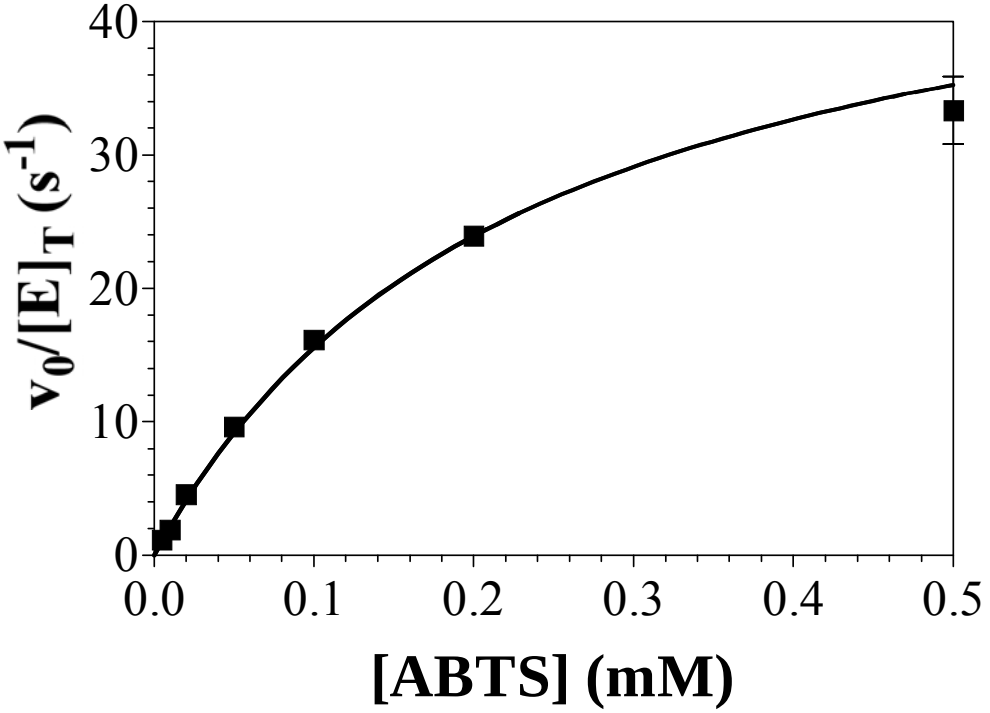

Figure 3.8. Effect of ABTS Concentration on the Peroxidase Activity of wtKatG.

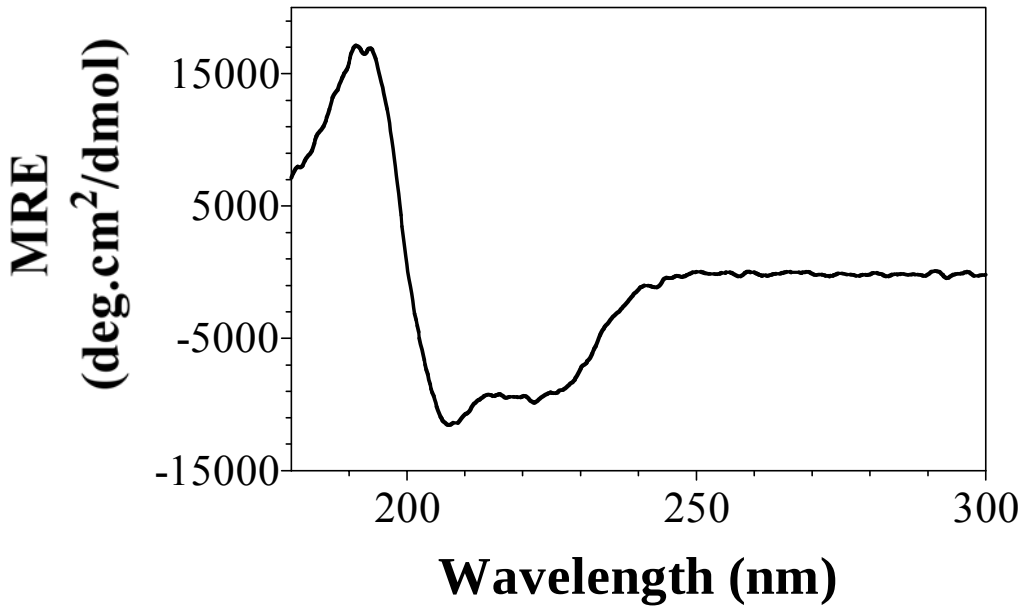

Figure 3.9. Far-UV CD Spectrum Recorded for Reconstituted wtKatG.

negative signals at 222 nm and 208 nm represent substantial α–helical content in the structure, and the positive signal at 190 nm is contributed by both α–helix and β–sheet. The resulting spectrum was analyzed using the K2D algorithm [127, 128]. The results indicated there were 29% α-helicity, and 15% β-sheet composition in the structure of wtKatG, which is compatible with the high percentage of α–helices in wtKatG.

3.1.7 Stopped-flow kinetic studies of CN^- binding to wtKatG

The accessibility of the heme iron of wtKatG to peroxide substrates can be evaluated by the ability of added CN^- to bind the heme and form the Fe^{III}-CN complex. The dissociation constant of CN^-, K_D, was evaluated by stopped-flow kinetic methods. The change in absorbance due to the coordination of CN^- was monitored over a short period of time (several milliseconds). In each trace, the observed rate constant, k_{obs}, was related to the rate constants k_{on} and k_{off} according to the following equation:

$$k_{obs} = k_{off} + k_{on} [CN^-]$$

The k_{obs} values were calculated at different NaCN concentrations and a linear relationship between the k_{obs} value and the NaCN concentration was obtained (Figure 3.10). A k_{on} value of 6.67×10^5 $M^{-1}s^{-1}$ was calculated from the graph. However, the k_{off} value, 9.7 ± 8.9 s^{-1}, was difficult to establish precisely because of the high standard deviation of the measurement. Thus, a precise K_D value was not obtained.

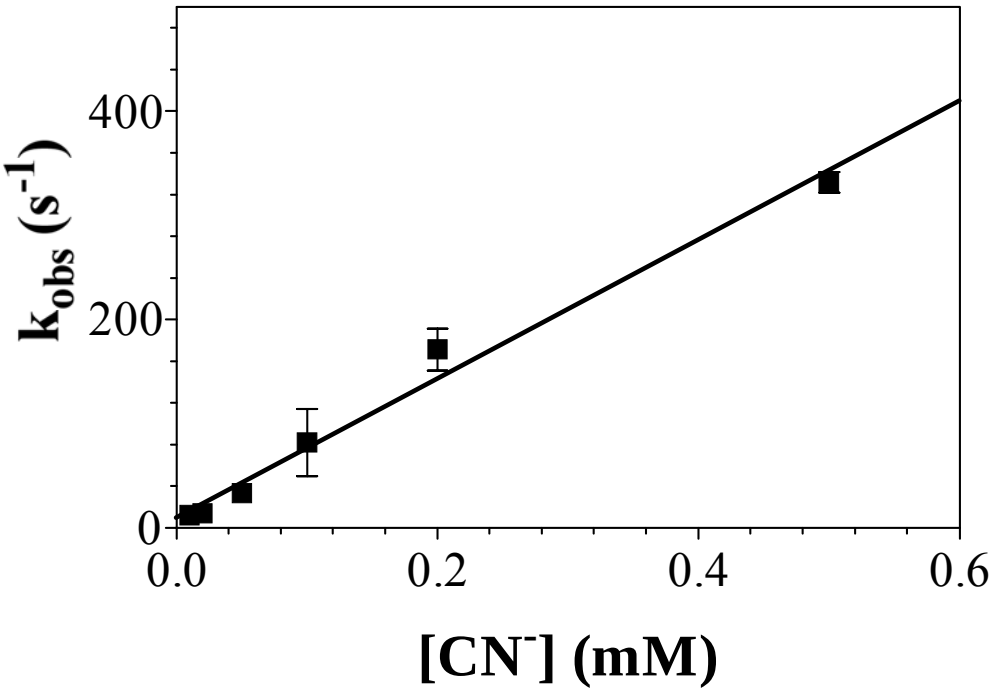

Figure 3.10. Effect of Cyanide Concentration on the Rate of Formation of the Fe^{III}-CN Complex of wtKatG.

3.1.8 Studies of CN^- binding to wtKatG by visible spectra

The accessibility of the heme iron of wtKatG was also evaluated by visible spectral study upon the addition of CN^-. The visible spectrum of wtKatG indicated a mainly penta-coordinate heme. Upon the addition of CN^-, the Soret band red-shifted from 408 nm to 424 nm gradually, indicating a change from penta-coordinate high-spin to hexa-coordinate low-spin heme species, concomitant with the increase in absorbance at 423.6 nm (Figure 3.11). A K_D value (the CN^- concentration which gave half of the maximal absorbance change) of 1.0 μM was obtained.

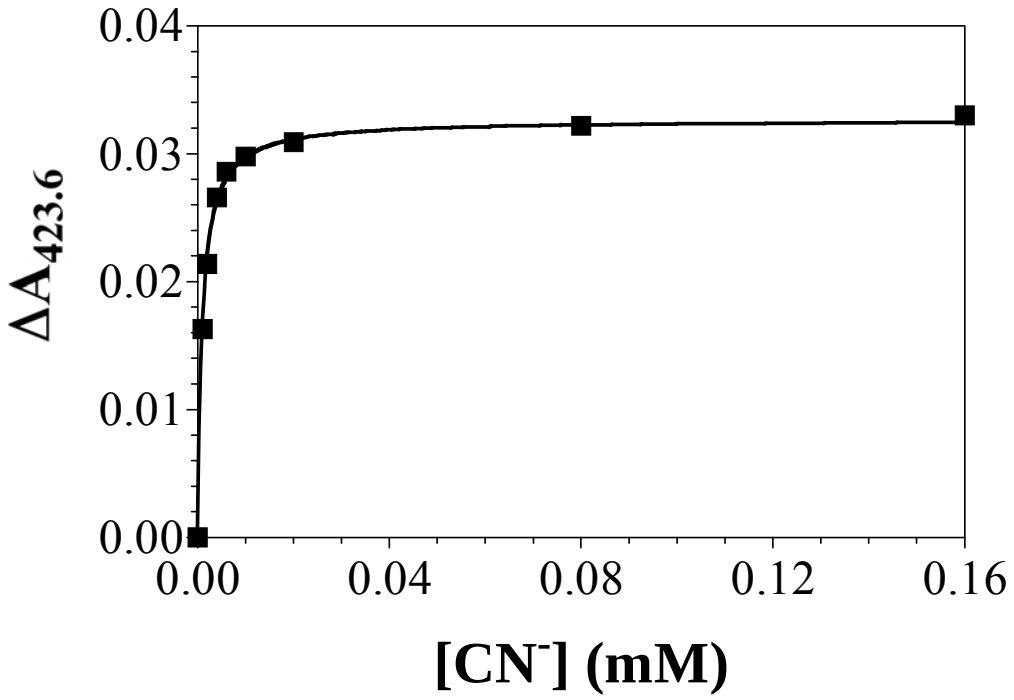

Figure 3.11. Change in Absorbance at 423.6 nm with Cyanide Added to wtKatG.

3.2 *KatG$^{\Delta FG}$*

3.2.1 Mutagenesis, expression, and isolation of KatG$^{\Delta FG}$

We first developed a deletion mutagenesis procedure to specifically delete the FG insertion from *E. coli* catalase-peroxidase (KatG). The codons corresponding to Pro 277 – Thr 311 (i.e., the FG insertion) were eliminated from the *katG* gene. The resulting variant, KatG$^{\Delta FG}$, was expressed the same way as wtKatG except for that no δ-amino levulinic acid and ferrous ammonium sulfate were supplemented during expression. Roughly 5×10^{-7} moles of KatG$^{\Delta FG}$ were routinely obtained per liter of LB broth. Electrophoretic migration of the KatG$^{\Delta FG}$ monomer evaluated by SDS-PAGE was consistent with elimination of the targetted 35 amino-acid segment (data not shown).

3.2.2 Reconstitution of KatG$^{\Delta FG}$

Like wtKatG, titration of KatG$^{\Delta FG}$ with hemin resulted in a linear increase in peroxidase activity up to one equivalent. Addition of hemin beyond this point does not contribute any additional activity. To minimize effects of free or adventitiously bound hemin to spectral or kinetic measurements, KatG$^{\Delta FG}$ was also reconstituted

with 0.75 equivalents hemin in all studies in this dissertation, unless otherwise stated. Hemin concentration was determined by the method of Falk [119].

3.2.3 UV-Visible spectra of KatG$^{\Delta FG}$

Following reconstitution with hemin, UV-visible absorption spectra were recorded for the ferric, ferrous, and ferri-cyano forms of KatG$^{\Delta FG}$ (Figure 3.12). In the ferric state, the Soret maximum (408 nm) and charge transfer maxima (501 and 637 nm) are consistent with a mixture of states dominated by penta-coordinate and hexa-coordinate high-spin heme iron. A very weak shoulder at ~ 535 nm suggests a minor contribution from hexa-coordinate low-spin heme. The penta-coordinate high-spin species dominates in the ferrous state, as indicated by a Soret maximum of 438 nm in addition to a strong β band at 561 nm and a relatively weak α band at 590 nm. All spectra for KatG$^{\Delta FG}$ were highly similar to wtKatG, suggesting that removal of the FG insertion had little effect on the heme environment.

The most prominent spectral difference between wtKatG and KatG$^{\Delta FG}$ was the lower molar absorptivities for the absorption bands of the hemin in the KatG$^{\Delta FG}$ ferric state compared to wtKatG. One possible explanation would be that a portion of the hemin from reconstitution remained unbound by the enzyme. However, we have recently been able to express and isolate KatG$^{\Delta FG}$ in its holoenzyme form using an expression system developed in our laboratory [129]. We observe spectral and catalytic properties highly similar to the reconstituted enzyme (data not shown).

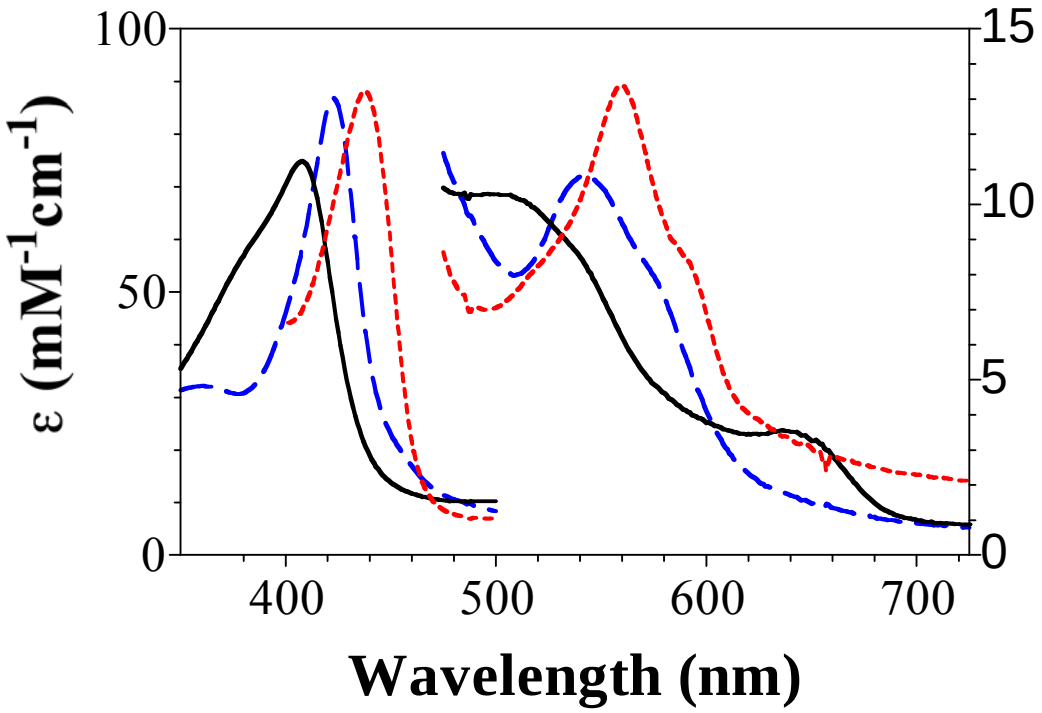

Figure 3.12. Absorption Spectra Recorded for Ferric (solid line), Ferrous (dotted line), and Ferri-cyano (dashed line) Forms of $KatG^{\Delta FG}$.

3.2.4 Electron paramagnetic resonance spectroscopy of KatG$^{\Delta FG}$

The EPR spectrum of KatG$^{\Delta FG}$ is consistent with other catalase-peroxidases and monofunctional peroxidases [130-133]. The rhombic signals at g = 6.69, 4.97, and 1.95 were contributed by penta-coordinate high-spin heme species. The axial signals at g = 5.75, and 1.99 indicated the presence of hexa-coordinate high-spin heme species (Figure 3.13).

3.2.5 Catalase and peroxidase activities of KatG$^{\Delta FG}$

Removal of the FG insertion produced a precipitous reduction in catalase activity, decreasing the apparent second-order rate constant by a factor of ~ 500 from 2.8×10^6 $M^{-1}s^{-1}$ to 5.7×10^3 $M^{-1}s^{-1}$ when compared to wtKatG. This effect was due primarily to a decrease in k_{cat} from 1.2×10^4 s^{-1} for wtKatG to 26 s^{-1} for KatG$^{\Delta FG}$. The apparent K_M for H_2O_2 as measured from catalase activity was 4.5 mM, essentially unchanged compared to wtKatG. In addition to the sharp decrease in catalase activity, a change in pH dependence was observed. The pH optimum shifted slightly from ~ pH 6.5 to ~ 7.0. More strikingly, the decrease in activity below pH 7.0 was much more dramatic with KatG$^{\Delta FG}$ than wtKatG. (Figure 3.14).

Compared to wtKatG, KatG$^{\Delta FG}$ retained appreciable peroxidase activity. With respect to H_2O_2, a k_{cat} value of 28 s^{-1} was obtained, roughly half of that observed for wtKatG (Figure 3.15). A K_M value of 2.2 mM was observed, representing a moderate

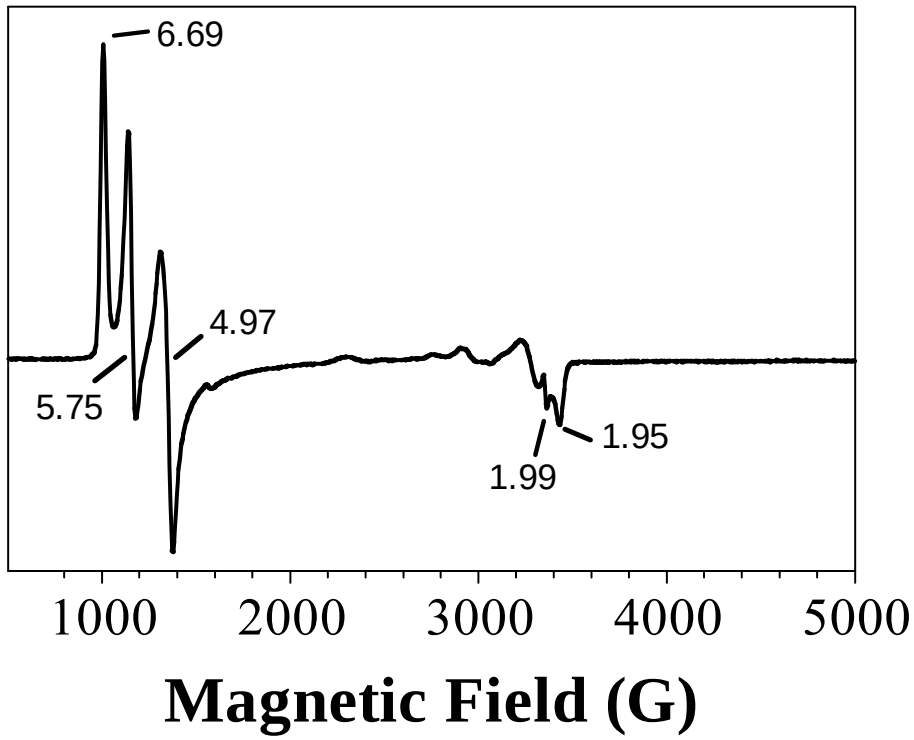

Figure 3.13. EPR Spectrum Recorded for $KatG^{\Delta FG}$.

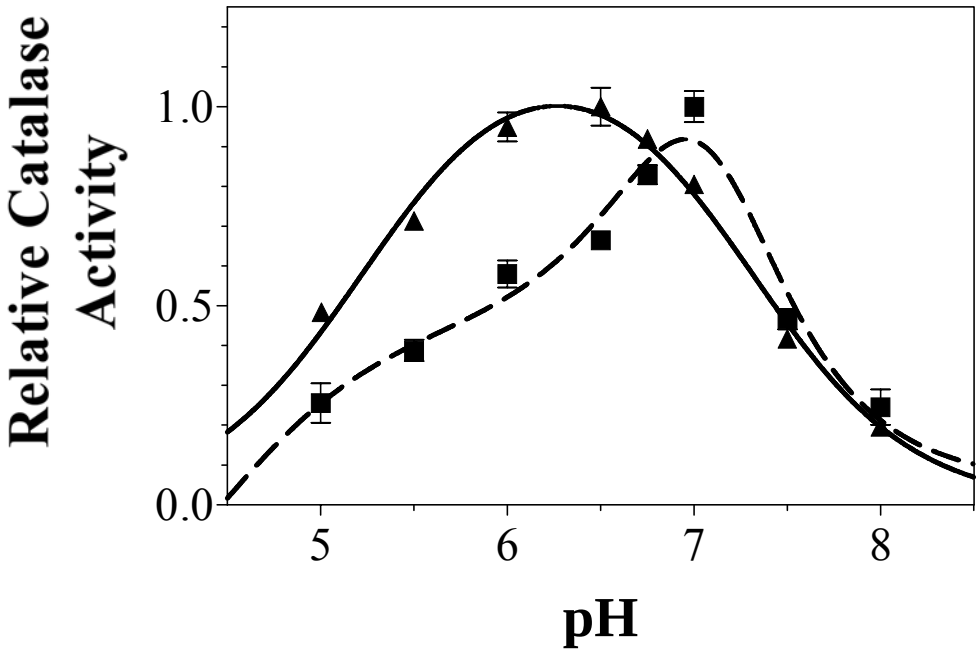

Figure 3.14. Comparison of pH Optima for Catalase Activity of wtKatG (▲) and $KatG^{\Delta FG}$ (■).

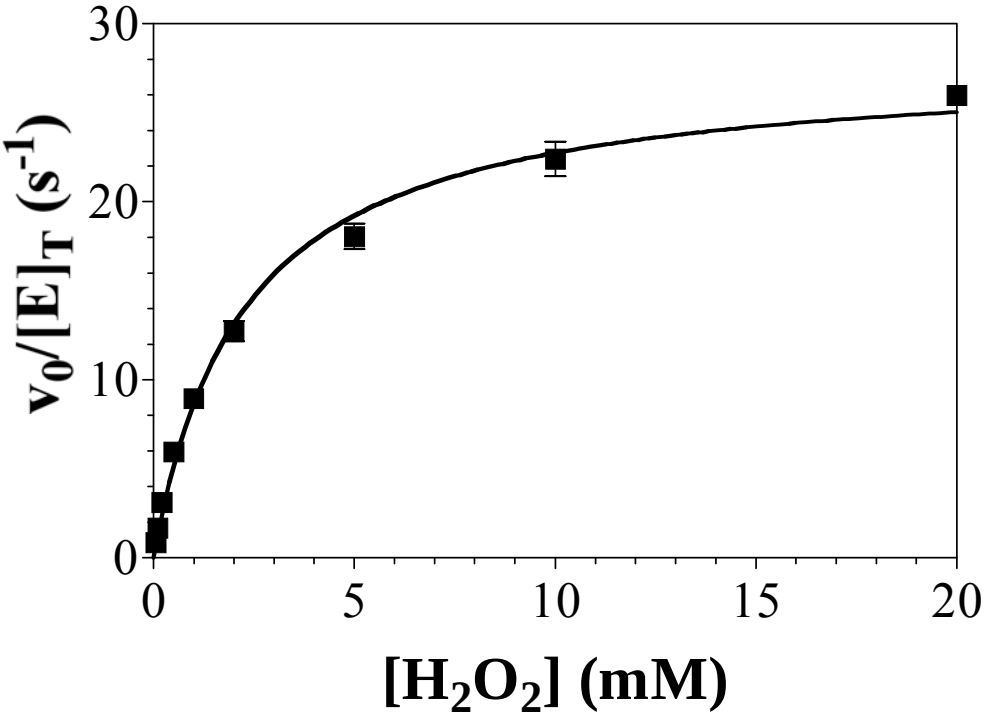

Figure 3.15. Effect of H_2O_2 Concentration on Peroxidase Activity of $KatG^{\Delta FG}$.

increase (~ two fold) compared to wtKatG. From these, an apparent second-order rate constant of 1.3×10^4 $M^{-1}s^{-1}$ was obtained. With respect to ABTS as the substrate, a k_{cat} of 28 s^{-1} was also observed (Figure 3.16). However, a dramatic decrease in the apparent K_M for ABTS was detected (0.012 mM vs. 0.23 mM). Consequently, the removal of the FG insertion resulted in a ten-fold increase in the apparent second order rate constant (2.2×10^6 $M^{-1}s^{-1}$ for $KatG^{\Delta FG}$ vs. 2.2×10^5 $M^{-1}s^{-1}$ for wtKatG).

The kinetic parameters obtained with respect to H_2O_2 have been used to describe reactions leading to the formation of compound I. Elimination of the FG insertion led to a five-fold decrease in the apparent second-order rate constant (k_{H2O2}) governing these steps. On the other hand, kinetic parameters obtained with respect to the reducing substrate (in this case ABTS) describe the reactions that result in conversion of compound I back to ferric enzyme. The apparent second-order rate constant (k_{ABTS}) governing these steps increased by a factor of ten. Regardless of the changes in peroxidase kinetic parameters, the pH profiles for peroxidase activity of $KatG^{\Delta FG}$ remained essentially unchanged compared to wtKatG. Peroxidase activities showed a sharp pH dependence with optimal peroxidase activity observed around pH 5.0 (Figure 3.17), which is the same as wtKatG.

In addition to a dramatically reduced K_M for ABTS, we also observed ABTS-dependent inhibition of $KatG^{\Delta FG}$ peroxidase activity at concentrations above 0.1 mM (Figure 3.16). At 1 mM ABTS, a 33% decrease in activity from the recorded maximum was observed. No inhibition was apparent for wtKatG over this same

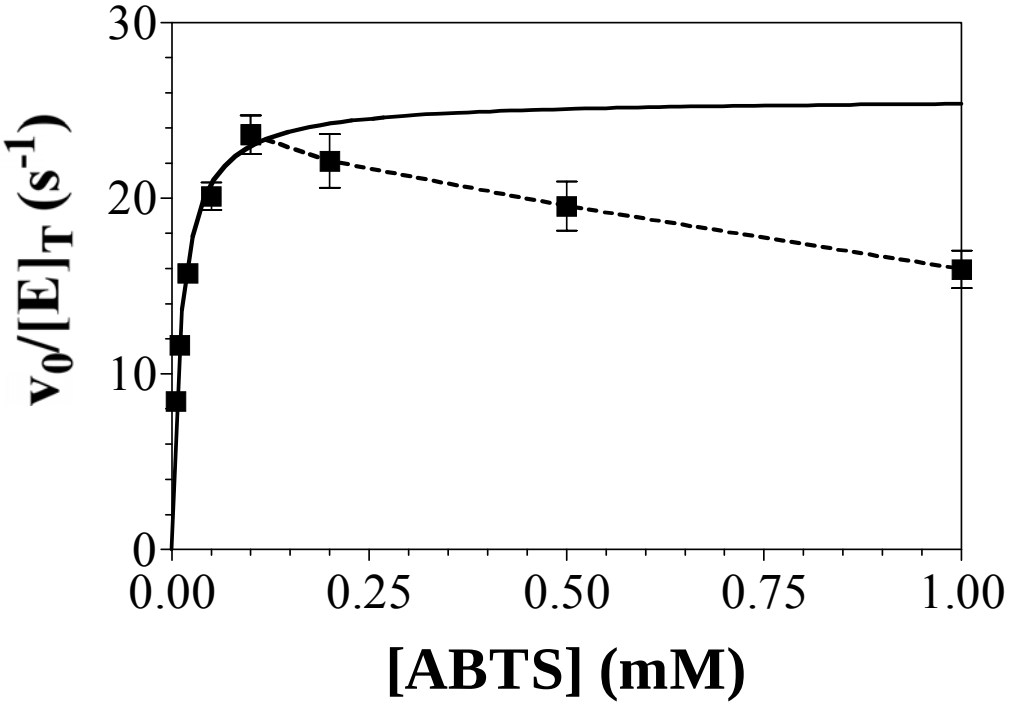

Figure 3.16. Effect of ABTS Concentration on Peroxidase Activity of $KatG^{\Delta FG}$.

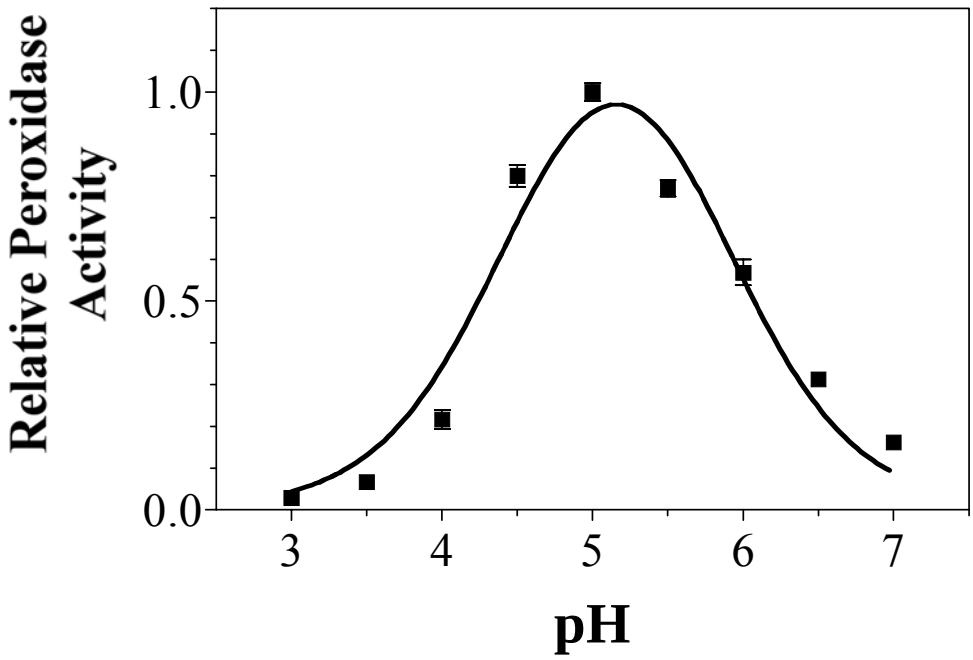

Figure 3.17. Effect of pH on Peroxidase Activity of $KatG^{\Delta FG}$.

concentration range. Likewise, the peroxidase activity of neither wtKatG nor KatG$^{\Delta FG}$ was sensitive to peroxide-dependent inhibition.

3.2.6 Far-UV CD spectrum of KatG$^{\Delta FG}$

The far-UV CD spectra of apo-KatG$^{\Delta FG}$ and reconstituted KatG$^{\Delta FG}$ both bear high similarity to that of wtKatG (Figure 3.18), indicating there was no global misfolding of the protein due to removal of the FG insertion. These spectra were analyzed using the K2D algorithm [127, 128], and the results indicated there was 30% helicity and 12% β-sheet in the structure of both apo-KatG$^{\Delta FG}$ and reconstituted KatG$^{\Delta FG}$. The results are compatible with the loss of β-sheet composition when the FG insertion was removed from wtKatG.

3.2.7 Studies of CN^- binding to KatG$^{\Delta FG}$ by visible spectra

Like wtKatG, the visible spectrum of KatG$^{\Delta FG}$ also showed a mainly penta-coordinate heme. Upon the addition of CN^-, the spectrum gradually changed in accordance with the appearance of a hexa-coordinate low-spin heme as evident in the increase in absorbance at 423.5 nm (Figure 3.19). A K_D value of 14.5 μM was obtained. This represents a 15 fold increase compared to that measured for wtKatG by the same method.

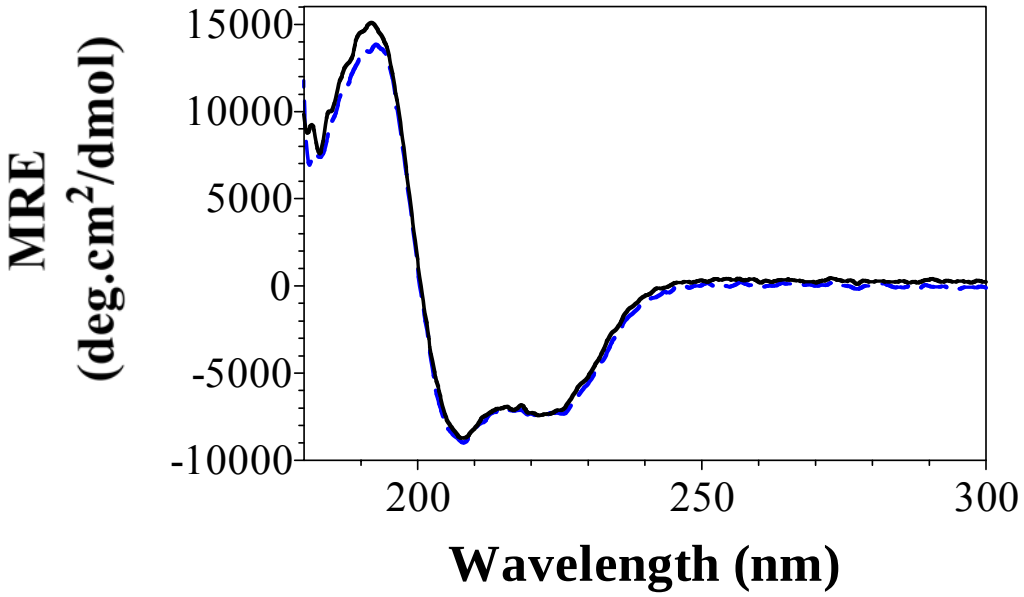

Figure 3.18. Far-UV CD Spectra of apo-KatG$^{\Delta FG}$ (solid line) and Reconstituted KatG$^{\Delta FG}$ (dashed line).

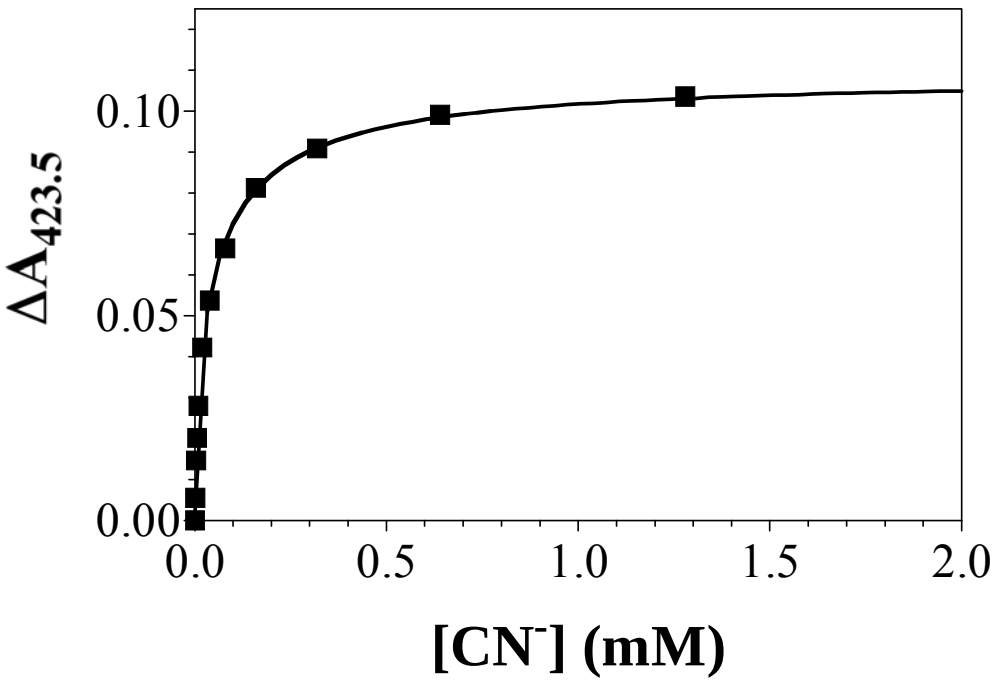

Figure 3.19. Change in Absorbance at 423.5 nm with Cyanide Added to KatG$^{\Delta FG}$.

3.3 KatG$^{\Delta DE}$

3.3.1 Mutagenesis, expression, purification, and reconstitution of KatG$^{\Delta DE}$

Using our seamless deletion mutagenesis procedure, the DE insertion of KatG (Leu193 – Asn228) was successfully eliminated. The resulting variant, KatG$^{\Delta DE}$, was expressed by the same methods as KatG$^{\Delta FG}$. However, unlike wtKatG and KatG$^{\Delta FG}$, KatG$^{\Delta DE}$ was expressed in inclusion bodies. Thus, the purification of this variant was accomplished under denaturing conditions. Refolding was accomplished using dialysis against buffer **A** (50 mM phosphate buffer, pH 8.0; 200 mM NaCl). Our SDS-PAGE analysis showed a band consistent with the elimination of the 36 amino acid segment from wtKatG (data not shown). Routinely, we obtained 5×10^{-8} moles of purified KatG$^{\Delta DE}$ per liter of LB broth.

Following purification and refolding, KatG$^{\Delta DE}$ was reconstituted with hemin. The peroxidase activity of the variant increased linearly with hemin added up to 0.25 equivalents, after which no further increase in peroxidase activity was observed. Optimal activity was observed 18 hours (4 °C) after reconstitution. Based on these observations, all KatG$^{\Delta DE}$ used for assays and spectra was reconstituted with 0.25 equivalents of hemin and incubated on ice for 18 hours, unless otherwise stated.

3.3.2 UV-visible spectra of KatG$^{\Delta DE}$

Spectra of ferric, ferrous, and ferri-cyano forms of KatG$^{\Delta DE}$ were recorded (Figure 3.20). Compared to wtKatG, KatG$^{\Delta DE}$ showed a 2 nm red shift in Soret λ_{max} from 408 nm to 410 nm. A broad mixture of spectral features from 500-550 nm as well as a persistent long-wavelength charge transfer transition (645 nm) was also observed. These data suggested the presence of high-spin species, as well as a substantial contribution from hexa-coordinate low-spin complex.

3.3.3 CD spectra of KatG$^{\Delta DE}$

CD spectrum of apo-KatG$^{\Delta DE}$ showed a similar pattern to that of wtKatG, indicating no significant overall structural change occurred when DE insertion was removed from the enzyme (Figure 3.21). However, small deviations between the spectra suggested that some adjustments had taken place to adjust for the missing amino acids. This adjustment was confirmed by fitting the data using the K2D algorithm [127, 128], which indicated 29% α-helicity, 13% β-sheet content for KatG$^{\Delta DE}$. CD spectra of 0.25 equivalent hemin reconstituted KatG$^{\Delta DE}$ immediate and 22 hours after reconstitution were also recorded (Figure 3.21). Though not dramatic, reconstitution of KatG$^{\Delta DE}$ with hemin showed both immediate and gradual effects on the enzyme structure. Fitting these data to the K2D algorithm gave us 30% helicity, 12% β-sheet content and 31% helicity, 12% β-sheet content for KatG$^{\Delta DE}$ immediate

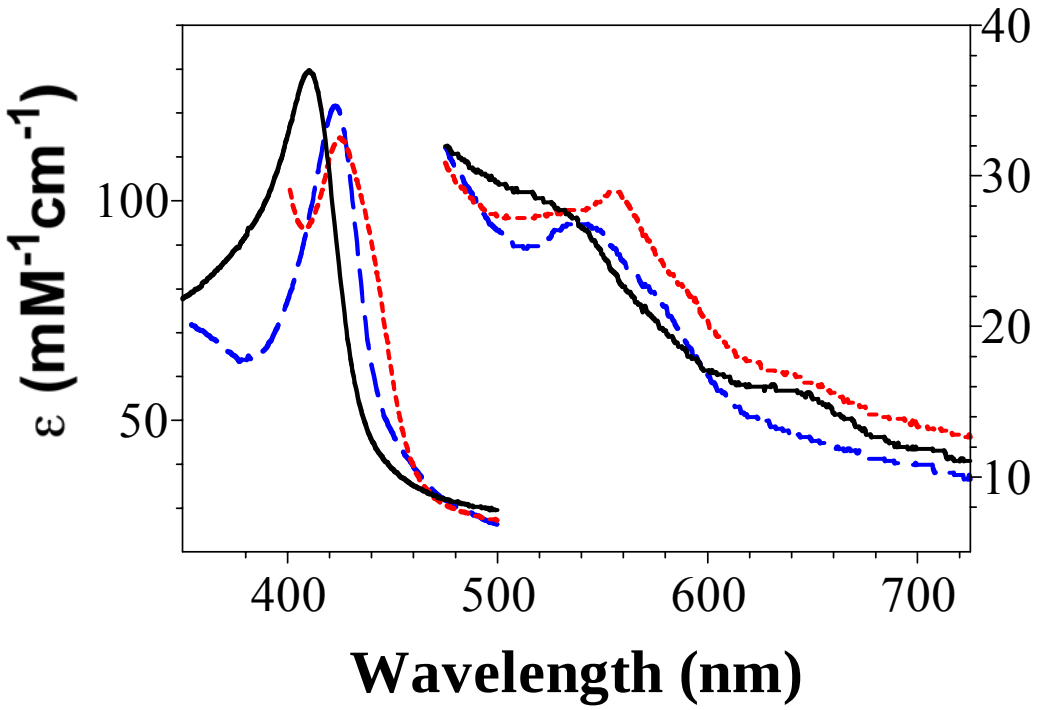

Figure 3.20. Absorption Spectra Recorded for Ferric (solid line), Ferrous (dotted line), and Ferri-cyano (dashed line) Forms of KatG$^{\Delta DE}$.

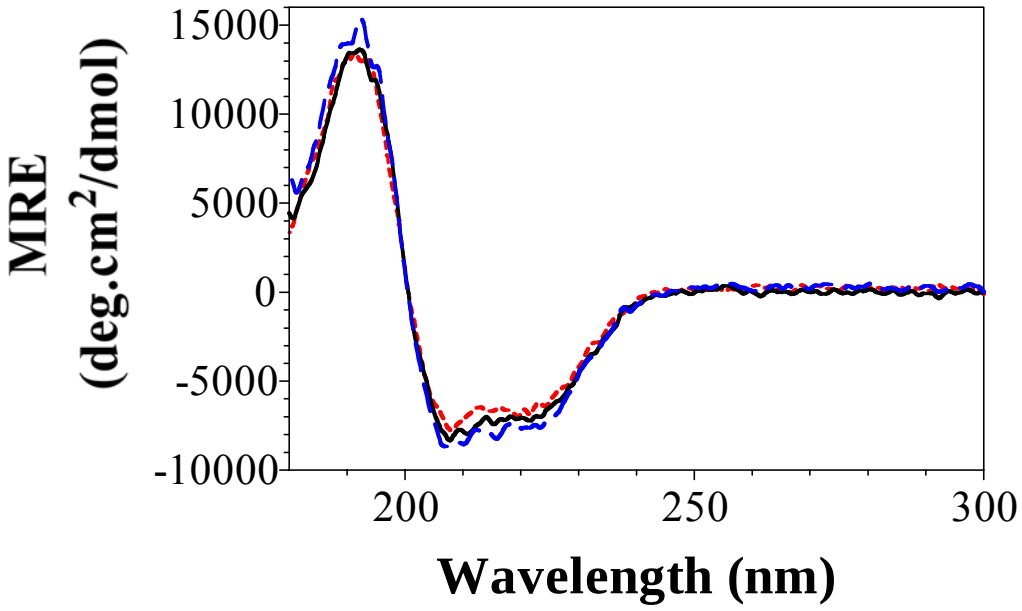

Figure 3.21. Far-UV CD Spectra of apo-KatG$^{\Delta DE}$ (dashed line), KatG$^{\Delta DE}$ 0 Hour After Reconstitution (solid line), and KatG$^{\Delta DE}$ 22 Hours After Reconstitution (dotted line).

and 22 hours after reconstitution, respectively. These observations were also consistent with the increase in peroxidase activity during the 22 hour period after reconstitution.

3.3.4 Electron paramagnetic resonance spectroscopy of KatG$^{\Delta DE}$

EPR spectrum of KatG$^{\Delta DE}$ showed a much lower composition of high-spin heme species compared to KatG$^{\Delta FG}$ with a much reduced signal at g = 5.98 and no detectable signal at g = 6.6. Signals below g = 3 suggested a hexa-coordinate low-spin heme environment (Figure 3.22).

3.3.5 Catalase activities of KatG$^{\Delta DE}$

Unlike KatG$^{\Delta FG}$, which still showed some residual catalase activity, KatG$^{\Delta DE}$ had no detectable catalase activity. When this 36 amino acid insertion is deleted from wtKatG, this bifunctional enzyme with substantial catalase activity loses its ability to catalyze this reaction completely.

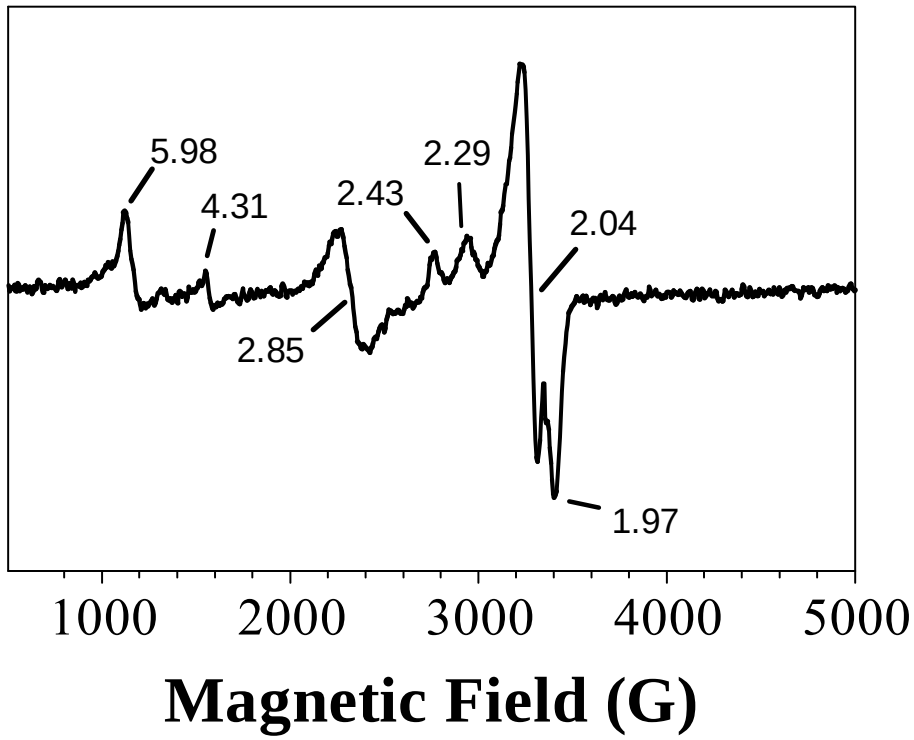

Figure 3.22. EPR Spectrum of KatG$^{\Delta DE}$.

3.3.6 Peroxidase activities of KatG$^{\Delta DE}$

In stark contrast to the catalase results, KatG$^{\Delta DE}$ had substantially *enhanced* peroxidase activity relative to the wtKatG. With respect to H_2O_2 as the substrate, a k_{cat} of 404 s^{-1} was projected, representing a seven fold increase over wtKatG. Even the maximum *observed* activity (280 s^{-1}) represents a five fold increase in peroxidase activity compared to wtKatG. The apparent K_M for H_2O_2 for KatG$^{\Delta DE}$ was 0.46 mM, yielding an apparent second-order rate constant of 8.8×10^5 $M^{-1}s^{-1}$ (Figure 3.23).

We also evaluated the kinetics of the peroxidase activity of KatG$^{\Delta DE}$ with respect to the reducing substrate, ABTS. A k_{cat} value of 406 s^{-1}, together with a K_M value of 0.23 mM, were obtained, giving an apparent second-order rate constant of 1.8×10^6 $M^{-1}s^{-1}$. However, these kinetic parameters must be interpreted with caution because a sigmoidal response in rate of peroxidase activity to increasing ABTS concentrations was observed with KatG$^{\Delta DE}$ (Figure 3.24). This is in contrast to the hyperbolic response of wtKatG (see Figure 3.8). Nevertheless, the maximum observed turnover rate of KatG$^{\Delta DE}$ was 270 s^{-1}, which also represents a five fold increase in activity over that observed for wtKatG.

Interestingly, the time course of ABTS oxidation by KatG$^{\Delta DE}$ revealed the presence of a lag phase which was not observed with wtKatG (Figure 3.25). The absorbance increase at 417 nm is due to the formation of ABTS radical, resulting from the oxidation of ABTS. At low ABTS concentrations, the lag phase was

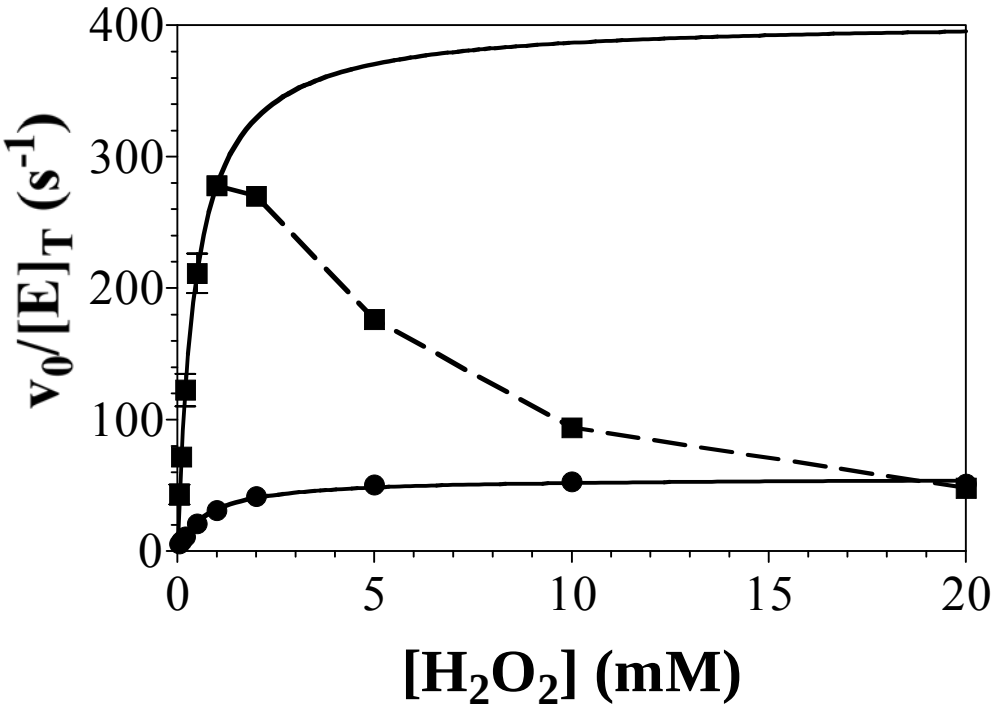

Figure 3.23. Comparison of Peroxidase Activity of wtKatG (●) and $KatG^{\Delta DE}$(■) with Respect to H_2O_2 as the Substrate.

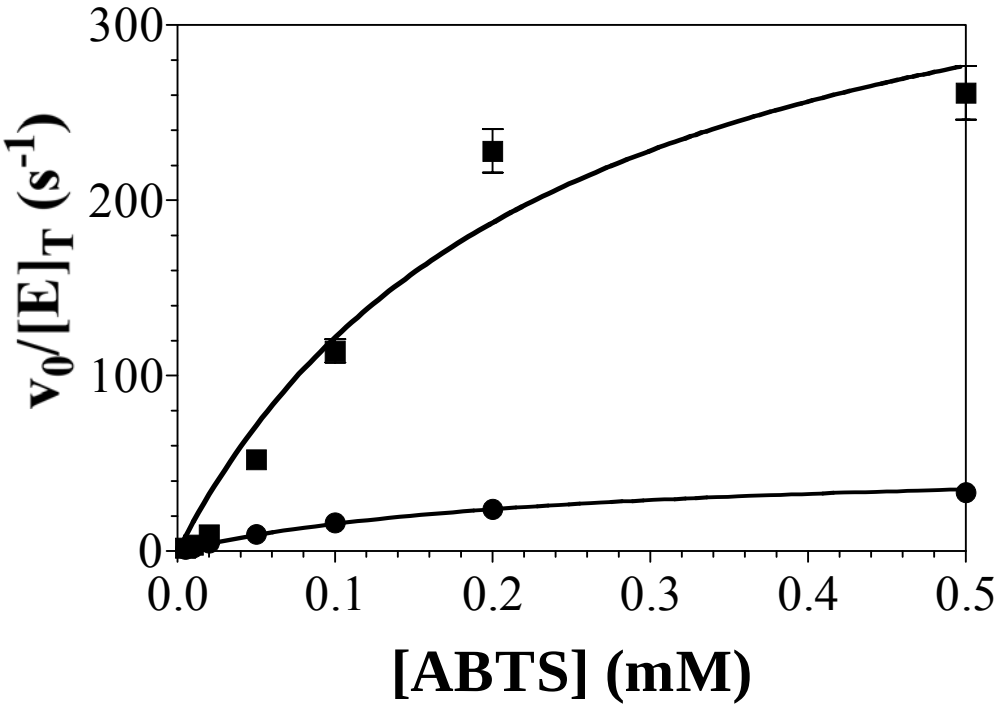

Figure 3.24. Comparison of Peroxidase Activity of wtKatG (●) and $KatG^{\Delta DE}$(■) with Respect to ABTS as the Substrate.

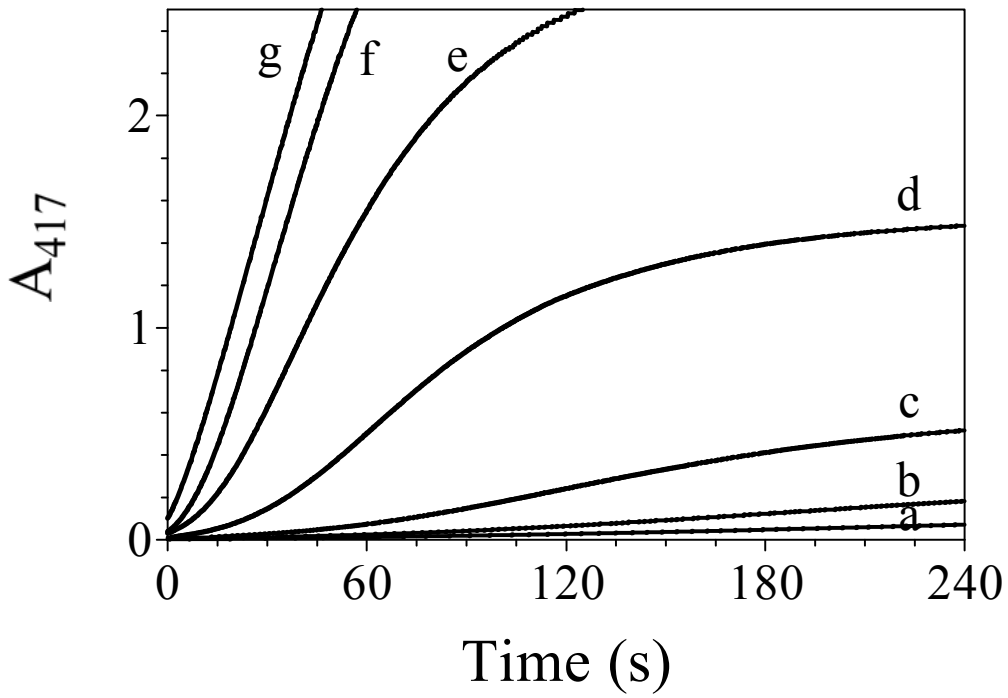

Figure 3.25. Effect of ABTS Concentration on Lag Phase of Peroxidase Activity of KatG$^{\Delta DE}$. Peroxidase activity reactions were performed with 0.005 mM (a), 0.01 mM (b), 0.02 mM (c), 0.05 mM (d), 0.1 mM (e), 0.2 mM (f), and 0.5 mM (g) ABTS.

prominent. Increasing the concentration of ABTS led to a dramatic decrease in the length of the lag phase (Figure 3.25 and Figure 3.26). Moreover, the maximum activity observed following the lag period increased in a non-linear fashion, giving rise to the sigmoidal response to ABTS concentration noted in Figure 3.24.

The effect of H_2O_2 concentration on the lag period was in contrast to ABTS. At low concentrations of H_2O_2 (50 – 500 μM), no lag phase was apparent. However, with increasing concentrations of H_2O_2 (1 – 20 mM), the lag phase became more pronounced (Figure 3.27). The length of the lag phase increased in a linear relationship with the concentration of H_2O_2 (Figure 3.28). Meanwhile, the maximum activity following the lag phase decreased with increasing concentrations of H_2O_2, giving rise to the peroxide-dependent inhibition observed at high concentrations (Figure 3.23).

In summary, we observed a counteracting effect between ABTS, which tended to shorten the lag phase and preserve activity, and H_2O_2, which tended to lengthen the lag phase, and concomitantly, eliminate activity.

3.3.7 Peroxide-dependent inactivation of KatG$^{\Delta DE}$ and formation of compound III

The peroxide-dependent inhibition of KatG$^{\Delta DE}$ peroxidase activity at relatively low H_2O_2 concentrations is noteworthy and reminiscent of peroxide-dependent irreversible inactivation of monofunctional peroxidases. The preserving effect of

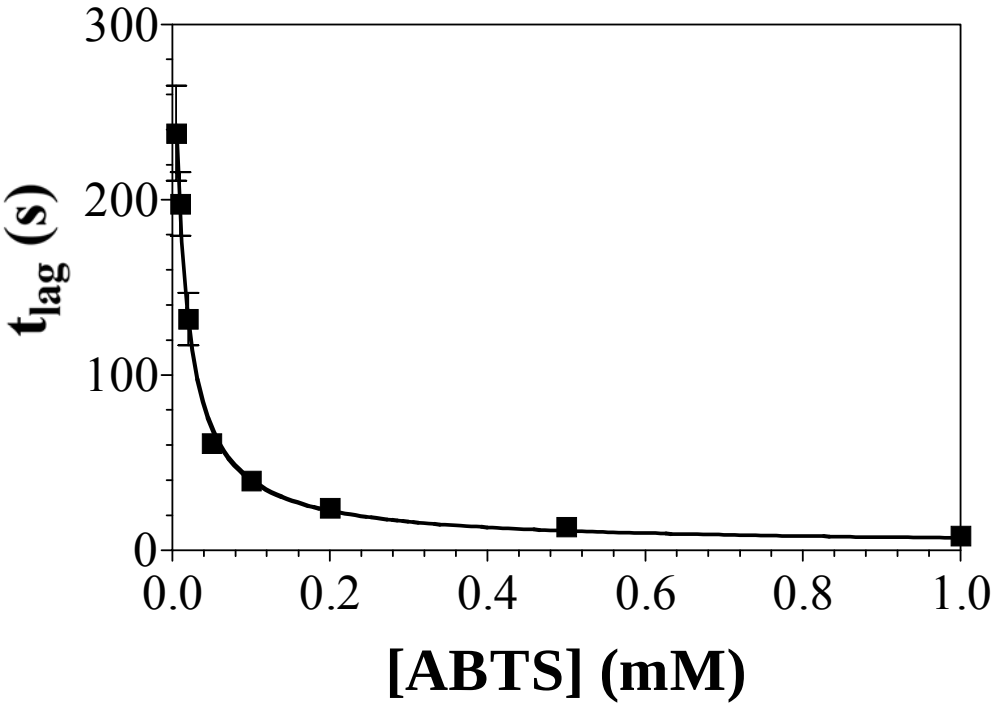

Figure 3.26. Effect of ABTS Concentration on Lag Time of Peroxidase Activity of $KatG^{\Delta DE}$.

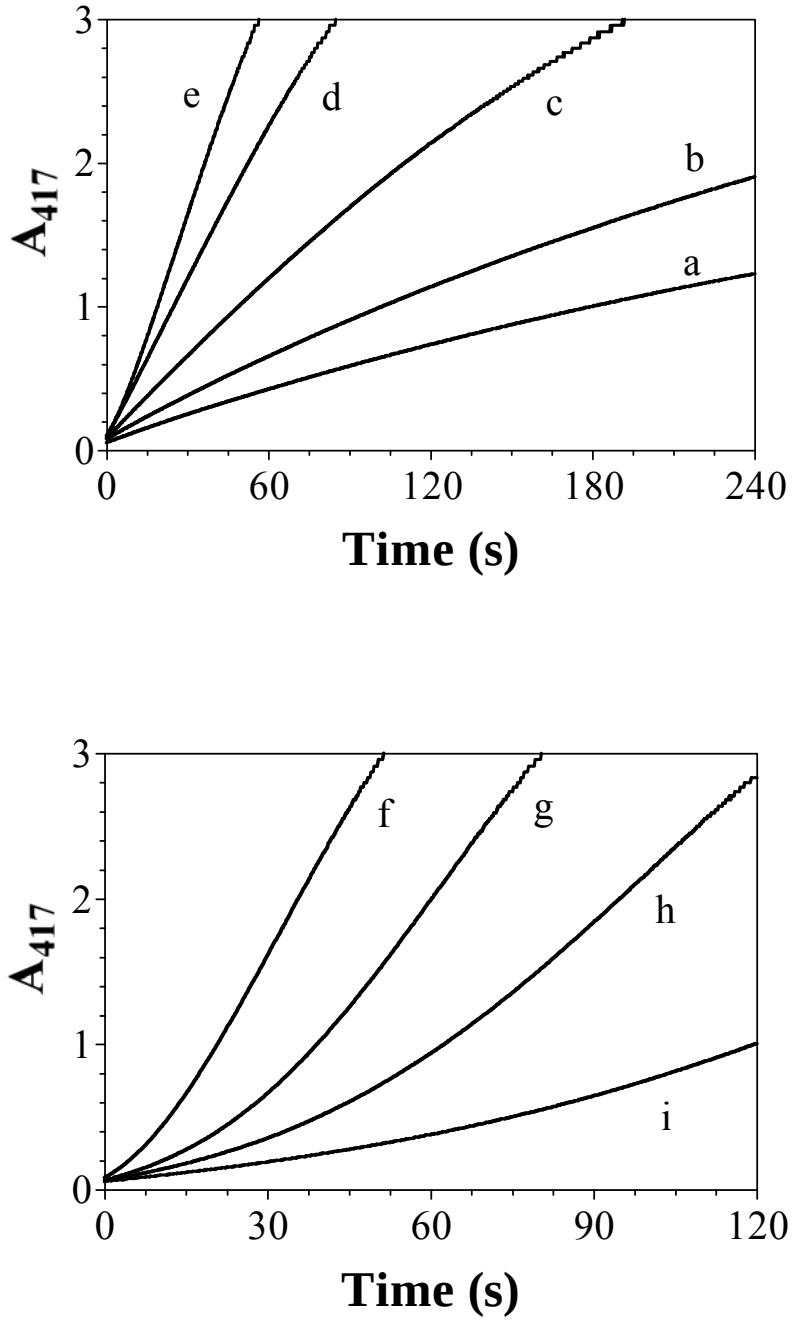

Figure 3.27. Effect of H_2O_2 Concentration on Lag Phase of Peroxidase Activity of $KatG^{\Delta DE}$. Peroxidase activity reactions were performed with 0.05 mM (a), 0.1 mM (b), 0.2 mM (c), 0.5 mM (d), 1 mM (e), 2 mM (f), 5 mM (g), 10 mM (h), and 20 mM (i) H_2O_2.

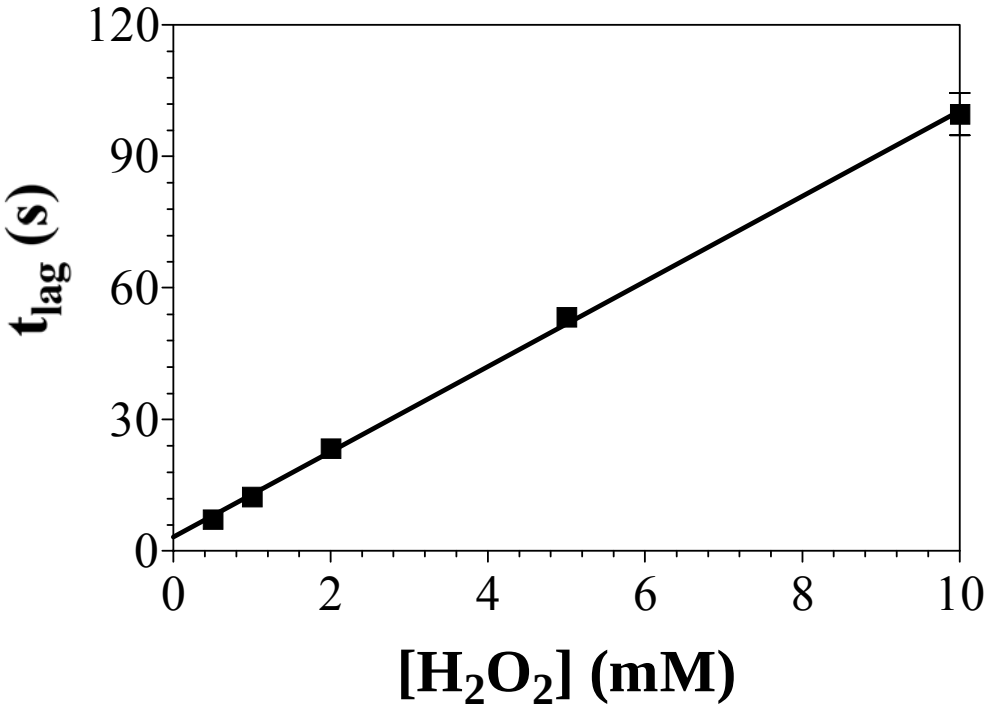

Figure 3.28. Effect of H_2O_2 Concentration on Lag Time of Peroxidase Activity of $KatG^{\Delta DE}$.

ABTS suggests that the inactivation process is by way of compound III (see Figure 1.7). Following the reduction of compound I to compound II in the typical peroxidase catalytic cycle, reducing substrate and H_2O_2 compete for reaction with compound II. Reducing substrate, ABTS in our studies, keeps the enzyme in its catalytic cycle by reducing compound II to the ferric state. Conversely, reaction of compound II with H_2O_2 results in the formation of compound III, which is inactive. Accordingly, reaction of $KatG^{\Delta DE}$ with a relatively low concentration of H_2O_2 (1×10^{-4} M) in the absence of a reducing substrate resulted in a spectrum (λ_{max} 416, 540, and 580) consistent with formation of the Fe^{III}-$O_2^{\bullet -}$ complex known as compound III (Figure 3.29) [116]. This phenomenon is frequently observed in monofunctional peroxidases, but only detected in catalase-peroxidases at much higher H_2O_2 concentrations (0.4 M and above) [134].

3.3.8 Lag phase vs [$ABTS^{\bullet +}$]

In the peroxidase catalytic cycle, H_2O_2 and ABTS compete with each other for the reaction with compound II. The reaction of H_2O_2 with compound II leads to the formation of inactive compound III, while the reaction of ABTS with compound II keeps the enzyme in the catalytic cycle. This peroxide-dependent inactivation explains why we observed the sigmoidal response to ABTS concentration in the maximal activity following the lag period (Figure 3.24). It also explains the peroxide-dependent decrease in maximal activity following the lag period at concentrations

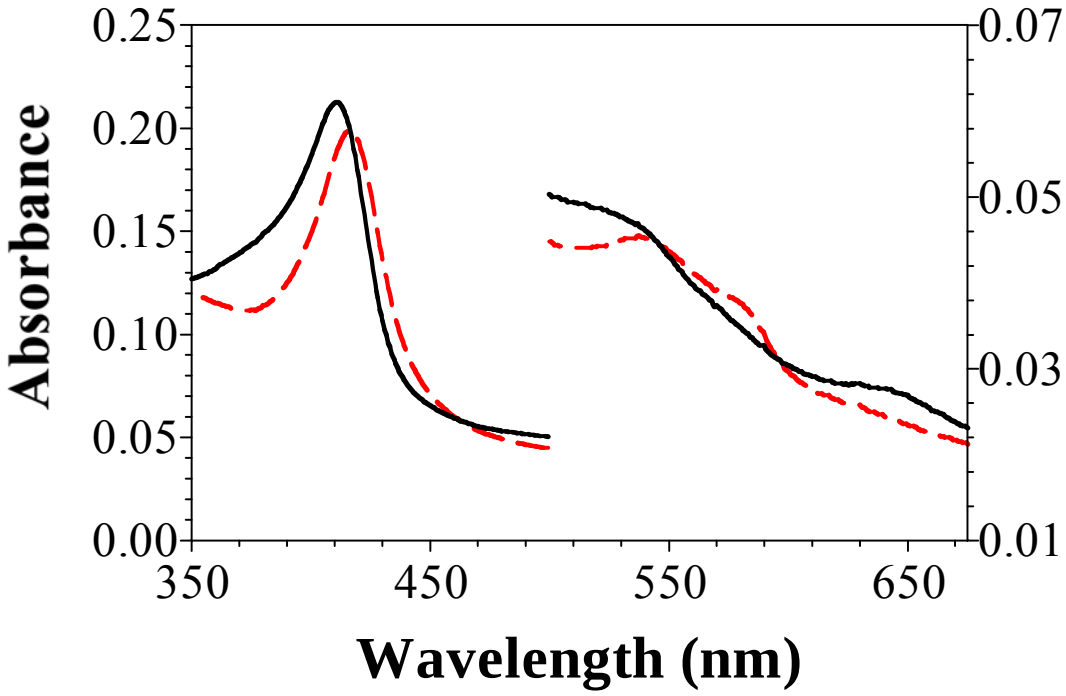

Figure 3.29. Heme Absorption Spectra of KatG$^{\Delta DE}$ Before (solid line) and After (dashed line) the Addition of 0.1 mM H_2O_2.

exceeding 1 mM (Figure 3.23). However, the reason for the lag period itself still remained unclear. A lag phase indicates that the activity of the enzyme increases as the reaction proceeds. More than likely, the lag phase in the peroxidase activity of $KatG^{\Delta DE}$ indicates that some inactivated $KatG^{\Delta DE}$ in the form of compound III is returned back to the peroxidase catalytic cycle. One possible reason could be that the formation of compound III by the reaction of compound II with H_2O_2 is reversible. Thus, as the reactions proceeds and the amount of H_2O_2 decreases, the equilibrium shifts toward compound II. Alternatively, the product of the peroxidase activity may be able to rescue the inactive compound III and return it to the catalytic cycle. Because $ABTS^{\bullet+}$ is the only product of the peroxidase activity of KatG other than H_2O, it was evaluated for its ability to lessen the lag phase. We observed that as little as 30 μM $ABTS^{\bullet+}$ caused a five-fold reduction in lag time (Figure 3.30). Meanwhile, the peroxidase activity following the lag phase increased with more ABTS radical present (Figure 3.31).

3.3.9 Stopped-flow kinetic studies of CN^- binding to $KatG^{\Delta DE}$

Like wtKatG, a precise K_D value could not be obtained because of the high standard deviation of the k_{off} value. We observed a k_{on} value of 1.9×10^6 $M^{-1}s^{-1}$, which indicates a more accessible active site compared to wtKatG (6.67×10^5 $M^{-1}s^{-1}$), and a k_{off} value of 13.6 ± 16.9 s^{-1} (Figure 3.32).

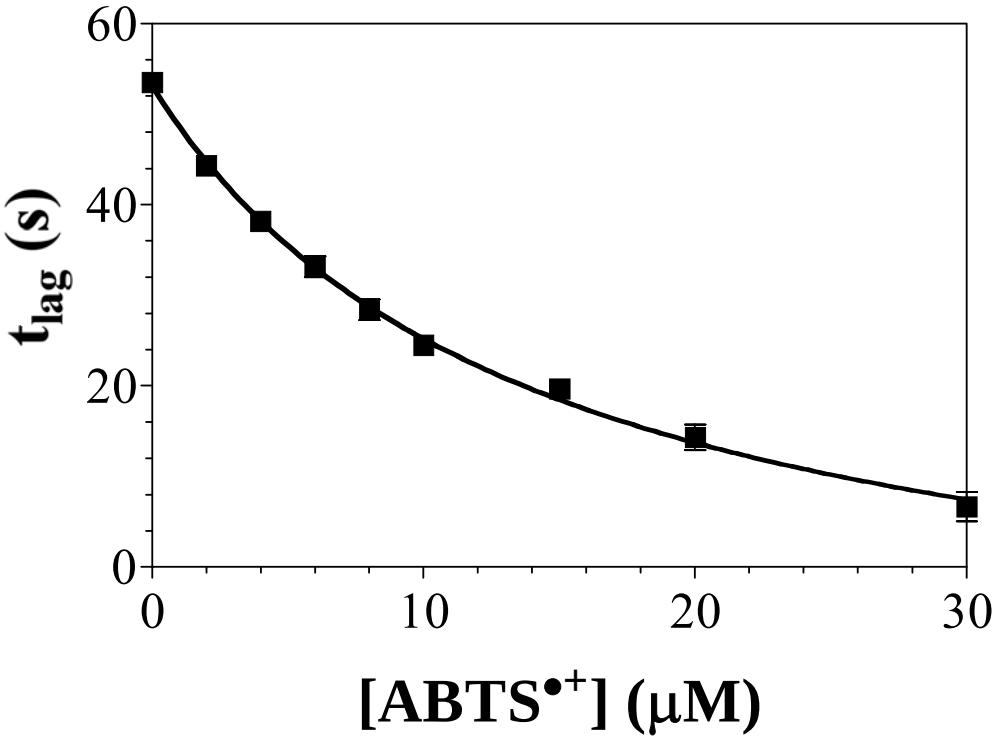

Figure 3.30. Effect of ABTS Radical Concentration on Lag Time of Peroxidase Activity of $KatG^{\Delta DE}$.

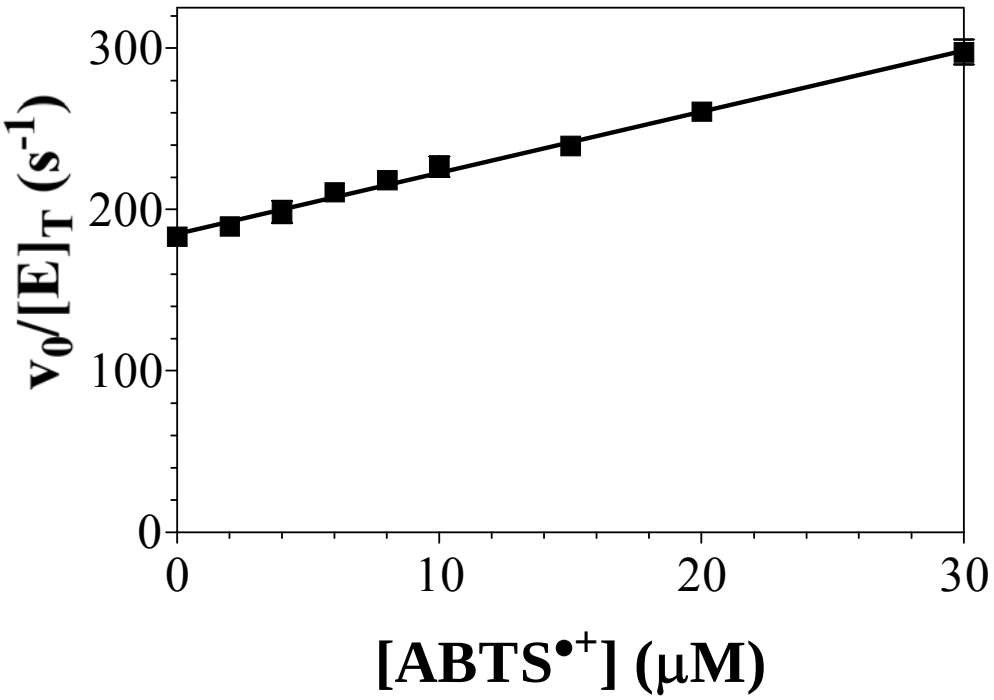

Figure 3.31. Effect of ABTS Radical Concentration on Peroxidase Activity of $KatG^{\Delta DE}$.

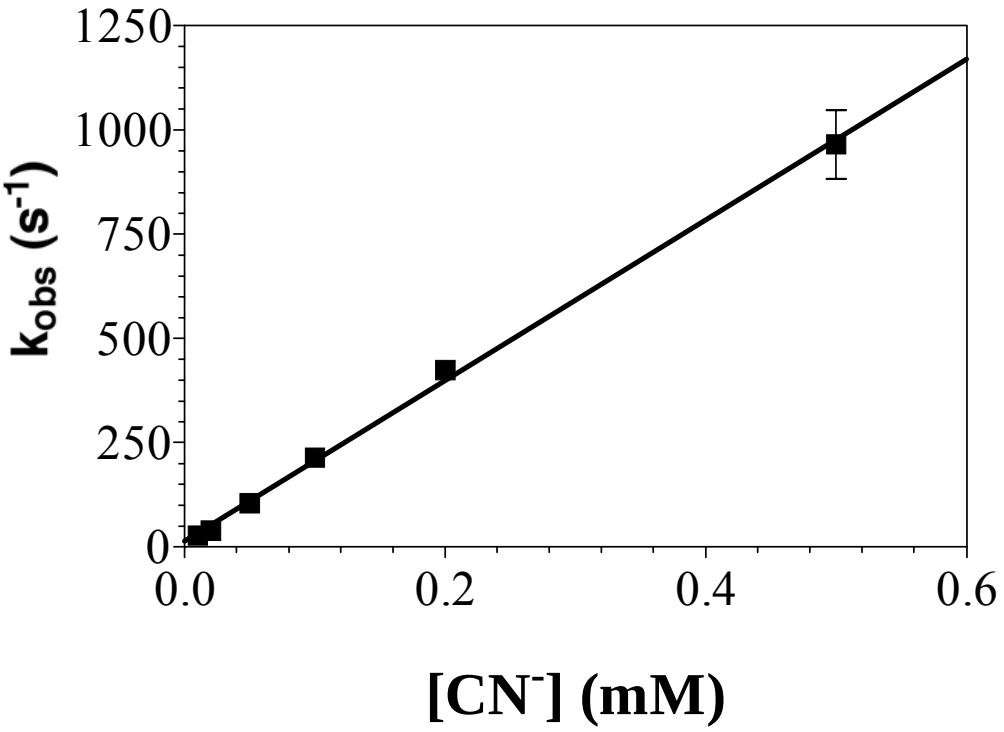

Figure 3.32. Effect of Cyanide Concentration on Observed Rate of Cyanide Binding to $KatG^{\Delta DE}$.

3.3.10 Studies of CN^- binding to $KatG^{\Delta DE}$ by visible spectra

Upon addition of CN^-, a decrease in absorbance at 390 nm was observed (Figure 3.33). The data fit well to a two-site binding equation, indicating two separate processes were taking place with CN^- added. Because $KatG^{\Delta DE}$ contained both penta-coordinate and hexa-coordinated heme species, it is suggested that the two processes are related to these two different heme species, respectively. A K_D value of about 3.6 μM for penta-coordinate heme species and a K_D value of about 1.8 mM for hexa-coordinate heme species were obtained.

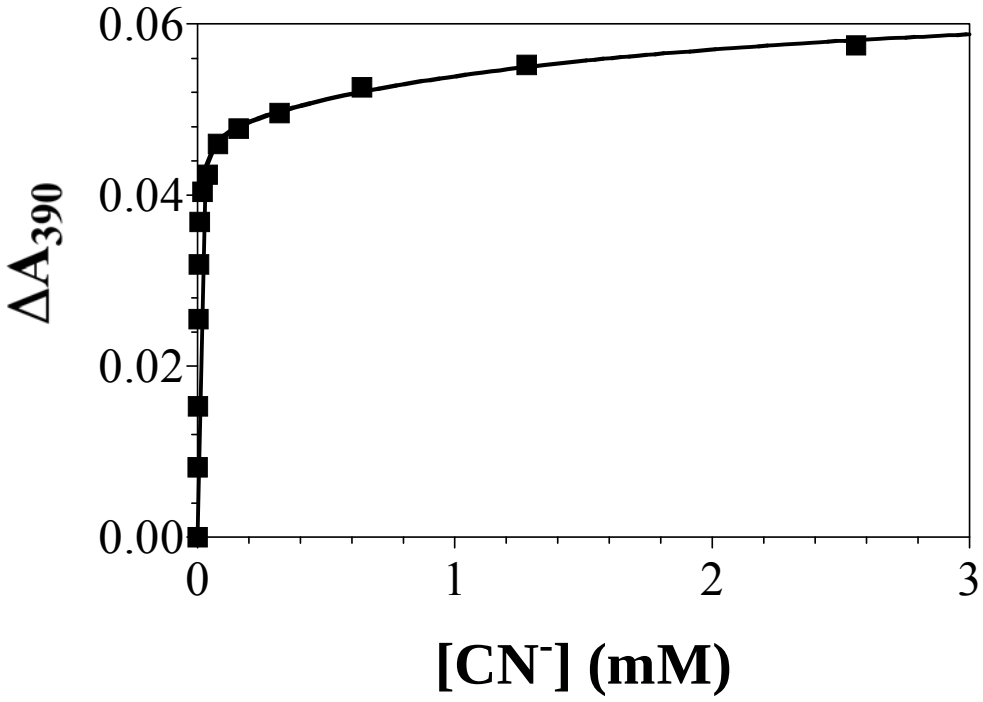

Figure 3.33. Change in Absorbance at 420 nm with Cyanide Added to KatG$^{\Delta DE}$.

3.4 KatG$^{\Delta DE/FG}$

3.4.1 Mutagenesis, expression, purification, and reconstitution of KatG$^{\Delta DE/FG}$

The plasmid pKatG$^{\Delta DE/FG}$ was successfully constructed using our seamless deletion mutagenesis procedure. Transformation and expression of this variant was carried out following the same procedure described for the other variants. The resulting variant, KatG$^{\Delta DE/FG}$, was expressed in inclusion bodies. Thus, like KatG$^{\Delta DE}$, the purification of this variant was accomplished under denaturing conditions, followed by dialysis against buffer **A** (50 mM phosphate buffer, pH 8.0; 200 mM NaCl) for refolding. Roughly 5×10^{-8} moles of KatG$^{\Delta DE}$ were routinely obtained per liter of LB broth.

Following purification and refolding, KatG$^{\Delta DE/FG}$ was reconstituted with hemin. The peroxidase activity of the variant increased linearly with hemin added up to 0.5 equivalents, after which no further increase in peroxidase activity was observed. In all studies in this dissertation, KatG$^{\Delta DE/FG}$ was reconstituted to 0.5 equivalents, unless otherwise stated.

3.4.2 UV-visible spectra of KatG$^{\Delta DE/FG}$

Spectra of ferric, ferrous, and ferri-cyano forms of KatG$^{\Delta DE/FG}$ were recorded

(Figure 3.34). These spectra are highly similar to KatG$^{\Delta DE}$ in almost all respects, suggesting that a greater proportion of the heme is in a hexa-coordinate low-spin state compared to wtKatG.

3.4.3 Catalase and Peroxidase activitis of KatG$^{\Delta DE/FG}$

Like KatG$^{\Delta DE}$, when both of the interhelical insertions were removed from the KatG structure, this bifunctional enzyme lost all catalase activity.

Also like KatG$^{\Delta DE}$, KatG$^{\Delta DE/FG}$ showed an elevated peroxidase activity compared to wtKatG. With respect to H_2O_2, a k_{cat} of 117 s^{-1} was observed, representing a more than two fold increase over wtKatG. However, the apparent K_M for H_2O_2 for KatG$^{\Delta DE/FG}$ also increased drastically (5.0 mM vs. 0.83 mM), yielding an apparent second-order rate constant that is lower than wtKatG (2.3 $\times 10^4$ $M^{-1}s^{-1}$ vs. 7.1 $\times 10^4$ $M^{-1}s^{-1}$) (Figure 3.35). Interestingly, in contrast to KatG$^{\Delta DE}$, when the FG insertion was also absent, KatG$^{\Delta DE/FG}$ showed hyperbolic dependence on H_2O_2, as well as the absence of inactivation at high H_2O_2 concentrations.

With respect to ABTS, a turnover number of 170 s^{-1} was obtained. This represents an extrapolated value due to inhibition observed at ABTS concentrations above 0.1 mM. This turnover number represents a three fold increase over wtKatG. The apparent K_M for ABTS decreased significantly compared to wtKatG (0.051 mM

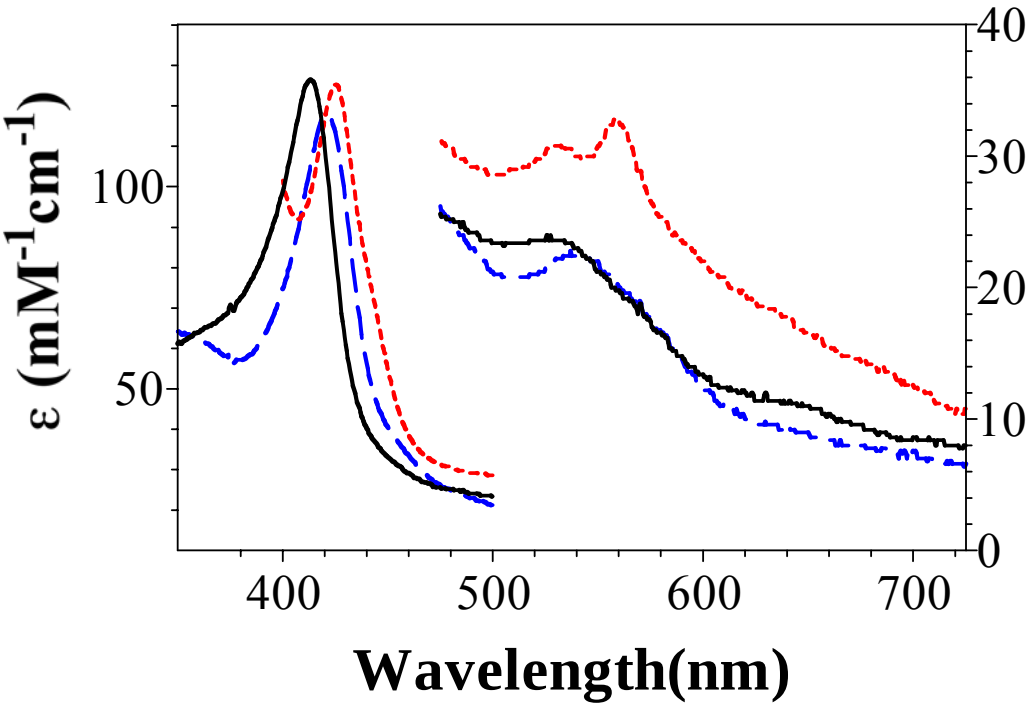

Figure 3.34. Absorption Spectra Recorded for Ferric (solid line), Ferrous (dotted line), and Ferri-cyano (dashed line) Forms of KatG$^{\Delta DE/FG}$.

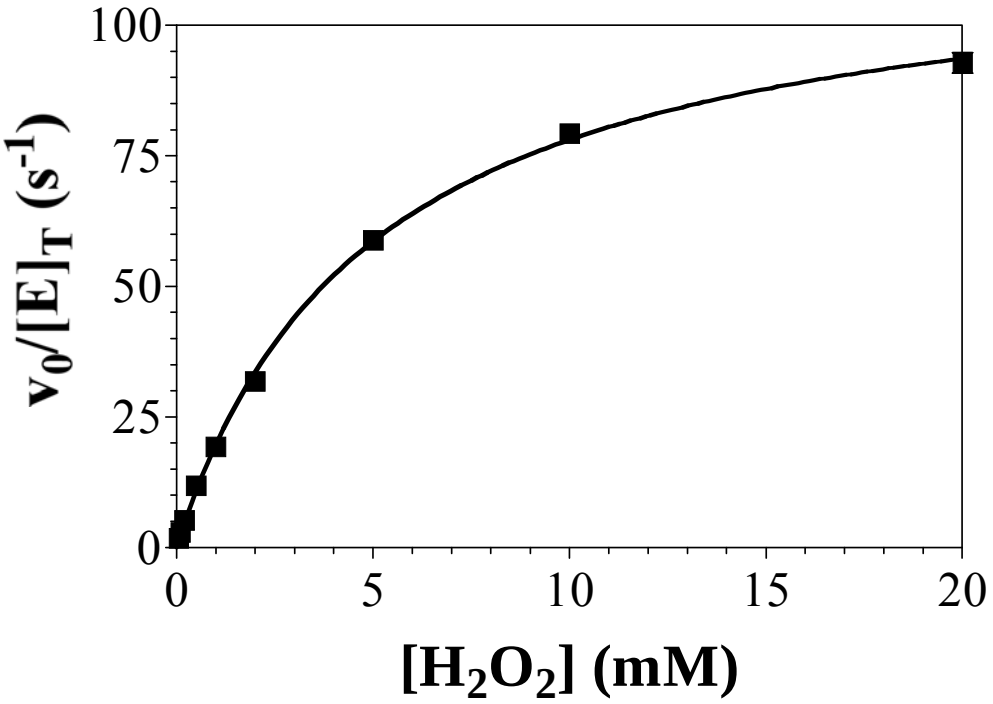

Figure 3.35. Effect of H_2O_2 Concentration on Peroxidase Activity of $KatG^{\Delta DE/FG}$.

vs. 0.23 mM). Consequently we obtained a 15 fold higher apparent second-order rate constant (3.3×10^6 $M^{-1}s^{-1}$ vs. 2.2×10^5 $M^{-1}s^{-1}$) (Figure 3.36).

3.4.4 Studies of CN^- binding to $KatG^{\Delta DE/FG}$ by visible spectra

Upon addition of CN^-, $KatG^{\Delta DE/FG}$ showed a decrease in absorbance at 401 nm (Figure 3.37). The data also fit well to a two-site binding equation, suggesting the binding of CN^- to both penta-coordinate and hexa-coordinate heme species. The K_D values of about 0.7 μM and 0.15 mM were obtained for penta-coordinate heme species and hexa-coordinate heme species, respectively.

3.4.5 Stopped-flow kinetic studies of CN^- binding to $KatG^{\Delta DE/FG}$

We observed a much higher k_{on} value of 4.3×10^6 $M^{-1}s^{-1}$ compared to wtKatG (6.67×10^5 $M^{-1}s^{-1}$) and $KatG^{\Delta DE}$ (1.9×10^6 $M^{-1}s^{-1}$), suggesting the active site is more accessible to peroxide substrates when either one of the two insertions was removed. However, with the high deviation of the k_{off} value (63.1 ± 58.0 s^{-1}), a precise K_D value could not be obtained (Figure 3.38).

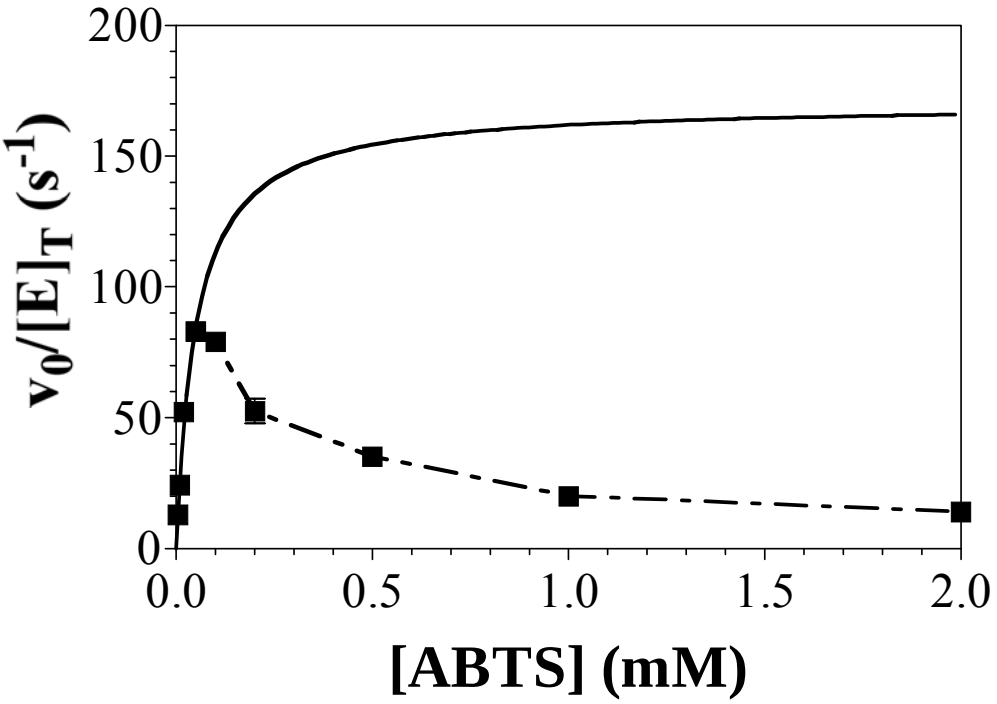

Figure 3.36. Effect of ABTS Concentration on Peroxidase Activity of $KatG^{\Delta DE/FG}$.

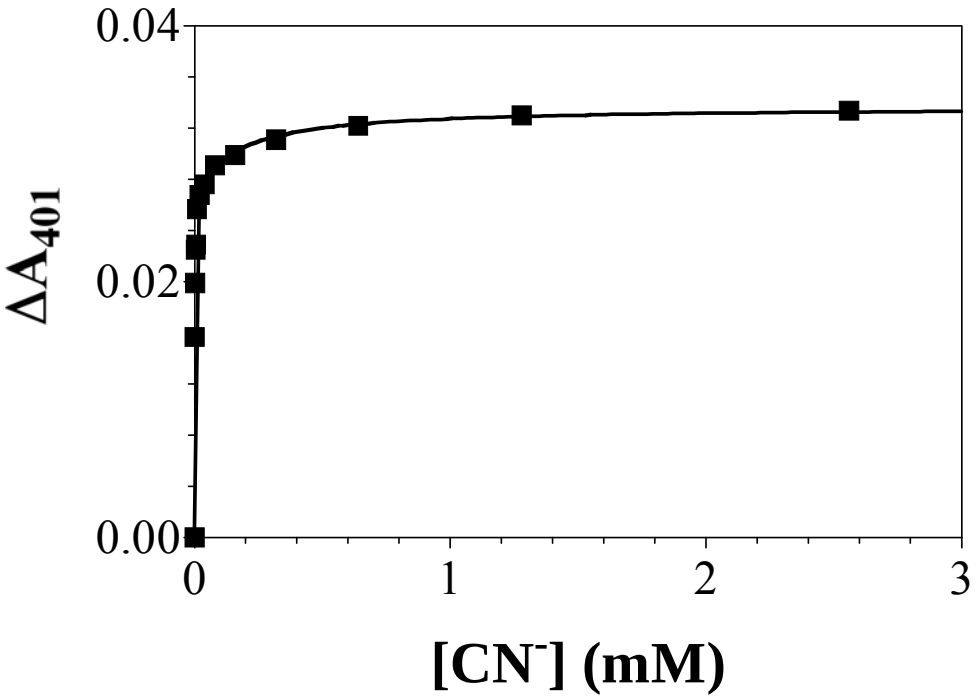

Figure 3.37. Change in Absorbance at 401 nm with Cyanide Added to KatG$^{\Delta DE/FG}$.

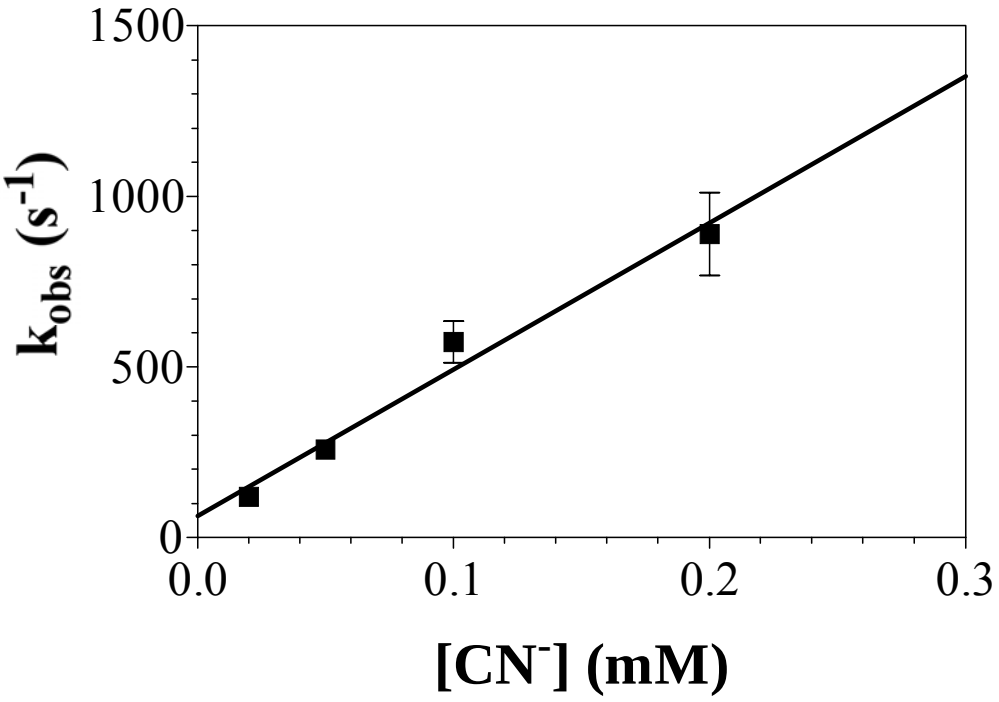

Figure 3.38. Effect of Cyanide Concentration on Observed Constant of Cyanide Binding for $KatG^{\Delta DE/FG}$.

3.5 KatG$^{N\text{-}term/\Delta DE}$ and KatG$^{N\text{-}term/\Delta FG}$

Compared to monofunctional peroxidases, the C-terminal domain of catalase-peroxidases is also an extra structural feature [108]. The main role of this domain has been proposed as maintaining the correct architecture of the active site for both activities [109]. To verify this role of the C-terminal domain, and further explore its collaboration with the two insertions, the variants lacking this domain as well as each of the two insertions, KatG$^{N\text{-}term/\Delta DE}$ and KatG$^{N\text{-}term/\Delta FG}$, were expressed, purified, and characterized.

3.5.1 Expression, purification, and reconstitution of KatG$^{N\text{-}term/\Delta DE}$ and KatG$^{N\text{-}term/\Delta FG}$

Using our deletion mutagenesis procedure, the plasmids pkatG$^{N\text{-}term/\Delta DE}$ and pkatG$^{N\text{-}term/\Delta FG}$ were constructed. Transformation and expression of these variants followed the procedure described for other variants. The resulting variants, KatG$^{N\text{-}term/\Delta DE}$ and KatG$^{N\text{-}term/\Delta FG}$, were both expressed in inclusion bodies. Thus, the purification of these proteins followed denaturing purification conditions, followed by dialysis against buffer **A** (50 mM phosphate buffer, pH 8.0; 200 mM NaCl) for ding. Roughly 1×10^{-6} moles of each protein were routinely obtained per liter of LB broth.

Following purification and refolding, both variants were reconstituted with one equivalent hemin and incubated at 4 °C for 24 hours. None of these reconstituted variants showed any catalase or peroxidase activity. Then these variants were recombined with equal amount of $KatG^{C\text{-}term}$, and peroxidase activity was monitored. It showed that the peroxidase activity of these recombined variants increased substantially over time. Maximal peroxidase activity was observed after 24-hour incubation at 4 °C for the recombined $KatG^{N\text{-}term/\Delta FG}$, and 48 hours for $KatG^{N\text{-}term/\Delta DE}$. Therefore, all kinetic data were obtained after this 24-hour incubation post-recombination for $KatG^{N\text{-}term/\Delta FG}$ and after 48 hours for $KatG^{N\text{-}term/\Delta DE}$, unless otherwise stated. UV-visible spectra were taken before and after the recombination with $KatG^{C\text{-}term}$.

3.5.2 *UV-vis Spectra of $KatG^{N\text{-}term/\Delta DE}$ and $KatG^{N\text{-}term/\Delta FG}$*

Consistent with the emergence of peroxidase activity, the spectra of these two variants underwent slow but obvious changes after recombination with $KatG^{C\text{-}term}$. Immediately following recombination, the spectra of both variants were dominated by low-spin heme species. After 24-hour incubation with $KatG^{C\text{-}term}$ at 4 °C, the spectrum for $KatG^{N\text{-}term/\Delta FG}$ was dominated by penta-coordinate high-spin heme (Figure 3.39). Spectral shifts for $KatG^{N\text{-}term/\Delta DE}$ were much more subtle. However, an increase in high-spin species was observed over 48 hours at 4 °C following addition

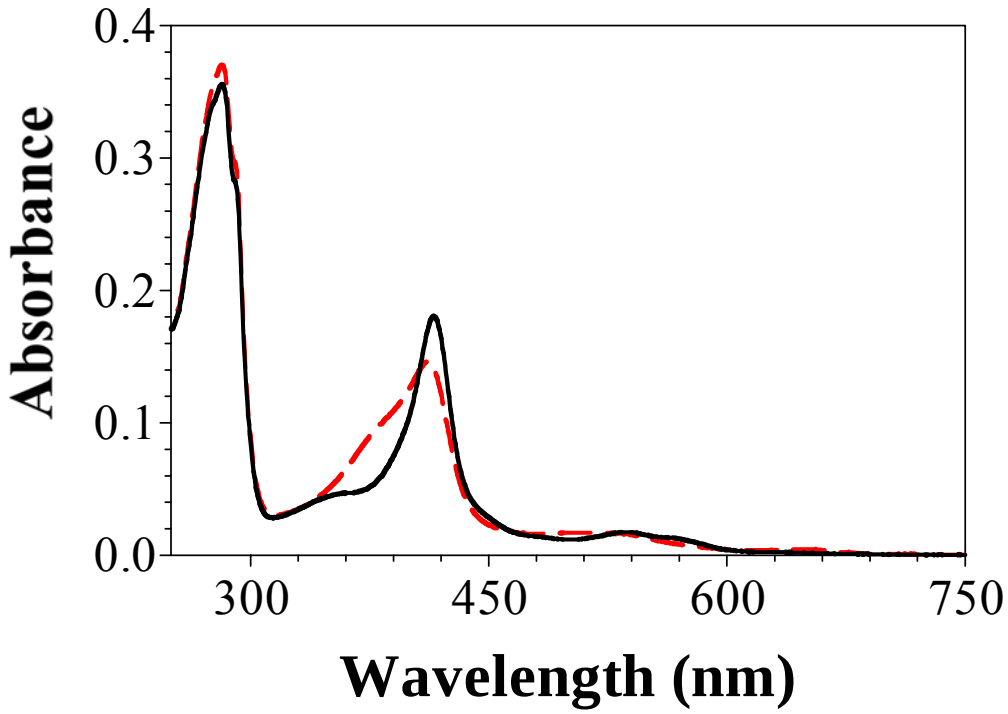

Figure 3.39. Spectra of Recombined KatG$^{N\text{-term}/\Delta FG}$ Immediately Following (solid line) and 24 Hours After (dashed line) Recombination with Equimolar KatG$^{C\text{-term}}$.

of equimolar KatG$^{C\text{-term}}$ (Figure 3.40). This was consistent with the return of peroxidase activity.

3.5.3 Catalase and peroxidase activities of Recombined KatG$^{N\text{-term}/\Delta DE}$ and KatG$^{N\text{-term}/\Delta FG}$

Both of these variants showed no detectable catalase activity.

Immediately after recombination, KatG$^{N\text{-term}/\Delta FG}$ showed appreciable peroxidase activity, which reached maximum after 24 hours. With respect to ABTS as the substrate, KatG$^{N\text{-term}/\Delta FG}$ showed maximal peroxidase activity with a k_{cat} value of 16.3 s^{-1}, and a K_M value of 7.3 μM (Figure 3.41). With respect to H_2O_2 as the substrate, KatG$^{N\text{-term}/\Delta FG}$ showed maximal peroxidase activity with a k_{cat} value of 20.2 s^{-1}, and a K_M value of 2.6 mM (Figure 3.42). All these data were comparable to those of KatG$^{\Delta FG}$. Indeed, even the inhibition of activity at high ABTS concentrations was detected for KatG$^{N\text{-term}/\Delta FG}$ in the presence of KatG$^{C\text{-term}}$.

In contrast, KatG$^{N\text{-term}/\Delta DE}$ showed very little peroxidase activity immediately following addition of KatG$^{C\text{-term}}$. However, substantial peroxidase activity was eventually observed. After 48 hours, the peroxidase activity reached 233 s^{-1} with respect to ABTS (Figure 3.43), and 134 s^{-1} with respect to H_2O_2 (Figure 3.44). Together with the apparent K_M values of 0.43 mM and 1.0 mM for ABTS and H_2O_2,

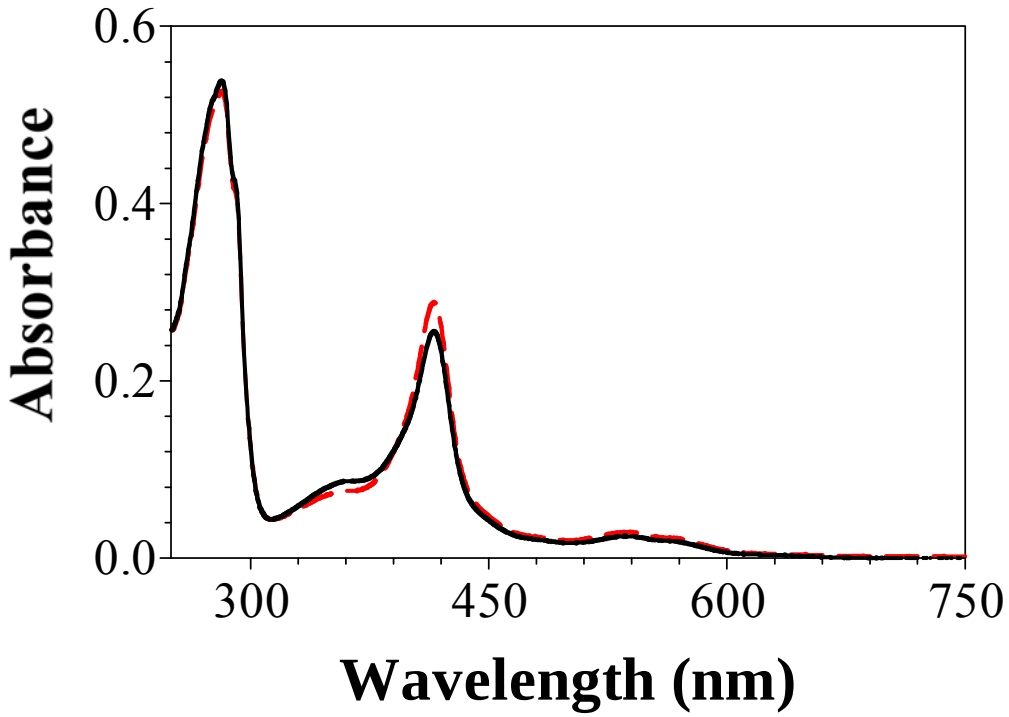

Figure 3.40. Spectra of Recombined KatG$^{N\text{-term}/\Delta DE}$ Immediately Following (solid line) and 48 Hours After (dashed line) Recombination with Equimolar KatG$^{C\text{-term}}$.

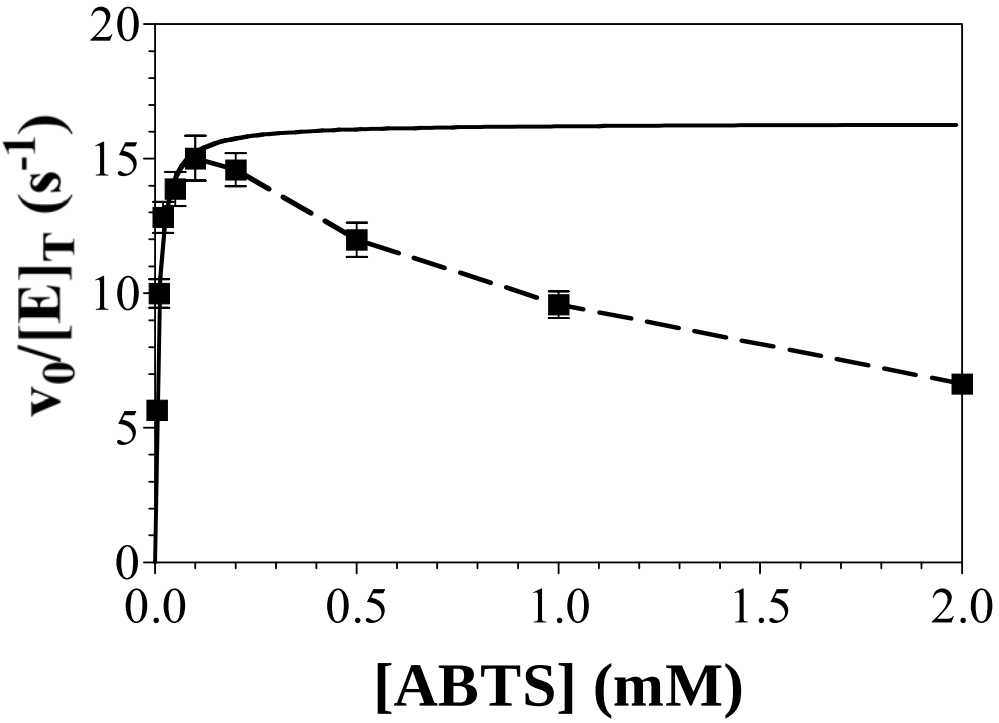

Figure 3.41. Effect of ABTS Concentration on Peroxidase Activity of Recombined $KatG^{N\text{-}term/\Delta FG}$.

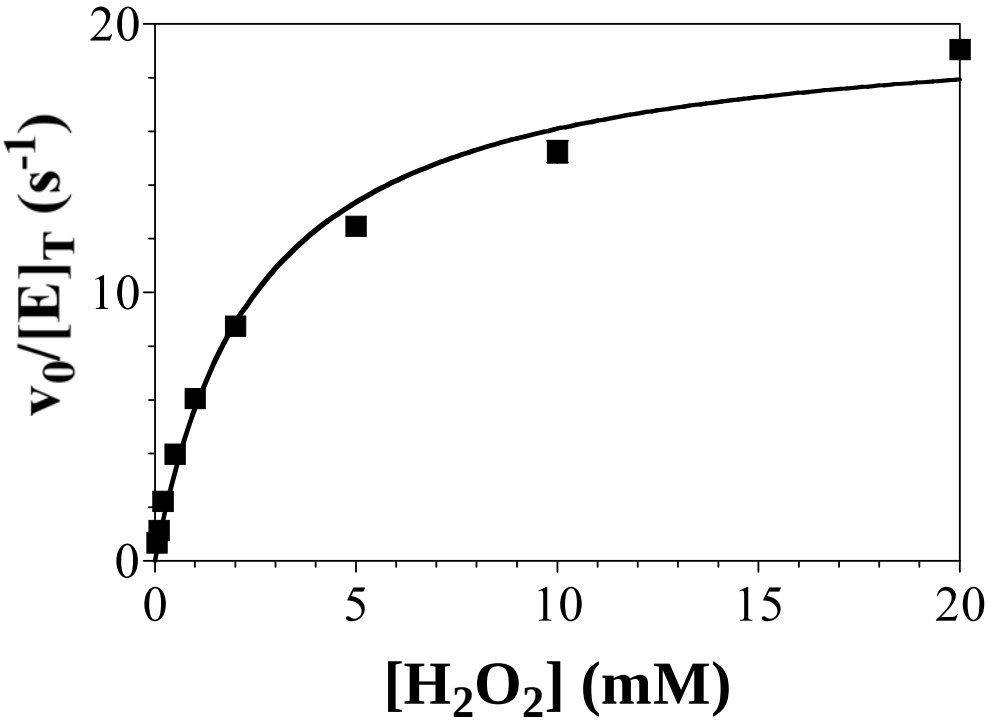

Figure 3.42. Effect of H_2O_2 Concentration on Peroxidase Activity of Recombined $KatG^{N\text{-}term/\Delta FG}$.

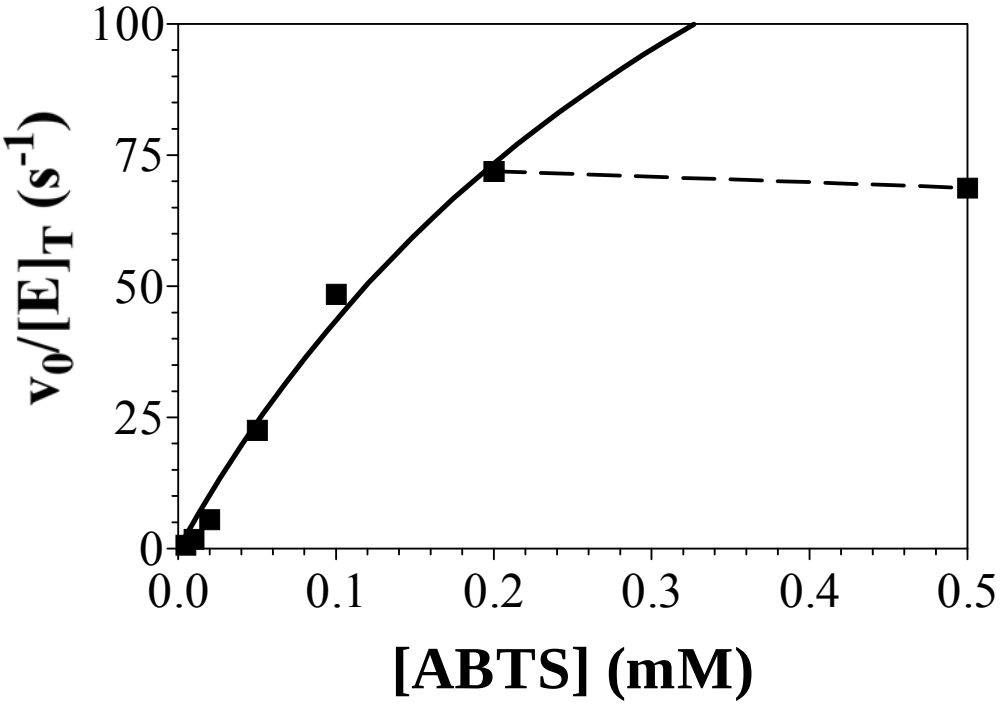

Figure 3.43. Effect of ABTS Concentration on Peroxidase Activity of Recombined $KatG^{N\text{-}term/\Delta DE}$.

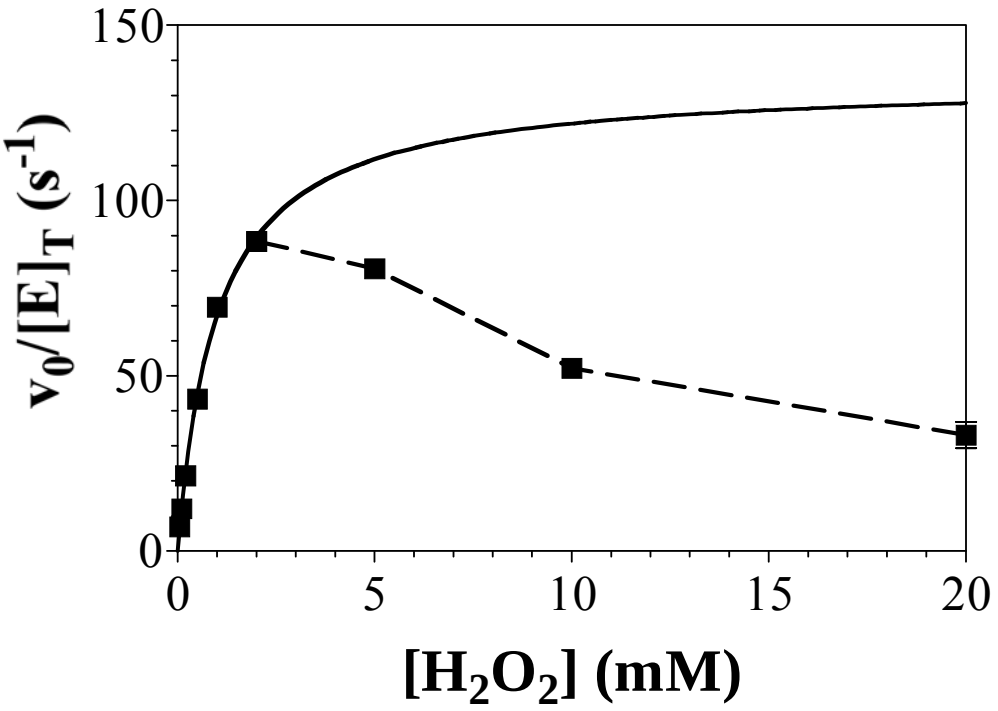

Figure 3.44. Effect of H_2O_2 Concentration on Peroxidase Activity of Recombined $KatG^{N\text{-}term/\Delta DE}$.

respectively, we obtained apparent second-order rate constants of 5.4×10^5 $M^{-1}s^{-1}$ for ABTS and 1.3×10^5 $M^{-1}s^{-1}$ for H_2O_2.

Remarkably, recombined $KatG^{N\text{-}term/\Delta DE}$ with $KatG^{C\text{-}term}$ showed a sigmoidal response to ABTS concentration, and peroxide-dependent inactivation, which were both compatible with $KatG^{\Delta DE}$ (Figure 3.44). The optimal H_2O_2 concentration recorded for the recombined enzyme was 2 mM, very close to the optimal H_2O_2 concentration for $KatG^{\Delta DE}$, which was 1 mM. Also similar to $KatG^{\Delta DE}$, the lag time showed a linear relationship with H_2O_2 concentration (Figure 3.45), and could be greatly reduced with increasing ABTS concentrations (Figures 3.46).

3.5.4 EPR spectra of $KatG^{N\text{-}term/\Delta FG}$

The EPR spectrum for ferric $KatG^{N\text{-}term/\Delta FG}$ showed an overwhelming hexa-coordinate low-spin heme signal with principal g-values of 2.91, 2.27, and 1.52 (Figure 3.47). These g values suggested that the sixth ligand of heme was a histidine [109, 135, 136]. Remarkably, upon the addition of just one equivalent of $KatG^{C\text{-}term}$ and a 24 hour incubation process at 4 °C, the EPR spectrum was almost identical to $KatG^{\Delta FG}$. The rhombic signals at g = 6.63, 4.99, and 1.95 indicated the presence of penta-coordinate high-spin species, and the axial signals at g = 5.74, and 1.99 suggested the presence of hexa-coordinate high-spin heme species. Meanwhile, in the spectrum, the signals at g =

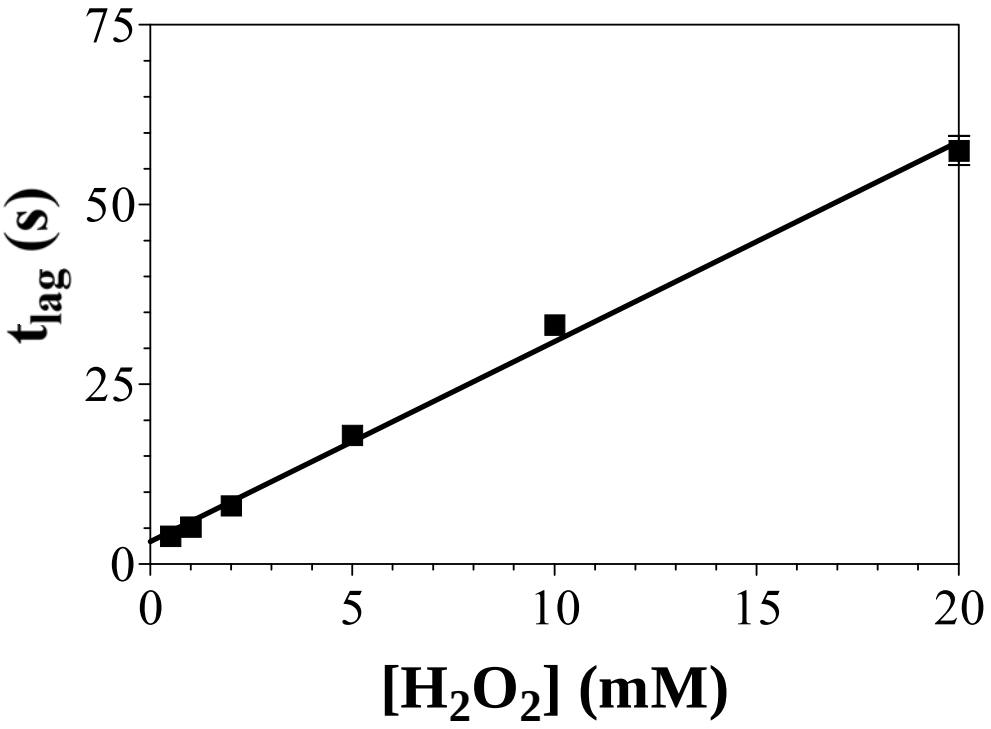

Figure 3.45. Effect of H_2O_2 Concentration on Lag Time of Peroxidase Activity of Recombined $KatG^{N\text{-}term/\Delta DE}$.

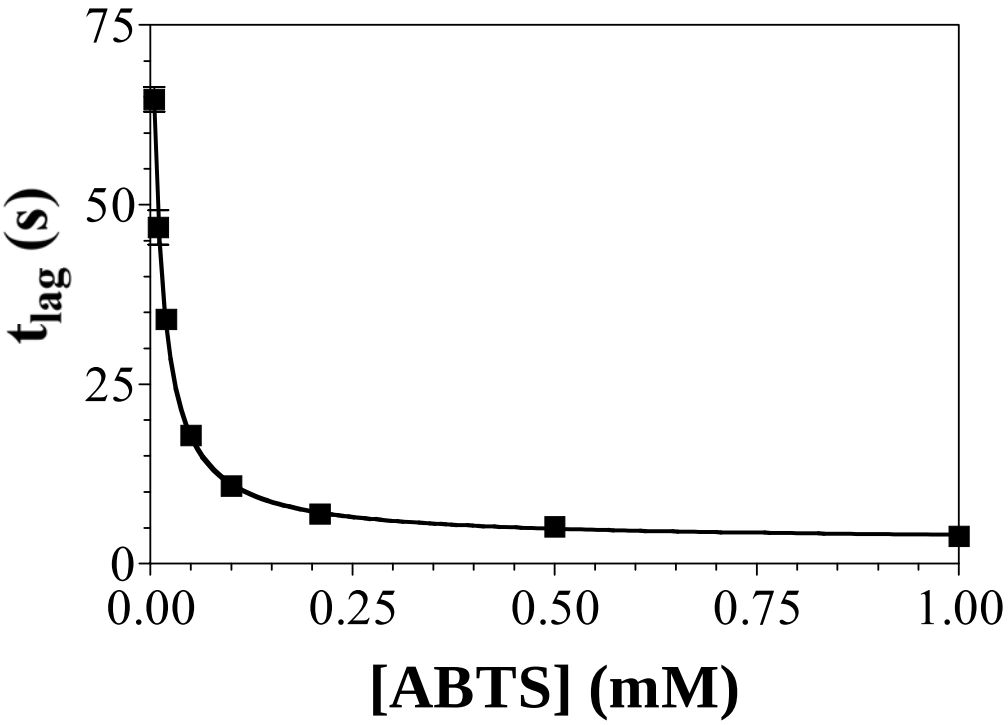

Figure 3.46. Effect of ABTS Concentration on Lag Time of Peroxidase Activity of Recombined $KatG^{N\text{-}term/\Delta DE}$.

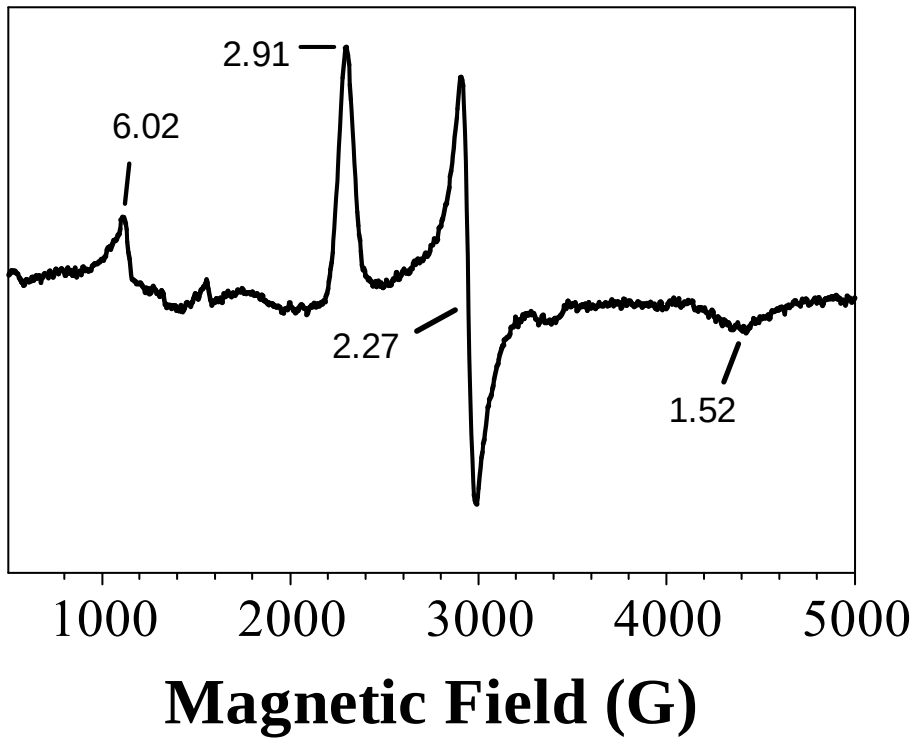

Figure 3.47. EPR Spectrum Recorded for $KatG^{N\text{-}term/\Delta FG}$.

2.92, and 2.26 indicated a slightly higher composition of hexa-coordinate low-spin heme species, compared to KatG$^{\Delta FG}$ (Figure 3.48).

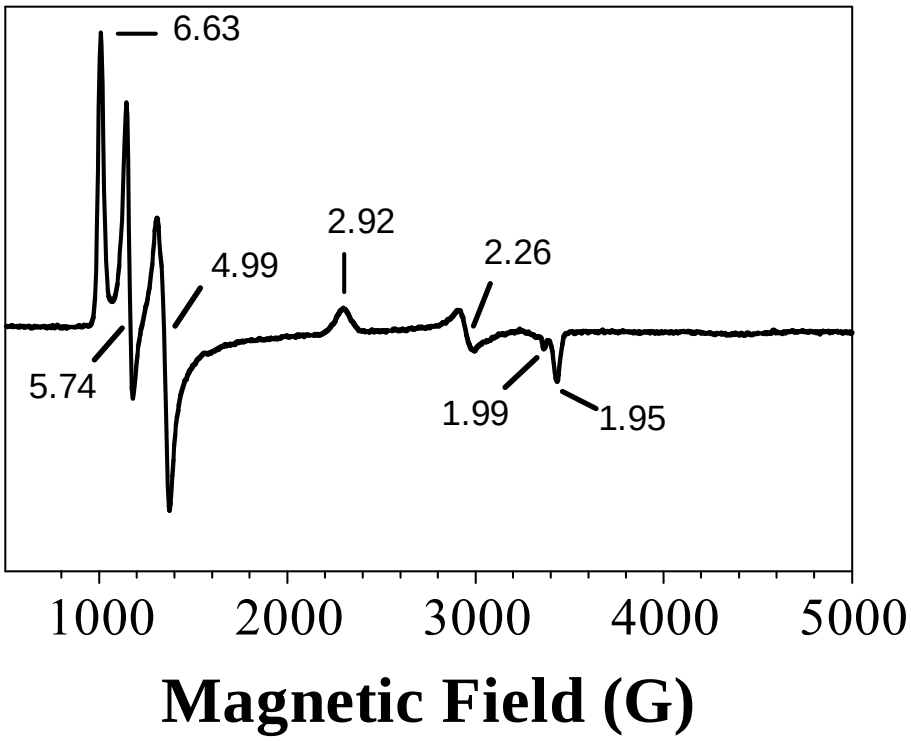

Figure 3.48. EPR Spectrum Recorded for $KatG^{N\text{-}term/\Delta FG}$ 24 Hours after Recombination with $KatG^{C\text{-}term}$.

CHAPTER FOUR

DISCUSSION

Heme enzymes use heme, a simple metallo-organic compound, to perform diverse functions ranging from oxygen storage and transport to electron transfer, from peroxide-dependent redox reactions, signal transduction, to control of gene expression. This astounding diversity of function is dictated at four structural levels: the structure of heme itself, the identity of protein-derived heme ligands, the non-ligand heme environment, and the global structure of the protein.

Although intense effort has been directed toward the study of the first three structural levels and how they regulate heme enzyme function, little is known about the regulation of heme-dependent catalysis at the global protein structural level. Indeed, the universal inability of synthetic inorganic complexes to reproduce the catalytic power of metalloenzymes stands as a testament to the importance of the global protein structure. Furthermore, enzymes that share almost identical active site arrangement can show different functions, for instance, monofunctional peroxidases share a nearly superimposable active-site arrangement with bifunctional catalase-peroxidases (Figure 4.1) [87, 137], yet the latter shows substantial catalase activity

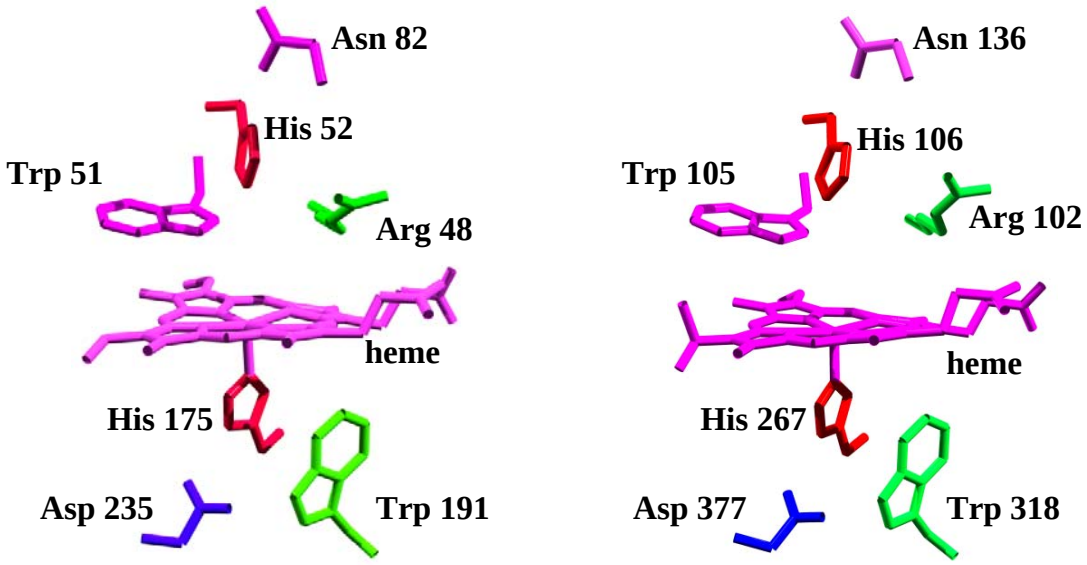

Cytochrome *c* Peroxidase **_E. coli_ Catalase-peroxidase**

Figure 4.1. Active Site Comparison of Cytochrome *c* Peroxidase and *E. coli* Catalase-peroxidase.

(Wang, J., et al. [1990] *Biochemistry* **29**, 7160-7173)

(Carpena, X., et al. [2003] *J. Mol. Biol.* **327**, 475-489)

which peroxidases lack. Clearly, the difference in function between these two important groups of enzymes can not be explained by the first three levels of structure alone. All these indicate that global protein structure plays an important role in the enzyme function. There are certainly fundamental reasons, though many of them remain unexplored, that nature goes to such great lengths to perform biological functions using large and complex structures for catalysis rather than simple active-site analogs.

Given the importance of global protein structure on heme enzyme function and the lack of information in this area, models to evaluate this critical aspect of heme enzyme structure/function are sorely needed. Fortunately, catalase-peroxidases stand out as ideal models. Catalase-peroxidases have drawn much attention because of their unique ability to catalyze two types of reactions using a *single* active site. As mentioned previously, the *functional* difference is obvious: the bifunctional enzymes have appreciable catalase activity, yet monofunctional peroxidases do not. Strangely, the catalase-peroxidase active site is nearly identical to that of monofunctional peroxidases. Structural comparison of these two types of enzymes reveals only three major differences: two interhelical insertions, and a C-terminal domain. Among them, the interhelical insertions contain about 35 amino acids each. One (the DE insertion) connects helices D and E. The other (the FG insertion) connects helices F and G. The C-terminal domain, which is also structurally similar to monofunctional peroxidases, is thought to be the product of a gene duplication event.

The work of the Goodwin laboratory, including that described in this dissertation, demonstrates that each structure is essential for the function of catalase-peroxidases. Importantly, all three of these structural components are peripheral to the active site. This highlights the functions of the structural features unique to the catalase-peroxidases, even with their peripheral locations to the active site. Consequently, it suggests that catalase-peroxidases are great models for the study of how the enzyme function is regulated at the global protein structural level.

4.1 Impacts of the FG Insertion

It has now been shown that the FG insertion is critical for the bifunctional capabilities of catalase-peroxidases. WtKatG showed substantial catalase activity with a turnover number of $(1.1 \pm 0.4) \times 10^4$ s^{-1}. The removal of the FG insertion caused a 99.8% loss of catalase activity (Table 4.1). Removal of this interhelical insertion, which is absent from monofunctional peroxidases, influences KatG catalytic function profoundly and makes this bifunctional enzyme function like a monofunctional peroxidase.

To explore how the FG insertion affects KatG function, the effects of the removal of this peripheral structural feature on the protein structure and function were examined.

Table 4.1. Steady-state Kinetic Parameters for Catalase and Peroxidase Activities of wtKatG and the Variants.

Substrate	Enzyme	K_M (mM)	k_{cat} (s^{-1})	k_{cat}/K_M ($M^{-1}s^{-1}$)
				k_{H2O2}
H_2O_2	wtKatG	0.83	58	7.1×10^4
(peroxidase activity)	$KatG^{\Delta DE}$	0.46	404	8.8×10^5
	$KatG^{\Delta FG}$	2.2	28	1.3×10^4
	$KatG^{\Delta DE/FG}$	5.0	117	2.3×10^4
				k_{ABTS}
ABTS	wtKatG	0.23	52	2.2×10^5
	$KatG^{\Delta DE}$	0.23	406	1.8×10^6
	$KatG^{\Delta FG}$	0.012	26	2.2×10^6
	$KatG^{\Delta DE/FG}$	0.051	170	3.3×10^6
H_2O_2	wtKatG	3.9	1.1×10^4	2.8×10^6
(catalase activity)	$KatG^{\Delta DE}$	-	-	-
	$KatG^{\Delta FG}$	4.5	26	5.7×10^3
	$KatG^{\Delta DE/FG}$	-	-	-

4.1.1 Roles of the FG insertion in KatG structure

The effects of the removal of the FG insertion on KatG structure were inspected to illuminate to what extent the structural changes were concomitant with the profound functional influence.

- *Heme coordination environment*

Removal of the FG insertion seemed to have no or little effect on KatG heme coordination environment. This is supported by UV-vis spectra of $KatG^{\Delta FG}$, which were very similar to those of wtKatG. Furthermore, EPR spectrum of $KatG^{\Delta FG}$ indicated dominance by a penta-coordinate high-spin heme species. This is similar to the heme environment observed in wtKatG [109], as well as other catalase-peroxidases and monofunctional peroxidases [130-133].

- *Non-ligand heme environment*

The FG insertion is essential to the catalase activity of KatG. Removal of this interhelical insertion caused a 500-fold decrease in the apparent second-order rate constant of catalase activity compared to wtKatG. However, $KatG^{\Delta FG}$ retained apparent k_{cat} values of peroxidase activity with respect to both H_2O_2 and ABTS

comparable to wtKatG (Table 4.1), suggesting that there is no fundamental change in the non-ligand heme environment when the FG insertion is removed from the KatG structure. Nevertheless, the removal of the FG insertion increased the apparent K_M for H_2O_2, suggesting that the peroxide molecule transport is interfered somehow when the FG insertion is removed. One possible reason is that the removal of the FG insertion interferes with the H-bonding system required for the reactions with H_2O_2.

- *Global protein structure*

Comparison of CD spectra of $KatG^{\Delta FG}$ and wtKatG showed about the same α–helical composition and a reasonable decrease in β-sheet composition in $KatG^{\Delta FG}$, indicating that no significant change in global protein structure occurred when the FG insertion was removed from the enzyme. Other data collected for $KatG^{\Delta FG}$, including UV-vis spectra, EPR spectra, and the kinetics of peroxidase activity suggested that global misfolding of the enzyme did not occur when FG insertion was removed from the enzyme.

4.1.2 Roles of the FG insertion in KatG function

Clearly, the structural consequences of removing the FG insertion were subtle.

However, the subtle alteration in structure resulted in a profound effect on KatG catalytic function.

- *Catalase activity*

This significant drop can be explained, at least in part, by the fact that the FG insertion serves to help peroxide molecules properly access the active site. One possible reason is that when this insertion is removed, the distal histidine gets closer to the active site, and consequently interferes with the accessibility of the active site to peroxide molecules. Another possible reason is that the removal of the FG insertion interferes with the H-bonding system. The catalase cycle involves two principal reactions with H_2O_2, compound I formation and compound I reduction. The rate-limiting step for catalase activity is thought to be compound I formation [138]. A hydrogen-bonding network involving Asp 135 and Asn 136 appears to be important for the catalase activity of catalase-peroxidases. The analogous residues in *Synechocystis* KatG (Asp 152 and Asn 153) are essential for full catalase activity. Interestingly, replacement of each of these residues diminishes catalase activity, apparently by differing mechanisms. Disruption of a hydrogen bond between the distal histidine and Asn 153 primarily affects compound I formation [139], whereas replacement of Asp 152 disrupts compound I reduction [140].

The change in pH profile for $KatG^{\Delta FG}$ is consistent with either a change in rate-determining step or a dramatic shift in the pKa's associated with it. The pH

profile is reminiscent of that observed for D152N *Synechocystis* KatG, where peroxide-dependent compound I reduction is the principal reaction affected by the substitution.

Given the consecutive appearance of Asp 135 and Asn 136 in catalase-peroxidases, it is reasonable to suggest that H-bonding interactions involving each of them may be disrupted by structural modification such as that described here. Indeed, the ascending and descending limbs of the FG insertion run roughly parallel to the H-bonding network outlined by His 106 (the distal histidine), Asn 136, and Leu 130 (carbonyl oxygen) (Figure 4.2) [87]. Indeed, the residues Glu 284 and Trp 297 lies fairly close to the H-bonding network (Figure 4.3).

- *Peroxidase reactions involving H_2O_2*

Evidence suggests that the removal of the FG insertion resulted in a decrease in the rate of compound I formation. Our k_{H2O2} values derived from peroxidase activity decreased five fold relative to wtKatG. This is in spite of the near absent catalase activity. The *catalatic* consumption of H_2O_2 is expected to diminish observed peroxidase activity due to the "non-productive" consumption of H_2O_2 (i.e., it does not result in oxidation of ABTS or other reducing substrates). Indeed, catalase-negative catalase-peroxidase variants often show an increase in peroxidase activity.

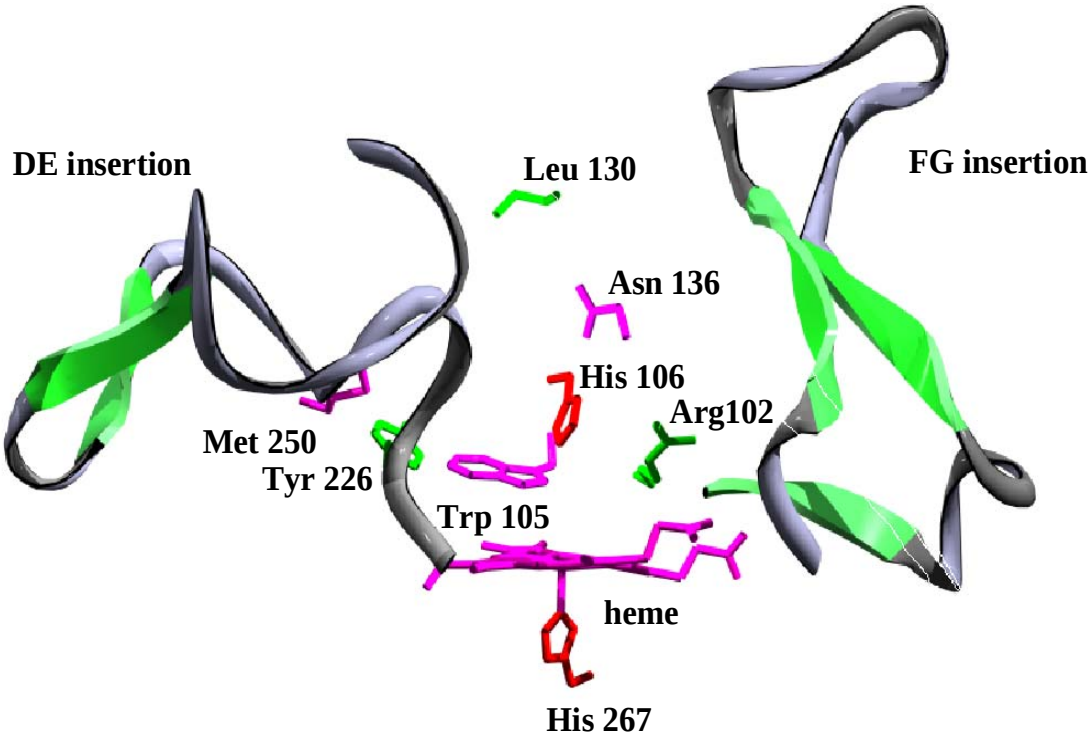

Figure 4.2. Position of the Insertions and Key Amino Acids within KatG Active Site.

(Carpena, X., et al. [2003] *J. Mol. Biol.* **327**, 475-489)

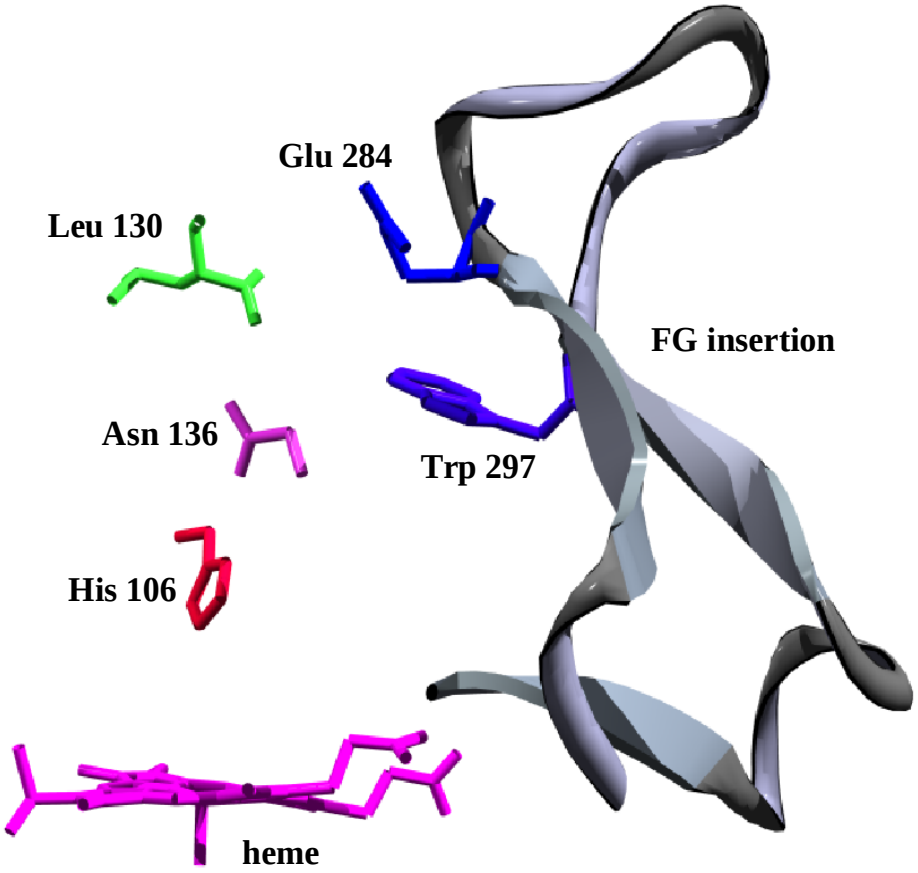

Figure 4.3. Position of the FG Insertion and the H-bonding Network Outlined by His 106, Asn 136, and Leu 130.

(Carpena, X., et al. [2003] *J. Mol. Biol.* **327**, 475-489)

Direct observation of peroxide-dependent KatG$^{\Delta FG}$ compound I formation by stopped-flow has been hampered by residual catalase activity and other difficulties. However, rates of CN^- binding, often monitored as a reaction analogous to the initial interaction of H_2O_2 with the heme iron, were diminished with KatG$^{\Delta FG}$ relative to wtKatG. An increase (~ 15 fold) in the dissociation constant for CN^- was also observed.

As discussed previously, efficient reactions with H_2O_2 required for catalase activity rely on properly aligned H-bonding networks. Compound I formation, common to both catalase and peroxidase activities, is no exception. In these properties, KatG$^{\Delta FG}$ resembles the N153A and N153D *Synechocystis* KatG variants [139].

- *Peroxidase reactions involving reducing substrate*

The rate-limiting step for peroxidase activity of catalase-peroxidases is typically compound I reduction [134]. Removal of the FG insertion caused a ten fold decrease in the apparent K_M for the reducing substrate, ABTS. As a result, k_{ABTS} observed for KatG$^{\Delta FG}$ increased drastically, and is more than 1200 fold higher than k_{H2O2} (Table 4.1), indicating the rate-limiting step has changed from compound I reduction to the one that requires the participation of H_2O_2, compound I formation. This effect is likely the combined effect of two consequences for removal of the FG insertion. The first

is the interference with the reaction with peroxide substrate as discussed above. The second is an apparent increase in access to the heme edge for electron donors.

Catalase-peroxidases have only a narrow aperture through which substrates enter the active site. The N-terminal (P277-S279) and C-terminal (G306-T311) ends of the FG insertion form a significant portion of the barrier separating the bulk solvent from the active site. Therefore, one possible function of the FG insertion is to favor catalase activity by lowering reaction rates with reducing substrate. It is reasonable to expect that the absence of this barrier would enhance electron transfer in the reductive steps of the peroxidase cycle. Generally, enhanced electron transfer would be apparent from k_{ABTS} and k_{cat} obtained with respect to ABTS. However, if the rate limiting step is compound I formation, not ABTS oxidation, only an increase in k_{ABTS} with a decrease in apparent K_M would be expected. Interestingly, the interaction of ABTS with $KatG^{\Delta FG}$ results in inhibition at moderate concentrations. The enhanced access of the reducing substrate to the active site may, at these concentrations, interfere with access of other substrates to the enzyme active site. The combined effect of lowered k_{H2O2} and increased k_{ABTS} tilts the balance toward peroxidase activity and away from catalase activity.

4.2 Impacts of the DE Insertion

The DE insertion seemed to be more critical for the bifunctionality of catalase-peroxidases than FG insertion. The removal of the DE insertion caused the total loss of

catalase activity. KatG$^{\Delta DE}$ showed some additional properties that were unique in comparison to either wtKatG or KatG$^{\Delta FG}$. KatG$^{\Delta DE}$ appeared to be less stable than either wtKatG or KatG$^{\Delta FG}$. First, it was expressed in inclusion bodies rather than in a soluble form. Second, maximal activity was observed with only 0.25 equivalent hemin, more hemin added could not contribute to more activity. In spite of the apparent compromise to structural stability, KatG$^{\Delta DE}$ also showed substantially elevated peroxidase activity compared to wtKatG, and similar to monofunctional peroxidases, KatG$^{\Delta DE}$ showed a propensity to peroxide-dependent inactivation.

4.2.1 Roles of the DE insertion in KatG structure

To illuminate how the KatG structure was affected by the removal of the DE insertion, and how the changes in the structure may influence KatG function, the effects of the DE insertion on KatG structure were inspected.

- *Heme coordination environment*

The DE insertion showed more influence on heme coordination state than FG insertion. UV-vis spectra of KatG$^{\Delta DE}$ revealed a decrease in intensity of the charge-transfer bands compared to wtKatG, indicating more hexa-coordinate low-spin species present compared to wtKatG. Similar phenomena were observed when comparing

UV-vis spectra of KatG$^{\Delta DE/FG}$ to KatG$^{\Delta FG}$. The high proportion of low-spin species was confirmed by EPR spectra of wtKatG and KatG$^{\Delta DE}$ [109]. The identity of this sixth ligand is still unclear. Due to the fact of low-spin state, this strong-field ligand could be the distal histidine, or a OH^- molecule.

- *Non-ligand heme environment*

The DE insertion appeared to have a greater influence on the heme coordination environment than the FG insertion. This suggests that there must also be some changes in the non-ligand heme environment. However, the high peroxidase activity and the susceptibility to the formation of compound III suggested that the non-ligand heme environment became more similar to monofunctional peroxidases.

- *Global protein structure*

Like KatG$^{\Delta FG}$, comparison of CD spectra of KatG$^{\Delta DE}$ with wtKatG showed similar α–helical composition and a reasonable decrease in β-sheet composition, indicating that changes in heme coordination and non-ligand environment were not accompanied by dramatic changes in overall secondary structural content.

4.2.2 Roles of the DE insertion in KatG function

Apparently DE insertion, though peripheral to the active site, plays important roles in maintaining the proper heme coordination environment and non-ligand active site environment. Though the phenomenon needs further exploration, the influence of the removal of the DE insertion on KatG function can be partly explained by these active site environmental changes.

- *Catalase activity*

Recent site-directed mutagenesis studies have identified three mechanisms by which the catalase activity of catalase-peroxidase is supported by the active site. Each participant in a novel covalent link (Trp 105, Tyr 226, and Met 252 [*E. coli* KatG numbering]) (Figure 4.2) has been shown in at least one catalase-peroxidase to be essential for catalase but not peroxidase activity [111, 116, 141]. The central residue of this covalent adduct, Tyr 226, is located in the DE insertion. Substitution of this tyrosine to phenylalanine causes the total loss of catalase activity [115, 116, 142]. This strongly suggests that the loss of catalase activity is due to the loss of this tyrosine. However, as will be discussed below, the function of the DE insertion clearly extends beyond simply positioning this critical tyrosine. It is not unreasonable to suggest that other features of the DE insertion are essential for catalase activity as well.

- *Peroxidase reactions involving H_2O_2*

a) Formation of compound III and peroxide-dependent inactivation

Peroxidase activity of KatG$^{\Delta DE}$ displayed a hyperbolic dependence on H_2O_2 at concentrations below 1 mM. However, in behavior distinct from wtKatG, the peroxidase activity of KatG$^{\Delta DE}$ decreased markedly at higher H_2O_2 concentrations. This observation coincided with the appearance of a lag phase in the peroxidase activity with H_2O_2 concentrations higher than 1 mM. As H_2O_2 concentrations were increased, the lag phase became more pronounced and the peroxidase activity following the lag phase decreased as well.

Conversely, ABTS showed the ability to reduce the lag phase. Increasing the concentration of ABTS reduced the duration of the lag phase and increased peroxidase activity following the lag phase. We even observed sigmoidal instead of hyperbolic response of KatG$^{\Delta DE}$ peroxidase activity to ABTS concentration, indicating that the reducing substrate is able to not only prevent the lag phase, but reverse it to some extent.

The counteracting effects of peroxide and reducing substrate in which H_2O_2 favors the inactivation of the enzyme while ABTS tends to keep the enzyme in the active form, suggest a mechanism involving the formation of compound III. Compound III, also known as oxyperoxidase, is an inactive complex with respect to peroxidase catalysis. Both ABTS and H_2O_2 compete to react with compound II

(Figure 4.3). The reaction of compound II with ABTS keeps KatG$^{\Delta DE}$ operating in its catalytic cycle. On the other hand, reaction of excess H_2O_2 with compound II leads to compound III formation. Compound III has no activity and further reactions involving H_2O_2 lead to the irreversible inactivation of the enzyme. For wtKatG, the formation of compound III is not observed unless H_2O_2 concentrations approach 0.4 M [116]. The rate-limiting step for wtKatG peroxidase activity is compound I reduction. Compound I, not compound II, accumulates as the steady-state intermediate. Conversely, when DE insertion is removed, compound II reduction becomes the rate-determining step, and thus, compound II accumulates in the steady-state. Consequently, the enzyme is much more susceptible to compound III formation, even in the presence of H_2O_2 concentrations as low as 0.1 mM.

b) Roles of ABTS$^{\bullet+}$ in the peroxidase activity of KatG$^{\Delta DE}$

When the concentration of H_2O_2 exceeded 1 mM, individual activity curves (A_{417} *vs.* time) exhibited an acceleration in the formation of ABTS$^{\bullet+}$ (the product of peroxidase activity). In other words, a lag phase was apparent (Figure 3.25). The presence of a lag phase indicated that the proportion of active KatG$^{\Delta DE}$ increased with time, suggesting a rescue from peroxide-dependent inactivation. The extent of the lag phase became greater with increasing concentrations of H_2O_2, and the activity observed following the lag phase dcreased. This indicated that with the more H_2O_2 present, there was more irreversible inactivation of the enzyme. Therefore, there was

less enzyme to recover, and less peroxidase activity can be recovered following the lag phase.

Since the rescue of the inactivated KatG$^{\Delta DE}$ occurs as a result of the reaction processes, it is reasonable to suggest that the key species in the rescue of the compound III is $ABTS^{\bullet+}$. First, $ABTS^{\bullet+}$ is the only product of the peroxidase activity of KatG during the reaction other than water. Second, there is some evidence to suggest that cation radicals prevent irreversible inactivation by H_2O_2 [82-85]. The effect of $ABTS^{\bullet+}$ addition on the peroxidase activity confirmed this hypothesis. It showed that $ABTS^{\bullet+}$ not only reduced the lag time of the reaction, but also increased the reaction rate following the lag phase as well. It is suggested that the rescue pathway of compound III occurs via ferric enzyme, because the rescue process involves the release of O_2, and there is evidence that the radical causes the disappearance of compound III in favor of ferric enzyme (data not shown) (Figure 4.4).

- *Peroxidase reactions involving reducing substrate*

One unique feature of KatG$^{\Delta DE}$ compared to wtKatG and KatG$^{\Delta FG}$ is that KatG$^{\Delta DE}$ showed a peroxidase activity that is seven fold higher than that of wtKatG, mainly because the DE insertion serves to regulate the access of the reducing substrate to the heme edge. Thus, the removal of DE insertion increased the rate of

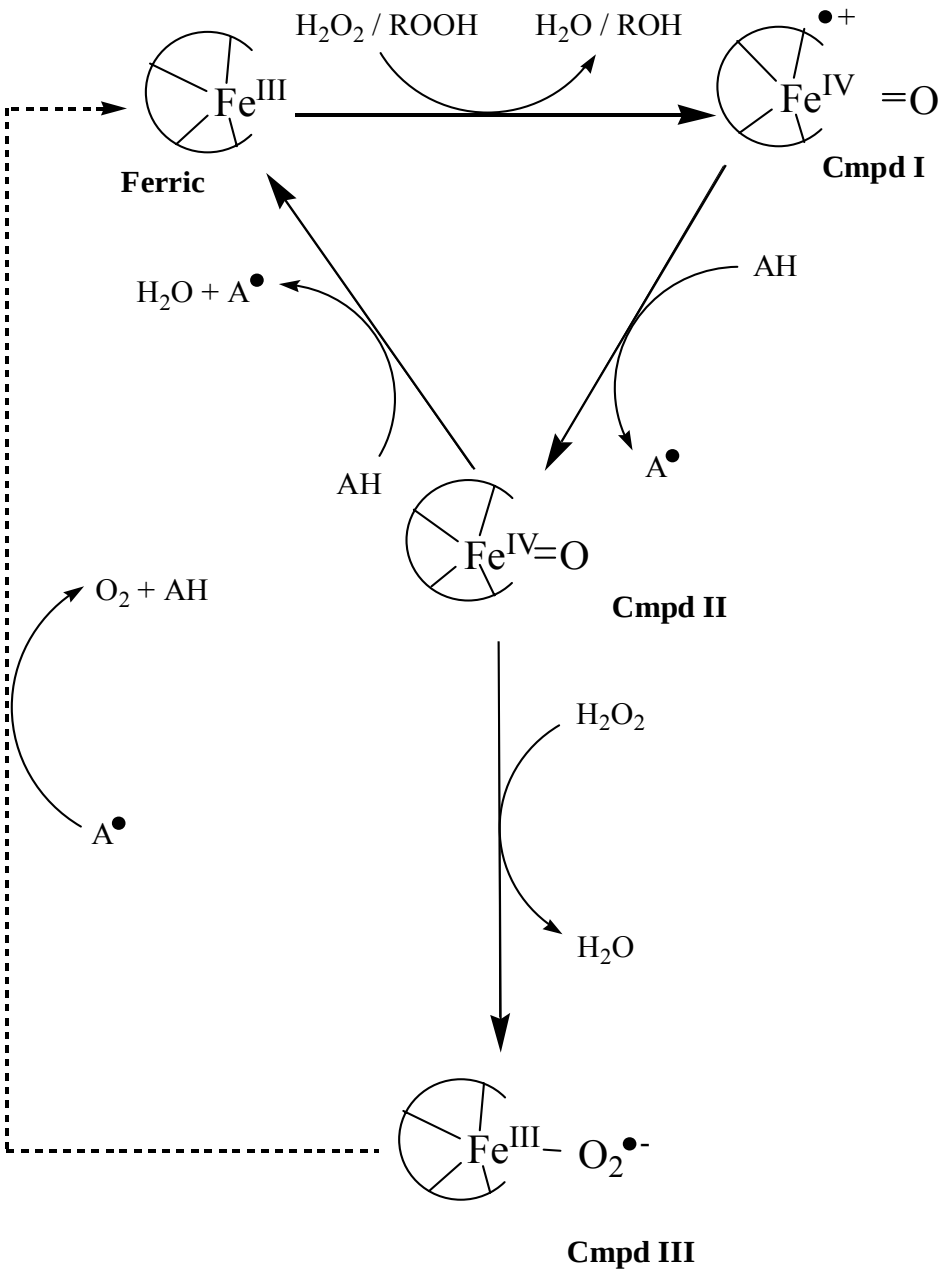

(AH: reducing substrate)

Figure 4.4. Proposed Catalytic Cycle of $KatG^{\Delta DE}$.

compound I reduction, which is typically the rate limiting step of KatG peroxidase activity catalytic cycle [134], and in turn made the compound II reduction step rate-limiting. The accumulation of compound II is, therefore, the major consequence. Interestingly, though the center piece of the novel covalent adduct (Trp-Tyr-Met), Tyr 226, is located in this insertion, these changes in reaction rate and rate limiting step were not observed in the single tyrosine to phenylalanine variant [116]. However, such results are compatible with monofunctional peroxidases, indicating the DE insertion as a whole has more roles in the enzyme bifunctionality than those explained by the tyrosine alone.

4.3 Collaboration of the Two Insertions and C-terminal Domain

4.3.1 Implication of roles of the interhelical insertions by KatG$^{\Delta DE/FG}$

Compared to KatG$^{\Delta FG}$, KatG$^{\Delta DE/FG}$ showed much higher apparent k_{cat}, and a higher apparent second-order rate constant with respect to ABTS (Table 4.1), confirming that the DE insertion serves to regulate the access of reducing substrate to the heme edge.

Compared to KatG$^{\Delta DE}$, the k_{on} value for CN^- of KatG$^{\Delta DE/FG}$ was higher, suggesting the active site is more accessible to peroxide substrates when the FG insertion is removed. However, the k_{H2O2} value of KatG$^{\Delta DE/FG}$ is much lower than that of KatG$^{\Delta DE}$, which indicates that the FG insertion is required for the reactions

with H_2O_2, most likely via an H-bonding system that includes Asp 135 and Asn 136. Meanwhile, $KatG^{\Delta DE/FG}$ showed a higher apparent second-order rate constant with respect to ABTS, confirming that the FG insertion regulates the access of reducing substrates to the heme edge. Consequently, the k_{ABTS} value of $KatG^{\Delta DE/FG}$ was more than 1400 fold higher than k_{H2O2}, which indicates that the rate-limiting step was compound I formation. Thus, it is reasonable to suggest that the ferric form of the enzyme accumulated instead of compound II. The prerequisite of the formation of compound III is compound II formation, as in the case of $KatG^{\Delta DE}$. This change in rate limiting step is also compatible with the proposition that the FG insertion helps poise the active site for reaction with peroxide, while simultaneously regulating the reducing substrate access to the heme edge.

4.3.2 Roles of $KatG^{C\text{-}term}$ in active site architecture

According to the research performed by our group, when C-terminal domain of KatG is removed, the active site is reorganized allowing distal histidine, His 106, to become the sixth coordination ligand of the active site heme [109]. The C-terminal domain executes this role of supporting the distal histidine by supporting the B-helix of the N-terminal domain via several polar interactions between the surfaces of both N- and C-terminal domains. Interestingly, incubation of $KatG^{N\text{-}term}$ with an equimolar concentration of the separately expressed and isolated C-terminal domain ($KatG^{C\text{-}term}$) results in partial recover of both catalase *and* peroxidase activities [109].

When KatG$^{N\text{-term}/\Delta FG}$ with hemin present was mixed with KatG$^{C\text{-term}}$, the peroxidase activity was restored to a level observed for KatG$^{\Delta FG}$. However, the process was slow. It took 24 hours for the recombined domains to reach maximal activity.

The visible absorption spectrum of KatG$^{N\text{-term}/\Delta FG}$ was dominated by a low-spin heme species. This low-spin state was confirmed by EPR. However, after a 24-hour incubation with equimolar KatG$^{C\text{-term}}$, both visible and EPR spectra indicated a substantial shift to a penta-coordinate high-spin heme species. All these data indicated that, though slowly, KatG$^{C\text{-term}}$ was able to interact with KatG$^{N\text{-term}/\Delta FG}$ and form the proper interactions required for reconstructing the architecture of the active site.

Similar phenomena in visible spectra were also observed for KatG$^{N\text{-term}/\Delta DE}$, only in that the spectrum of KatG$^{\Delta DE}$ had a greater contribution of low-spin species when compared to KatG$^{\Delta FG}$. The restoration of peroxidase activity took longer than KatG$^{N\text{-term}/\Delta FG}$, most likely because DE also plays a role in directing the hemin to the active site and maintaining the proper architecture of the active site. Moreover, recombined KatG$^{N\text{-term}/\Delta DE}$ with KatG$^{C\text{-term}}$ showed other properties similar to KatG$^{\Delta DE}$, like peroxide-dependent inactivation, supporting that the reformation of the enzyme structure by KatG$^{C\text{-term}}$ was precise.

All these results confirm that though slowly, KatG$^{C\text{-term}}$ added extrinsically is capable of getting to the proper position and restoring the suitable heme environment

for the activities by preventing the coordination of the distal histidine, despite of its peripheral position to the active site. Indeed, the C-terminal domain comes no closer to the active site than 30 Å.

4.4 Summary

Though clearly heme is very important to enzyme function, little is understood about the influence of protein structural features peripheral to an active site on the function heme enzymes. Progress in understanding the mechanisms by which global protein structure support and fine-tune catalysis has been hindered by a lack of adequate models for research in this area. The size and complexity of most enzymes make it difficult to identify critical residues or structures for study. Moreover, results can be difficult to interpret due to the multiple effects of amino acids in the structural features.

The work described in this dissertation demonstrates that KatG is an excellent model to evaluate protein structure-function relationships. Furthermore, we have demonstrated that KatG is amenable to considerable fine-tuning, making it an ideal target for enzyme engineering. With KatG, we first introduced a novel deletion mutagenesis procedure to demonstrate how some heme enzyme structural features, though peripheral to the active site, influence the inner heme enzyme structural levels and enzyme functions. The effects of removal of the two interhelical insertions of KatG

confirm that changes of the structures peripheral to the active site will affect heme coordination state, as well as non-ligand heme environment; furthermore, the structures peripheral to the active site are important for dictating the catalytic properties of the enzyme. However, the changes in enzyme function induced by the changes in peripheral structures also rely on some other factors other than its effects on the inner structural levels.

We first introduced this novel procedure for deletion mutagenesis to eliminate some structural features that are unique to catalase-peroxidase, the FG insertion, and the DE insertion. One of the resulting variants, KatG$^{\Delta FG}$, had very little catalase activity but retained peroxidase activity comparable to the wild-type enzyme. The selective loss of catalase activity was observed despite the peripheral position of the FG insertion relative to the active site. This indicates that the FG insertion has a role in fine-tuning the catalase-peroxidase active site for its unique bifunctionality. The spectral and kinetic properties of KatG$^{\Delta FG}$ suggest that it supports hydrogen-bonded networks that are integral to catalase activity and regulates access of peroxidatic electron donors to the active site. Moreover, the FG insertion seemed to help peroxide substrates get into the active site, and as a result, the rate limiting step of peroxidase catalytic cycle of KatG$^{\Delta FG}$ changed from compound I reduction, as for wtKatG, to compound I formation.

Another resulting variant, KatG$^{\Delta DE}$, helped us look further into the mechanisms of catalase-peroxidases and monofunctional peroxidases. The DE insertion functions to regulate the access of reducing substrates to the heme edge.

Thus, with the DE insertion removed, KatG$^{\Delta DE}$ showed a change in rate limiting step to compound II reduction. Consequently, KatG$^{\Delta DE}$ showed peroxidase activity about seven fold greater than that of the wtKatG, together with the accumulation of compound II. Compound II is the precursor to the formation of inactive compound III in the presence of H_2O_2, and further leads to the peroxide-dependent inactivation. Meanwhile, to keep the enzyme in the active form, not only the reducing substrate can compete with H_2O_2 in reacting with compound II, inactive compound III can also be rescued back to the catalytic cycle by means of peroxidase-generated cation radicals. Furthermore, a novel covalent adduct Trp-Tyr-Met, which was also absent in monofunctional peroxidases, was discovered and proved to be critical for catalase activity [110, 111, 115, 116], and the center tyrosine is located in the DE insertion [86-88]. However, alteration of this tyrosine alone did not stimulate the change in rate limiting step, nor affect the accessibility of the heme to the reducing substrate or H_2O_2, indicating the regulation of the access to the heme and thus keeping the rate limiting step to be the co mpound I reduction requires more than the tyrosine in the covalent adduct.

Both of its insertions, despite of their peripheral positions relative to the active site, serve to fine-tune the active site, and collaborate for the full function of these enzymes. KatG has helped us better understand how enzyme function is dictated at the global structure level. Not only do such studies provide a fundamental understanding necessary for protein structure and function, which will be useful for understanding the resistance to isoniazid, how these enzymes may be used by pathogens as virulence factors,

as well as better utilizing catalase-peroxidase for generation of new redox-activated antibiotics, but they also provide the essential components for enzyme engineering using KatG as a starting point. Such enzyme engineering using KatG could be used to explore how to fine-tune the active site for manipulating enzyme function by modifying structures at the global protein structural level, which could be practical for development of new catalysts to remove recalcitrant and toxic environmental pollutants.

REFERENCES

[1] L. Stawiarski, Ration. Med. 3 (1853) 375.

[2] C. A. McMunn, J. Physiol. 5 (1886) 34.

[3] D. Keilin, Proc. R. Soc. London, B 98 (1925) 312.

[4] J. E. Erman, L. P. Hager, and S. G. Sligar, Cytochrome P-450 and peroxidase chemistry, Adv Inorg Biochem 10 (1994) 71-118.

[5] M. Paoli, J. Marles-Wright, and A. Smith, Structure-function relationships in heme-proteins, DNA Cell Biol 21 (2002) 271-280.

[6] T. Mogi, K. Saiki, and Y. Anraku, Biosynthesis and functional role of haem O and haem A, Mol Microbiol 14 (1994) 391-398.

[7] G. R. Moore, Cytochrome c: evolutionary, structural and physiochemical aspects, ed. 1990.

[8] L. Thony-Meyer, Haem-polypeptide interactions during cytochrome c maturation, Biochim Biophys Acta 1459 (2000) 316-324.

[9] J. M. Stevens, O. Daltrop, J. W. Allen, and S. J. Ferguson, C-type cytochrome formation: chemical and biological enigmas, Acc Chem Res 37 (2004) 999-1007.

[10] J. W. Allen, N. Leach, and S. J. Ferguson, The histidine of the c-type cytochrome CXXCH heme-binding motif is essential for heme attachment by the Escherichia coli cytochrome c maturation (Ccm) apparatus, Biochem J (2005).

[11] E. J. Tomlinson, and S. J. Ferguson, Conversion of a c type cytochrome to a b type that spontaneously forms in vitro from apo protein and heme: implications for c type cytochrome biogenesis and folding, Proc Natl Acad Sci U S A 97 (2000) 5156-5160.

[12] G. W. Pettigrew, J. L. Leaver, T. E. Meyer, and A. P. Ryle, Purification, properties and amino acid sequence of atypical cytochrome c from two protozoa, Euglena gracilis and Crithidia oncopelti, Biochem J 147 (1975) 291-302.

[13] R. P. Ambler, M. D. Kamen, R. G. Bartsch, and T. E. Meyer, Amino acid sequences of Euglena viridis ferredoxin and cytochromes c, Biochem J 276 (Pt 1) (1991) 47-52.

[14] J. W. Priest, and S. L. Hajduk, Cytochrome c reductase purified from Crithidia fasciculata contains an atypical cytochrome c1, J Biol Chem 267 (1992) 20188-20195.

[15] B. K. Vainshtein, W. R. Melik-Adamyan, V. V. Barynin, A. A. Vagin, A. I. Grebenko, V. V. Borisov, K. S. Bartels, I. Fita, and M. G. Rossmann, Three-dimensional structure of catalase from Penicillium vitale at 2.0 A resolution, J Mol Biol 188 (1986) 49-61.

[16] G. N. Murshudov, A. I. Grebenko, V. Barynin, Z. Dauter, K. S. Wilson, B. K. Vainshtein, W. Melik-Adamyan, J. Bravo, J. M. Ferran, J. C. Ferrer, J. Switala, P. C. Loewen, and I. Fita, Structure of the heme d of Penicillium vitale and Escherichia coli catalases, J Biol Chem 271 (1996) 8863-8868.

[17] K. M. Barkigia, C. K. Chang, and J. Fajer, Molecular structure of a dihydroxychlorin. A model of the green heme d and of a photodynamic therapy sensitizer, Journal of the American Chemical Society 113 (1991) 7445 - 7447.

[18] T. L. Poulos, B. C. Finzel, and A. J. Howard, High-resolution crystal structure of cytochrome P450cam, J Mol Biol 195 (1987) 687-700.

[19] P. Kotsonis, L. G. Frohlich, C. S. Raman, H. Li, M. Berg, R. Gerwig, V. Groehn, Y. Kang, N. Al-Masoudi, S. Taghavi-Moghadam, D. Mohr, U. Munch, J. Schnabel, P.

Martasek, B. S. Masters, H. Strobel, T. Poulos, H. Matter, W. Pfleiderer, and H. H. Schmidt, Structural basis for pterin antagonism in nitric-oxide synthase. Development of novel 4-oxo-pteridine antagonists of (6R)-5,6,7,8-tetrahydrobiopterin, J Biol Chem 276 (2001) 49133-49141.

[20] R. E. Dickerson, T. Takano, D. Eisenberg, O. B. Kallai, L. Samson, A. Cooper, and E. Margoliash, Ferricytochrome c. I. General features of the horse and bonito proteins at 2.8 A resolution, J Biol Chem 246 (1971) 1511-1535.

[21] J. H. Dawson, Probing structure-function relations in heme-containing oxygenases and peroxidases, Science 240 (1988) 433-439.

[22] P. R. Ortiz, Cytochrome P450: structure, mechanism and biochemistry, ed., Plenum, New York 1995.

[23] O. Hayaishi, History and scope, in Oxygenases, Academic Press, New York, 1962, pp. 1-29.

[24] H. S. Mason, Mechanisms of oxygen metabolism, in Advances in Enzymology, in Nord, F. F., (Ed.), Academic Press, New York, 1957, pp. 79-134.

[25] S. G. Sligar, and I. C. Gunsalus, A thermodynamic model of regulation: modulation of redox equilibria in camphor monoxygenase, Proc Natl Acad Sci U S A 73 (1976) 1078-1082.

[26] C. F. Harford-Cross, A. B. Carmichael, F. K. Allan, P. A. England, D. A. Rouch, and L. Wong, Protein engineering of cytochrome P450cam (CYP101) for the oxidation of polycyclic aromatic hydrocarbons, Protein Eng. 13 (2000) 121-128.

[27] I. Schlichting, J. Berendzen, K. Chu, A. M. Stock, S. A. Maves, D. E. Benson, R. M. Sweet, D. Ringe, G. A. Petsko, and S. G. Sligar, The catalytic pathway of cytochrome p450cam at atomic resolution, Science 287 (2000) 1615-1622.

[28] D. Mansuy, The great diversity of reactions catalyzed by cytochromes P450, Comp Biochem Physiol C Pharmacol Toxicol Endocrinol 121 (1998) 5-14.

[29] J. H. Dawson, R. H. Holm, J. R. Trudell, G. Barth, R. E. Linder, E. Bunnenberg, C. Djerassi, and S. C. Tang, Letter: Oxidized cytochrome P-450. Magnetic circular

dichroism evidence for thiolate ligation in the substrate-bound form. Implications for the catalytic mechanism, J Am Chem Soc 98 (1976) 3707-3708.

[30] J. A. Hasler, Pharmacogenetics of cytochromes P450, Mol Aspects Med 20 (1999) 12-24, 25-137.

[31] M. Sono, J. H. Dawson, K. Hall, and L. P. Hager, Ligand and halide binding properties of chloroperoxidase: peroxidase-type active site heme environment with cytochrome P-450 type endogenous axial ligand and spectroscopic properties, Biochemistry 25 (1986) 347-356.

[32] J. B. Wittenberg, Oxygen transport: a new function proposed for myoglobin, Biol. Bull. 117 (1959) 402-403.

[33] P. George, and D. H. Irvine, A possible structure for the higher oxidation state of metmyoglobin, Biochem J 60 (1955) 596-604.

[34] R. Roncone, E. Monzani, M. Murtas, G. Battaini, A. Pennati, A. M. Sanangelantoni, S. Zuccotti, M. Bolognesi, and L. Casella, Engineering peroxidase activity in myoglobin: the haem cavity structure and peroxide activation in the T67R/S92D mutant and its derivative reconstituted with protohaemin-l-histidine, Biochem J 377 (2004) 717-724.

[35] J. C. Kendrew, G. Bodo, H. M. Dintzis, R. G. Parrish, H. Wyckoff, and D. C. Phillips, A three-dimensional model of the myoglobin molecule obtained by x-ray analysis, Nature 181 (1958) 662-666.

[36] M. F. Perutz, J. C. Kendrew, and H. C. Watson, Structure and function of haemoglobin II. Some relations between polypeptide chain configuration and amino acid sequence, J. Mol. Biol. 13 (1965) 669-678.

[37] V. Riveros-Moreno, and J. B. Wittenberg, The self-diffusion coefficients of myoglobin and hemoglobin in concentrated solutions, J Biol Chem 247 (1972) 895-901.

[38] W. B. Veldkamp, and J. R. Votano, Effects of intermolecular interaction on protein diffusion in solution, Journal of Physical Chemistry 80 (1976) 2794-2801.

[39] B. A. Wittenberg, and J. B. Wittenberg, Transport of oxygen in muscle, Annu Rev Physiol 51 (1989) 857-878.

[40] R. E. Dickerson, Hemoglobin: structure, function, evolution and pathology, ed., Benjammin/Cummings, Menlo Park, CA 1983.

[41] M. F. Perutz, Mechanisms of cooperativity and allosteric regulation in proteins, Q Rev Biophys 22 (1989) 139-237.

[42] C. F. Schonbein, J. Prakt. Chem. 98 (1863) 323.

[43] O. Warburg, Versuche und uberledbeudem carcinomgewebe (methoden). Biochem Z. 142 (1923) 317-333.

[44] D. Dolphin, A. Forman, D. C. Borg, J. Fajer, and R. H. Felton, Compounds I of catalase and horse radish peroxidase: pi-cation radicals, Proc Natl Acad Sci U S A 68 (1971) 614-618.

[45] G. N. Murshudov, W. R. Melik-Adamyan, A. I. Grebenko, V. V. Barynin, A. A. Vagin, B. K. Vainshtein, Z. Dauter, and K. S. Wilson, Three-dimensional structure of catalase from Micrococcus lysodeikticus at 1.5 A resolution, FEBS Lett 312 (1992) 127-131.

[46] P. Gouet, H. M. Jouve, and O. Dideberg, Crystal structure of Proteus mirabilis PR catalase with and without bound NADPH, J Mol Biol 249 (1995) 933-954.

[47] J. Bravo, N. Verdaguer, J. Tormo, C. Betzel, J. Switala, P. C. Loewen, and I. Fita, Crystal structure of catalase HPII from Escherichia coli, Structure 3 (1995) 491-502.

[48] B. K. Vainshtein, W. R. Melik-Adamyan, V. V. Barynin, A. A. Vagin, and A. I. Grebenko, Three-dimensional structure of the enzyme catalase, Nature 293 (1981) 411-412.

[49] S. Berthet, L. M. Nykyri, J. Bravo, M. J. Mate, C. Berthet-Colominas, P. M. Alzari, F. Koller, and I. Fita, Crystallization and preliminary structural analysis of catalase A from Saccharomyces cerevisiae, Protein Sci 6 (1997) 481-483.

[50] M. R. Murthy, T. J. Reid, 3rd, A. Sicignano, N. Tanaka, and M. G. Rossmann, Structure of beef liver catalase, J Mol Biol 152 (1981) 465-499.

[51] W. R. Melik-Adamyan, V. V. Barynin, A. A. Vagin, V. V. Borisov, B. K. Vainshtein, I. Fita, M. R. Murthy, and M. G. Rossmann, Comparison of beef liver and Penicillium vitale catalases, J Mol Biol 188 (1986) 63-72.

[52] J. Switala, J. O. O'Neil, and P. C. Loewen, Catalase HPII from Escherichia coli exhibits enhanced resistance to denaturation, Biochemistry 38 (1999) 3895-3901.

[53] M. Zamocky, and F. Koller, Understanding the structure and function of catalases: clues from molecular evolution and in vitro mutagenesis, Prog Biophys Mol Biol 72 (1999) 19-66.

[54] I. Fita, and M. G. Rossmann, The active center of catalase, J Mol Biol 185 (1985) 21-37.

[55] T. J. Reid, 3rd, M. R. Murthy, A. Sicignano, N. Tanaka, W. D. Musick, and M. G. Rossmann, Structure and heme environment of beef liver catalase at 2.5 A resolution, Proc Natl Acad Sci U S A 78 (1981) 4767-4771.

[56] C. Obinger, M. Maj, P. Nicholls, and P. Loewen, Activity, peroxide compound formation, and heme d synthesis in Escherichia coli HPII catalase, Arch Biochem Biophys 342 (1997) 58-67.

[57] H. N. Kirkman, S. Galiano, and G. F. Gaetani, The function of catalase-bound NADPH, J Biol Chem 262 (1987) 660-666.

[58] A. Hillar, P. Nicholls, J. Switala, and P. C. Loewen, NADPH binding and control of catalase compound II formation: comparison of bovine, yeast, and Escherichia coli enzymes, Biochem J 300 (Pt 2) (1994) 531-539.

[59] H. B. Dunford, Heme peroxidases, ed., Wiley-VCH, New York 1999.

[60] H. B. Dunford, and J. S. Stillman, On the function and mechanism of action of peroxidases, Coordination Chemistry Reviews 19 (1976) 187-251.

[61] D. E. Hultquist, and M. Morrison, Lactoperoxidase. I. The Prosthetic Group of Lactoperoxidase, J Biol Chem 238 (1963) 2843-2846.

[62] K. G. Welinder, Plant peroxidases. Their primary, secondary and tertiary structures, and relation to cytochrome c peroxidase, Eur J Biochem 151 (1985) 497-504.

[63] K. G. Welinder, Superfamily of plant, fungal and bacterial peroxidases, Current Opinion in Structural Biology 2 (1992) 388-393.

[64] C. A. Reddy, An overview of the recent advances on the physiology and molecular biology of lignin peroxidases of Phanerochaete chrysosporium, J Biotechnol 30 (1993) 91-107.

[65] B. C. Finzel, T. L. Poulos, and J. Kraut, Crystal structure of yeast cytochrome c peroxidase refined at 1.7-A resolution, J Biol Chem 259 (1984) 13027-13036.

[66] M. Sundaramoorthy, K. Kishi, M. H. Gold, and T. L. Poulos, The crystal structure of manganese peroxidase from Phanerochaete chrysosporium at 2.06-A resolution, J Biol Chem 269 (1994) 32759-32767.

[67] A. Henriksen, K. G. Welinder, and M. Gajhede, Structure of barley grain peroxidase refined at 1.9-A resolution. A plant peroxidase reversibly inactivated at neutral pH, J Biol Chem 273 (1998) 2241-2248.

[68] K. Wada, T. Tada, Y. Nakamura, T. Ishikawa, Y. Yabuta, K. Yoshimura, S. Shigeoka, and K. Nishimura, Crystal structure of chloroplastic ascorbate peroxidase from tobacco plants and structural insights into its instability, J Biochem (Tokyo) 134 (2003) 239-244.

[69] N. Kunishima, K. Fukuyama, H. Matsubara, H. Hatanaka, Y. Shibano, and T. Amachi, Crystal structure of the fungal peroxidase from Arthromyces ramosus at 1.9 A resolution. Structural comparisons with the lignin and cytochrome c peroxidases, J Mol Biol 235 (1994) 331-344.

[70] H. B. Dunford, Peroxidases in chemistry and biology, ed., CRC Press, Boca Raton, FL 1990.

[71] T. H. Moss, A. Ehrenberg, and A. J. Bearden, Mossbauer spectroscopic evidence for the electronic configuration of iron in horseradish peroxidase and its peroxide derivatives, Biochemistry 8 (1969) 4159-4162.

[72] J. E. Penner-Hahn, K. S. Eble, T. J. McMurry, M. Renner, A. L. Balch, J. T. Groves, J. H. Dawson, and K. O. Hodgson, Structural characterization of horseradish peroxidase using EXAFS spectroscopy. Evidence for Fe = O ligation in compounds I and II, Journal of the American Chemical Society 108 (1986) 7819-7825.

[73] G. N. La Mar, J. S. De Ropp, L. Latos-Grazynski, A. L. Balch, R. B. Johnson, K. M. Smith, D. W. Parish, and R. J. Cheng, Proton NMR characterization of the ferryl group in model heme complexes and hemoproteins: evidence for the FeIVO group in ferryl myoglobin and compound II of horseradish peroxidase, Journal of the American Chemical Society 105 (1983) 782-787.

[74] R. S. Koduri, and M. Tien, Kinetic analysis of lignin peroxidase: explanation for the mediation phenomenon by veratryl alcohol, Biochemistry 33 (1994) 4225-4230.

[75] H. E. Schoemaker, T. K. Lundell, A. I. Hatakka, and K. Piontek, The oxidation of veratryl alcohol, dimeric lignin models and lignin by lignin peroxidase: The redox cycle revisited, FEMS Microbiology Reviews 13 (1994) 321-331.

[76] B. Sauders, and B. P. Stark, Peroxidases, ed., Butterworth & Co., Washington, D. C. 1964.

[77] C. Jakopitsch, A. Wanasinghe, W. Jantschko, P. G. Furtmuller, and C. Obinger, Kinetics of interconversion of ferrous enzymes, compound II and compound III, of wild-type synechocystis catalase-peroxidase and Y249F: proposal for the catalatic mechanism, J Biol Chem 280 (2005) 9037-9042.

[78] D. Y. Cai, and M. Tien, Characterization of the oxycomplex of lignin peroxidases from Phanerochaete chrysosporium: equilibrium and kinetics studies, Biochemistry 29 (1990) 2085-2091.

[79] M. Huwiler, H. Jenzer, and H. Kohler, The role of compound III in reversible and irreversible inactivation of lactoperoxidase, Eur J Biochem 158 (1986) 609-614.

[80] S. A. Adediran, Kinetics of the formation of p-670 and of the decay of compound III of horseradish peroxidase, Arch Biochem Biophys 327 (1996) 279-284.

[81] H. Wariishi, and M. H. Gold, Lignin peroxidase compound III. Mechanism of formation and decomposition, J Biol Chem 265 (1990) 2070-2077.

[82] D. P. Barr, and S. D. Aust, Effect of superoxide and superoxide dismutase on lignin peroxidase-catalyzed veratryl alcohol oxidation, Arch Biochem Biophys 311 (1994) 378-382.

[83] D. P. Barr, and S. D. Aust, Conversion of lignin peroxidase compound III to active enzyme by cation radicals, Arch Biochem Biophys 312 (1994) 511-515.

[84] P. J. Harvey, G. F. Gilardi, M. L. Goble, and J. M. Palmer, Charge transfer reactions and feedback control of lignin peroxidase by phenolic compounds: significance in lignin degradation, J. Biotechnol. 30 (1993) 57-69.

[85] R. H. Nakajima, and I. Yamazaki, Biochemical, molecular, and physiological aspects of plant peroxidases, ed., University of Geneva Press, Geneva 1991.

[86] Y. Yamada, T. Fujiwara, T. Sato, N. Igarashi, and N. Tanaka, The 2.0 A crystal structure of catalase-peroxidase from Haloarcula marismortui, Nat Struct Biol 9 (2002) 691-695.

[87] X. Carpena, S. Loprasert, S. Mongkolsuk, J. Switala, P. C. Loewen, and I. Fita, Catalase-peroxidase KatG of Burkholderia pseudomallei at 1.7A resolution, J Mol Biol 327 (2003) 475-489.

[88] T. Bertrand, N. A. Eady, J. N. Jones, Jesmin, J. M. Nagy, B. Jamart-Gregoire, E. L. Raven, and K. A. Brown, Crystal structure of Mycobacterium tuberculosis catalase-peroxidase, J Biol Chem 279 (2004) 38991-38999.

[89] P. Bandyopadhyay, and H. M. Steinman, Catalase-peroxidases of Legionella pneumophila: cloning of the katA gene and studies of KatA function, J Bacteriol 182 (2000) 6679-6686.

[90] E. Garcia, Y. A. Nedialkov, J. Elliott, V. L. Motin, and R. R. Brubaker, Molecular characterization of KatY (antigen 5), a thermoregulated chromosomally encoded catalase-peroxidase of Yersinia pestis, J Bacteriol 181 (1999) 3114-3122.

[91] J. Amemura-Maekawa, S. Mishima-Abe, F. Kura, T. Takahashi, and H. Watanabe, Identification of a novel periplasmic catalase-peroxidase KatA of Legionella pneumophila, FEMS Microbiol Lett 176 (1999) 339-344.

[92] R. J. Mehigh, and R. R. Braubaker, Major stable peptides of Yersinia pestis synthesized during the low-calcium response, Infect Immun 61 (1993) 13-22.

[93] P. Bandyopadhyay, and H. M. Steinman, Legionella pneumophila catalase-peroxidases: cloning of the katB gene and studies of KatB function, J Bacteriol 180 (1998) 5369-5374.

[94] A. Hillar, L. Van Caeseele, and P. C. Loewen, Intracellular location of catalase-peroxidase hydroperoxidase I of Escherichia coli, FEMS Microbiol Lett 170 (1999) 307-312.

[95] D. M. Faguy, and W. F. Doolittle, Horizontal transfer of catalase-peroxidase genes between archaea and pathogenic bacteria, Trends Genet 16 (2000) 196-197.

[96] M. G. Klotz, and P. C. Loewen, The molecular evolution of catalatic hydroperoxidases: evidence for multiple lateral transfer of genes between prokaryota and from bacteria into eukaryota, Mol Biol Evol 20 (2003) 1098-1112.

[97] R. R. Brubaker, Mechanisms of bacterial virulence, Annu Rev Microbiol 39 (1985) 21-50.

[98] C. Dye, S. Scheele, P. Dolin, V. Pathania, and M. C. Raviglione, Consensus statement. Global burden of tuberculosis: estimated incidence, prevalence, and mortality by country. WHO Global Surveillance and Monitoring Project, Jama 282 (1999) 677-686.

[99] C. J. Murray, K. Styblo, and A. Rouillon, Tuberculosis in developing countries: burden, intervention and cost, Bull Int Union Tuberc Lung Dis 65 (1990) 6-24.

[100] G. Middlebrook, Sterilization of tubercle bacilli by isonicotinic acid hydrazide and the incidence of variants resistant to the drug in vitro, Am Rev Tuberc 65 (1952) 765-767.

[101] G. Middlebrook, Isoniazid-resistance and catalase activity of tubercle bacilli; a preliminary report, Am Rev Tuberc 69 (1954) 471-472.

[102] F. Winder, Catalase and peroxidase in mycobacteria. Possible relationship to the mode of action of isoniazid, Am Rev Respir Dis 81 (1960) 68-78.

[103] Y. Zhang, B. Heym, B. Allen, D. Young, and S. Cole, The catalase-peroxidase gene and isoniazid resistance of Mycobacterium tuberculosis, Nature 358 (1992) 591-593.

[104] A. Quemard, C. Lacave, and G. Laneelle, Isoniazid inhibition of mycolic acid synthesis by cell extracts of sensitive and resistant strains of Mycobacterium aurum, Antimicrob Agents Chemother 35 (1991) 1035-1039.

[105] K. Johnsson, D. S. King, and P. G. Schultz, Studies on the mechanism of action of Iioniazid and ethionamide in the chemotherapy of tuberculosis, Journal of the American Chemical Society 117 (1995) 5009-5010.

[106] V. Cannac-Caffrey, G. Hudry-Clergeon, Y. Petillot, J. Gagnon, G. Zaccai, and B. Franzetti, The protein sequence of an archaeal catalase-peroxidase, Biochimie 80 (1998) 1003-1011.

[107] M. Zamocky, G. Regelsberger, C. Jakopitsch, and C. Obinger, The molecular peculiarities of catalase-peroxidases, FEBS Lett 492 (2001) 177-182.

[108] K. G. Welinder, Bacterial catalase-peroxidases are gene duplicated members of the plant peroxidase superfamily, Biochim Biophys Acta 1080 (1991) 215-220.

[109] R. D. Baker, C. O. Cook, and D. C. Goodwin, Properties of catalase-peroxidase lacking its C-terminal domain, Biochem Biophys Res Commun 320 (2004) 833-839.

[110] G. Regelsberger, C. Jakopitsch, F. Ruker, D. Krois, G. A. Peschek, and C. Obinger, Effect of distal cavity mutations on the formation of compound I in catalase-peroxidases, J Biol Chem 275 (2000) 22854-22861.

[111] A. Hillar, B. Peters, R. Pauls, A. Loboda, H. Zhang, A. G. Mauk, and P. C. Loewen, Modulation of the activities of catalase-peroxidase HPI of Escherichia coli by site-directed mutagenesis, Biochemistry 39 (2000) 5868-5875.

[112] J. E. Erman, L. B. Vitello, M. A. Miller, A. Shaw, K. A. Brown, and J. Kraut, Histidine 52 is a critical residue for rapid formation of cytochrome c peroxidase compound I, Biochemistry 32 (1993) 9798-9806.

[113] T. L. Poulos, S. L. Edwards, H. Wariishi, and M. H. Gold, Crystallographic refinement of lignin peroxidase at 2 A, J Biol Chem 268 (1993) 4429-4440.

[114] G. Regelsberger, C. Jakopitsch, P. G. Furtmuller, F. Rueker, J. Switala, P. C. Loewen, and C. Obinger, The role of distal tryptophan in the bifunctional activity of catalase-peroxidases, Biochem Soc Trans 29 (2001) 99-105.

[115] S. Yu, S. Girotto, X. Zhao, and R. S. Magliozzo, Rapid formation of compound II and a tyrosyl radical in the Y229F mutant of Mycobacterium tuberculosis catalase-peroxidase disrupts catalase but not peroxidase function, J Biol Chem 278 (2003) 44121-44127.

[116] C. Jakopitsch, M. Auer, A. Ivancich, F. Ruker, P. G. Furtmuller, and C. Obinger, Total conversion of bifunctional catalase-peroxidase (KatG) to monofunctional peroxidase by exchange of a conserved distal side tyrosine, J Biol Chem 278 (2003) 20185-20191.

[117] E. Santoni, C. Jakopitsch, C. Obinger, and G. Smulevich, Manipulating the covalent link between distal side tryptophan, tyrosine, and methionine in catalase-peroxidases: an electronic absorption and resonance Raman study, Biopolymers 74 (2004) 46-50.

[118] J. M. Sambrook, and E. F. Fritsch, Molecular cloning: a laboratory manual, ed., Cold Spring Harbor, NY 1989.

[119] J. K. Falk, Porphyrins and Metalloporphyrins, ed., Elsevier Publishing, New York 1964.

[120] J. P. Kushner, G. R. Lee, and S. Nacht, The role of iron in the pathogenesis of porphyria cutanea tarda. An in vitro model, J Clin Invest 51 (1972) 3044-3051.

[121] K. Johnsson, W. A. Froland, and P. G. Schultz, Overexpression, purification, and characterization of the catalase-peroxidase KatG from Mycobacterium tuberculosis, J Biol Chem 272 (1997) 2834-2840.

[122] G. S. Jacob, and W. H. Orme-Johnson, Catalase of Neurospora crassa. 1. Induction, purification, and physical properties, Biochemistry 18 (1979) 2967-2975.

[123] S. Arun, R. Thirumurugan, R. Visakan, S. Balamurugan, V. Arunachalam, and P. Subramanian, Optimal analytical conditions for catalase in fresh water prawn, Mcrobrachium malcolmsonii, Biotechnic and Histochemistry 78 (2003) 1-4.

[124] R. R. Hamed, Characterization of catalase from Hyalomnta dromedarii cuticle, Comp Biochem Physiol 78 (1984) 499-505.

[125] D. R. Livingstone, F. Lips, G. P. Martinez, and R. K. Pipe, Antioxidant enzymes in the digestive gland of the common mussel Mytilus edulis, Mar Biol 112 (1992) 265-276.

[126] D. J. Sessa, and R. L. Anderson, Oybean peroxidases: purification and some properties, Journal of Agricultural and Food Chemistry 29 (1981) 960-965.

[127] L. Whitmore, and B. A. Wallace, DICHROWEB, an online server for protein secondary structure analyses from circular dichroism spectroscopic data, Nucleic Acids Res 32 (2004) W668-673.

[128] A. Lobley, L. Whitmore, and B. A. Wallace, DICHROWEB: an interactive website for the analysis of protein secondary structure from circular dichroism spectra, Bioinformatics 18 (2002) 211-212.

[129] C. L. Varnado, and D. C. Goodwin, System for the expression of recombinant hemoproteins in Escherichia coli, Protein Expr Purif 35 (2004) 76-83.

[130] T. Yonetani, and H. Anni, Yeast cytochrome c peroxidase. Coordination and spin states of heme prosthetic group, J Biol Chem 262 (1987) 9547-9554.

[131] S. Chouchane, S. Girotto, S. Kapetanaki, J. P. Schelvis, S. Yu, and R. S. Magliozzo, Analysis of heme structural heterogeneity in Mycobacterium tuberculosis catalase-peroxidase (KatG), J Biol Chem 278 (2003) 8154-8162.

[132] S. W. Kengen, F. J. Bikker, W. R. Hagen, W. M. de Vos, and J. van der Oost, Characterization of a catalase-peroxidase from the hyperthermophilic archaeon Archaeoglobus fulgidus, Extremophiles 5 (2001) 323-332.

[133] Y. Mino, H. Wariishi, N. J. Blackburn, T. M. Loehr, and M. H. Gold, Spectral characterization of manganese peroxidase, an extracellular heme enzyme from the lignin-degrading basidiomycete, Phanerochaete chrysosporium, J Biol Chem 263 (1988) 7029-7036.

[134] S. Chouchane, I. Lippai, and R. S. Magliozzo, Catalase-peroxidase (Mycobacterium tuberculosis KatG) catalysis and isoniazid activation, Biochemistry 39 (2000) 9975-9983.

[135] P. Gadsby, and A. J. Thomson, Assignment of the axial ligands of ferric ion in low-spin hemoproteins by near-infrared magnetic circular dichroism and electron paramagnetic resonance spectroscopy, J Am Chem Soc 112 (1990) 5003-5011.

[136] G. Palmer, Electron paramagnetic resonance of hemoproteins, in The porphyrins: physical chemistry, part B, in Dolphin, D., (Ed.), Academic Press, Inc, New York, 1979, pp. 313-350.

[137] Y. Cao, R. A. Musah, S. K. Wilcox, D. B. Goodin, and D. E. McRee, Protein conformer selection by ligand binding observed with crystallography, Protein Sci 7 (1998) 72-78.

[138] G. Regelsberger, C. Jakopitsch, M. Engleder, F. Ruker, G. A. Peschek, and C. Obinger, Spectral and kinetic studies of the oxidation of monosubstituted phenols and anilines by recombinant Synechocystis catalase-peroxidase compound I, Biochemistry 38 (1999) 10480-10488.

[139] C. Jakopitsch, M. Auer, G. Regelsberger, W. Jantschko, P. G. Furtmuller, F. Ruker, and C. Obinger, The catalytic role of the distal site asparagine-histidine couple in catalase-peroxidases, Eur J Biochem 270 (2003) 1006-1013.

[140] C. Jakopitsch, M. Auer, G. Regelsberger, W. Jantschko, P. G. Furtmuller, F. Ruker, and C. Obinger, Distal site aspartate is essential in the catalase activity of catalase-peroxidases, Biochemistry 42 (2003) 5292-5300.

[141] L. J. Donald, O. V. Krokhin, H. W. Duckworth, B. Wiseman, T. Deemagarn, R. Singh, J. Switala, X. Carpena, I. Fita, and P. C. Loewen, Characterization of the catalase-peroxidase KatG from Burkholderia pseudomallei by mass spectrometry, J Biol Chem 278 (2003) 35687-35692.

[142] C. Jakopitsch, A. Ivancich, F. Schmuckenschlager, A. Wanasinghe, G. Poltl, P. G. Furtmuller, F. Ruker, and C. Obinger, Influence of the unusual covalent adduct on the kinetics and formation of radical intermediates in synechocystis catalase peroxidase: a stopped-flow and EPR characterization of the MET275, TYR249, and ARG439 variants, J Biol Chem 279 (2004) 46082-46095.